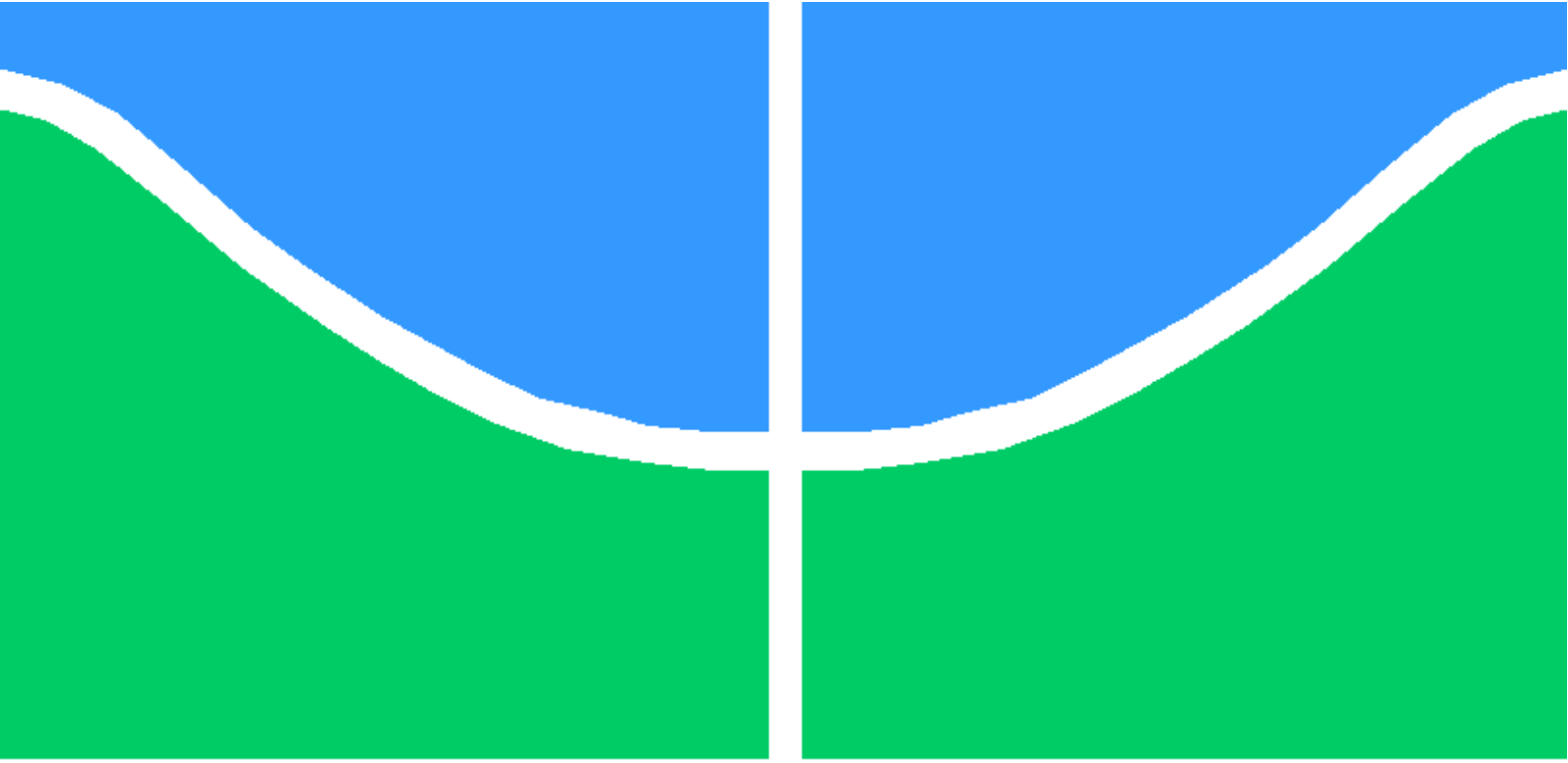

DISSERTAÇÃO DE MESTRADO

AN ANALYTICAL INVESTIGATION OF THE ATTENUATION PERFORMANCE OF DUCTS UNDER MEAN FLOW AND LINED WALLS

Guilherme Augusto Daniel da Silva

Brasília, Julho de 2022

UNIVERSIDADE DE BRASÍLIA

FACULDADE DE TECNOLOGIA

UNIVERSIDADE DE BRASILIA
Faculdade de Tecnologia

DISSERTAÇÃO DE MESTRADO

AN ANALYTICAL INVESTIGATION OF THE ATTENUATION PERFORMANCE OF DUCTS UNDER MEAN FLOW AND LINED WALLS

Guilherme Augusto Daniel da Silva

Relatório submetido ao Departamento de Engenharia Mecânica como requisito parcial para obtenção do grau de Mestre em Ciências Mecânicas

Banca Examinadora

Prof. Dr. Adriano Todorovic Fabro, ENM-FT/UnB
Orientador

Prof. Dr. Bráulio Gutierrez Pimenta, ENM-FT/UnB
Co-orientador

Prof. Dr. José Maria Campos dos Santos, FEM/UNICAMP
Examinador externo

Profa. Dra. Marcela Rodrigues Machado, ENM-FT/UnB
Examinador interno

Dedicatória

Dedico este trabalho ao meu pai Hélio à minha mãe Neusa e ao meu irmão João. Vocês são parte disso.

Guilherme Augusto Daniel da Silva

Agradecimentos

Gostaria de agradecer a minha família por terem me apoiado durante todo esse tempo. Agradeço especialmente ao meu pai Hélio e minha mãe Neusa por terem garantido a minha educação e tudo que precisei com seu trabalho honesto e árduo, além terem sido pais maravilhosos. Agradeço ao meu irmão João por sua amizade e companheirismo. Aagradeço também à minha namorada Eliza sempre me apoiou e encorajou apesar das adversidades. Agradeço aos ótimos professores da Universidade de Brasíla em especial ao meu orientador Adriano Fabro e ao Professor Bráulio por sua grande solicitude e disponibilidade para me ensinar e ajudar durante este e outros trabalhos. Agradeço a todos os amigos que fiz ao longo desses anos (Gustavo, Pedro, Caio,todos os demais) por proporcionarem ótimas lembranças.

Guilherme Augusto Daniel da Silva

Resumo

Turbo máquinas como fans, compressores e turbinas estão entre as mais importantes fontes de ruído aeroacústico. Tipicamente, a interação aeroacústica entre as pás do rotor e estator de turbofans aeronáuticos geram ruídos tonais que se propagam ao longo do duto da nacele e tem grande contribuição no ruído aeronáutico total gerado por aeronaves modernas. Os modos acústicos gerados dessa interação dependem do número de pás do rotor e do estator, conhecido como relação de Tyler e Sofrin. Nesse sentido, liners acústicos empregados nas paredes na nacele são comumente utilizados para controle de ruído, utilizando o mecanismo de ressonadores de Helmholtz para atenuação acústica. Neste trabalho, propõe-se uma investigação analítica dos modos acústicos resultantes da interação rotor-estator em dutos com liners e fluxo médio. Apesar da existência de expressões analíticas, estas não se apresentam de forma fechada e requerem esquemas numéricos para busca de raízes em equações transcedentais ao mesmo tempo que se faz o rastreamento dos modos correspondentes em uma certa banda de frequência. Estes resultados são utilizados para se contruir uma curva de dispersão de ondas dos modos acústicos, i.e., seus números de onda como uma função da frequência. A partir destas curvas, o desempenho de atenuação de liners pode ser investigado através da frequência de corte do modo e do comportamento da parte imaginária do número de onda. Primeiramente, propõe-se uma validação da metodologia implementada, que se utiliza do Método de Muller, a partir de resultados encontrados na literatura. Então, três modelos diferentes de liners são investigados, o modelo de *Tam and Auriault*, um modelo de um e dois grau de liberdade para ressonadores de Helmholtz. A evolução das formas modais radiais ao longo da frequência também é mostrada e discutida. Além disso, apresenta-se uma interpretação física das curvas de dispersão para cada modelo de liner. Mostra-se que eles apresentam diferenças qualitativas e quantitativas em termos de desempenho de atenuação e principal mecanismo de atenuação. A abordagem proposta tem o potencial de ser utilizada como uma metodologia de baixo custo computacional para projeto e desenvolvimetno atenuadores acústicos em dutos com liners.

Abstract

Turbo machines such as fans, compressors and turbines are among the most important sources of aeroacoustic noise. Typically, the aeroacoustic interaction between the rotor and stator blades of aeronautical turbofan generates tonal noises that propagate along the nacelle duct and has great contribution in the total aeronautical noise generated by modern aircraft. The acoustic modes generated from this interaction depend on the number of blades of the rotor and the stator, known as the Tyler and Sofrin relationship. In this sense, acoustic liners used in the nacelle walls are commonly used for noise control, using the Helmholtz resonator mechanism for acoustic attenuation. In this work, an analytical investigation is proposed for the acoustic modes resulting from the rotor-stator iteration of lined ducts with mean flow. Despite of the existence of analytical expression, these are not in closed form expression and require numerical schemes for root-finding in transcendental equations while also tracking their corresponding modes over a certain frequency band. Subsequently, these results are used to construct the wave dispersion curve of the acoustic modes, i.e., their wavenumber as a function of the frequency. From these curves, the attenuation performance of the liners can be investigated based on the frequency of the cut-on mode and on the behaviour of the imaginary part of the wavenumber. First, a numerical validation of the implemented methodology, using the Muller's method, is proposed using results from the literature. Then, three different models for liners are investigated, the *Tam and Auriault* model, and the single degree of freedom and the two degrees of freedom Helmholtz resonator models. The evolution of the radial mode shapes along the frequency is also shown and discussed. In addition, the physical interpretation of the obtained dispersion curves for the different liners' models is discussed. It is shown that they present significant qualitative and quantitative differences in terms of attenuation performance and main attenuation mechanism. The proposed approach has the potential of being used as a low cost computational design methodology for acoustic attenuation in lined ducts.

SUMÁRIO

LISTA DE FIGURAS

LISTA DE TABELAS

Chapter 1

Introduction

1.1 Aircraft Noise and the Urban Community

Several factors and environmental conditions elicit different psychological reactions in human beings and consequently how noise is perceived by them. For instance, according to the World Health Organisation traffic noise causes annoyance in 1 in 3 individuals during the daytime and 1 in 5 has their sleep disturbed at night because of it[15, 16]. Also according to the World Health Organisation increasing evidence from Epidemiological studies shows that there is a positive association between transportation noise (particularly road traffic and aircraft noise) and cardiovascular diseases such as hypertension and ischaemic heart diseases [16]. Therefore one of the factors that can generate annoyance for the urban community is the noise generated by aeroplanes and airports in populated regions.

The rapid expansion of commercial aviation and the resulting increase in noise, created a scenario where the society is greatly exposed to the aircraft noise [1]. Even though aircraft have had a tendency to become progressively quieter since the introduction of turbofans in the 1960s and 1970s, the reduction provided by new technologies has not sufficiently mitigated the problems and impacts caused by aircraft noise.

Although noise exposure levels can be quantified by physical variables, each person's reaction may vary as it depends on each individual's tolerance level which also depends on psychological factors. Thus, for control purposes, all aspects, objective or not, must be included in an indicator in order to quantify and judge the impacts caused by noise from aircraft.

Thus, national and international regulatory agencies began to impose rules for airports located in residential and habitational areas. As these restrictions were not enough to control noise levels, the aircraft models that can operate at a given airport were restricted. Certification processes for the new models have been adopted where a given level of noise is allowed for each class of aircraft [17].

1.2 Aircraft Noise Certification

The advent of low bypass ratio turbofan engines in commercial aircraft has taken commercial aviation to a new level. More powerful engines and more flights have revealed a previously not-so-addressed problem of excessive aircraft noise. In response to society's negative reaction to such conditions, authorities developed a concept implemented in the early 1970s, which is [1] aircraft certification.

The certification process involves both safety requirements and the level of noise produced. As discussed in the previous section, each individual's response to noise is variable and is linked to several factors. Thus, a metric was developed to quantify this response, the Effective Perceived Noise Level. Such a metric takes into account the spectral content, presence of tones and duration of the noise, as well as the individual's response to noise, aiming at a more representative way of how unsociable a noise is.

For certification, the noise radiated by the aircraft is measured by microphones located in certain positions on the ground. The measurement process takes place with the aircraft flying through the reference points under predetermined standard conditions. The certification process is made in three rating points that simulate the aircraft operating conditions: the approach measurements, lateral measurements and the flyover measurement.

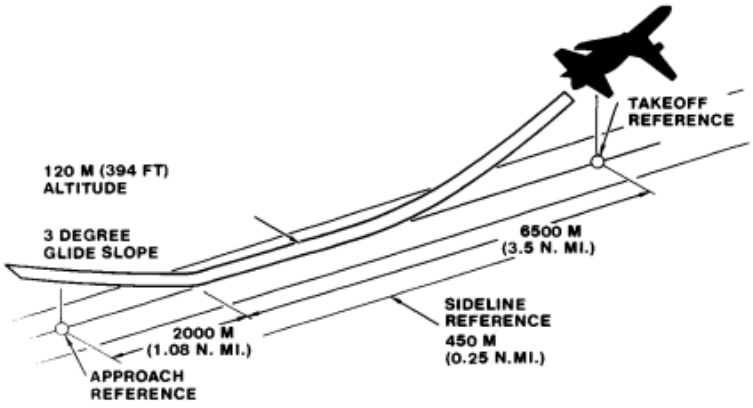

Figure 1.1: Scheme of the three reference points for aircraft certification [1]

The approach measurements take place in landing conditions with the measurement points located through the centre line of the runway at two kilometres from the runway end with an approach angle of 3 degrees and an altitude of 120 metres. For the lateral measurements are made with the aircraft at take-off operating conditions with the engines at full power, the altitude for the lateral measurements is defined by the results from the approach measurements. For this measurement, the microphones are positioned 450 metres from the centre line of the runway on both of its sides. The flyover measurement takes place with the aircraft in climbing conditions right after the take-off, the measurement point is 6500 metres distant from the point where the aircraft is airborne[17].

After the measurements, the values measured in the three stages are compared with the normalised values for that type of aircraft. If the aircraft has a noise level greater than the allowable at any of the three measurement points, the aircraft fails the certification process and is not allowed to operate at any civil airport.

Around 1 billion dollars are spent annually in research and development of new technologies that can mitigate aircraft noise as the regulatory agencies are periodically reducing the allowed noise levels in the certification procedures[1]. Therefore, manufacturers and governmental agencies hold great interest in advancements achieved in such fields.

1.3 Aircraft Noise Sources

The term jet was initially a colloquial term to refer to aircraft powered by gas turbine engines without propellants, such as those that entered service with the Comet in the 1950s. Today, this denomination also covers aircraft with modern turbofan engines, since these also do not have a visible propeller and also rely on energy from the flow that is exhausted by the nozzle located in the rear of turbines as driving force [1].

In a typical 50 kN thrust jet engine, about 40 kg of air per second is absorbed by the compression system and then mixed with the fuel and burned. At the exit of the combustion system, a turbine extracts enough energy to move the compressor, which is connected by the same shaft, before the jet is expelled through the nozzle at a speed of approximately 600 meters per second [1]. That is, the propulsive force is simply the force remaining in the jet after it overcomes all opposing forces in the engine nacelle.

A high jet speed is an essential feature to be able to fly at very high speeds such as supersonic flight. Accelerating a small mass of air is not the most effective aerodynamic process, but given the materials available at the time of the invention of jet turbines, this was one of the few possible processes. With the evolution of materials and engine cooling technologies, it was possible to produce more efficient blades and thus the bypass cycle improved its propulsive efficiency. The bypass cycle requires approximately 50% air for each unit of thrust generated, which consequently decreases the [1] exhaust velocity.

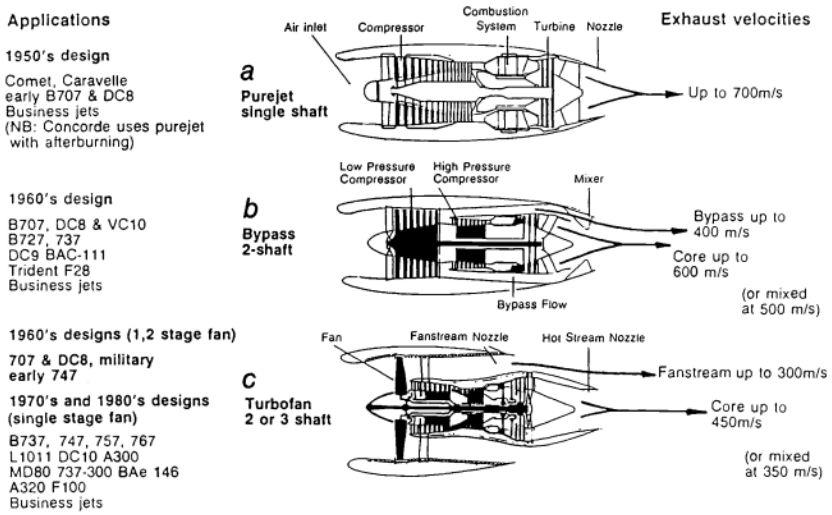

Figure 1.2: Schematic of types of jet turbines and their applications [1].

As part b of the figure 1.2 shows that the engine with bypass divides a large air intake into two similar streams, using one of these to feed the combustion chamber which in this case is smaller but more efficient than it has an exhaust velocity similar to that of a pure jet engine. The other stream is maintained at low pressure and flows through a separate duct and is exhausted by a different nozzle at a lower speed.

Modern turbofans, as schematic c of figure 1.2 represents, utilise even higher bypass levels using a large fan that is driven by an even more efficient air-cooled gas turbine that operates at even higher temperatures and pressures. This technology allows about three to four times more air for each unit of thrust generated compared to a pure jet. Of this amount of air only about 10% is used in the generation of gas for the turbine. The fan promotes a small compression in the air and the fan jet exit speed is around 300 meters per second, being the lowest of all cases. The compression ratio in the gas generating core is high, but energy is extracted to move the fan and compressors, which results in an exit velocity of the hot jet between 400 and 500 meters per second.

Since aerodynamic noise sources are intrinsically related to speed, and increasing the bypass ratio causes speeds to drop, noise for these types of engines is less. The engine power is also proportionally related to the bypass ratio, however, the noise generated by the fan, intermediate compressor and turbine system also increases with the increase of the bypass ratio. Such a scenario changes not only the noise composition but also the directivity with the acoustic field, as can be seen in the figure 1.3.

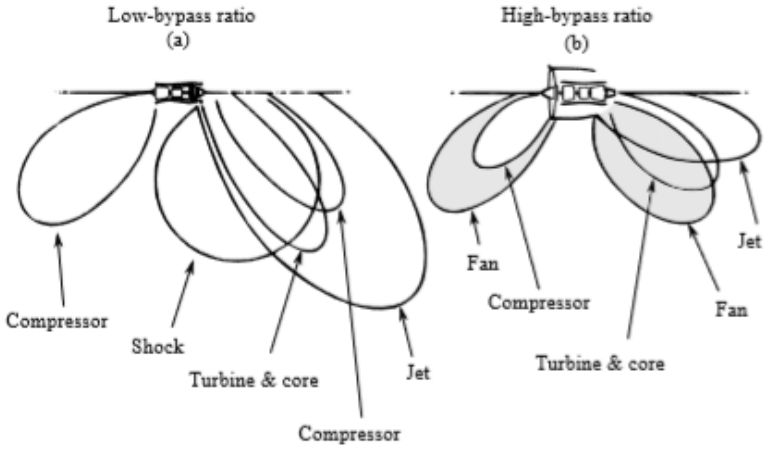

Figure 1.3: Comparison diagram between sound radiation in low and high bypass ratio motors [2]

If in pure jet engines or with a low bypass ratio the main source of the noise was the jet exhaust, in turbofan engines as the speeds are lower, however, to maintain the same thrust, the duct radius must be greater and consequently, the fan should be bigger so the fan has become one of the predominant sources of noise.

As with all rotating machines, the fan and compressors will emit sound with broad-band and tonal characteristics. The tonal component is the component penalised by the EPNL metric since they are extremely unsociable because they have a characteristic not found in nature.

Broadband noise is the result of sound propagation produced near the surface of the blades as a result of pressure fluctuations associated with turbulent flow in the vicinity. Turbulence in general is induced in any situation where there is flow over a solid surface or when there are discontinuities between two flows. The generation of tonal noise is extremely complex and comes from the interactive effect between the disturbances in the flow in the path of blade rotation.

Most of the noise generated by high bypass ratio turbofans is a product of the interaction between the rotor and stator blades. The pressure and vorticity fields generated by the rotor blades interact with the stator blades, generating noise with tonal and broadband components [18]. The tonal component is associated with the cyclical nature of the interaction due to the frequency of passage of the blades and their harmonics. Broadband noise is associated with the non-cyclic components of these interactions [8].

1.4 Work Background

The study of the sound attenuation in aircraft engines is closely related to the duct acoustics especially duct sound attenuation. There are various approaches to such a theme, this chapter aims to present an overview of the topic by listing some of the most relevant methodologies present in the literature. Huge efforts have been made in order to develop tools for prediction of the noise generation and propagation in aeronautic turbofans [8]. Nevertheless, there are various approaches

to the field in different aspects, since the noise generation due to the interaction of the rotor blades and the stator vanes to its propagation through the engine's nacelle. Computational Fluid Dynamics (CFD) and its primarily traditional methods have been applied to the flow calculations of the rotor-stator interaction. The usage of the linearised Euler's equations is typical when the rotor outlet flow field is unilaterally imposed on the stator vanes domain. In general, those perturbations are then propagated using linear equations as the Pridmore-Brown equations. The linearised Euler's equations are also used for the noise propagation in ducts coupled with different discretizations methods as the boundary element methods, finite element methods, finite volumes methods and finite differences methods. Also, analytical methods like the use of the Green's Functions or with other kind os methods for solving differential equations as shown by Tester in the works [19] [20].

1.4.1 Computational Fluid Dynamics Approach

Over the last decades, the Computational Fluid Dynamics has developed at a rapid pace, greatly influenced by aerospace engineering. Nowadays, new CFD algorithms have been developed to fill the gaps where the traditional CFD methods do not have the required precision in order to describe the physical phenomena correctly. Such a scenario created a new branch of the computational fluid dynamics: the computational aeroacoustics (CAA). The new CAA methods attempt to describe the physical processes with high temporal gradients where the wave propagation is the main problem [8].

One of the approaches of the CFD modelling of the noise generation due to the rotor-stator interaction is the usage of the mathematical model known as Reynolds Averaged Navier-Stokes equations (RANS). The RANS makes use of the idea of the Reynolds decomposition which preconizes a decomposition of the instantaneous quantities in time-averaged and fluctuating quantities allying that with a turbulent model to solve the system [21] [22] [23] [3].

A similar approach, however considering a transient flow, is also used, the Unsteady Averaged Navier-Stokes equations (URANS) comes from the same principles behind the RANS model and such a model is applied in a broad set of cases [24] [25] [26] [27].

Another simulation method applied to such cases is the Large Eddy Simulation (LES), differently of the RANS and the URANS rather than averaging all spectrum of the flow's fluctuations the LES adds a filtering method to the vector's field removing certain fluctuations modes of small time and spacial scales[4]. Such a method has a higher computational cost when compared with the URANS however in high complexity cases its applicability is needed.

All these methods have been proved significantly robust in the solutions presented, as all the works cited here present comparisons of their code results with experimental results or benchmarks cases showing an acceptable level of error and, when not, presenting the reasons and discussions around it. Their applicability varies along with the computational resources at hand and the complexity of the case of interest and also, it is noted that a High-Performance Computing (HPC) architecture is needed and also a good error and uncertainties management. Those facts elevate the

computational costs. However, the methods, codes and softwares shown in the works cited in this chapter demonstrate the flexibility of its applications both in large scales and high computational demanding cases. The interface between such approaches with Computational Assisted Design (CAD) and the Computational Assisted Manufacturing.

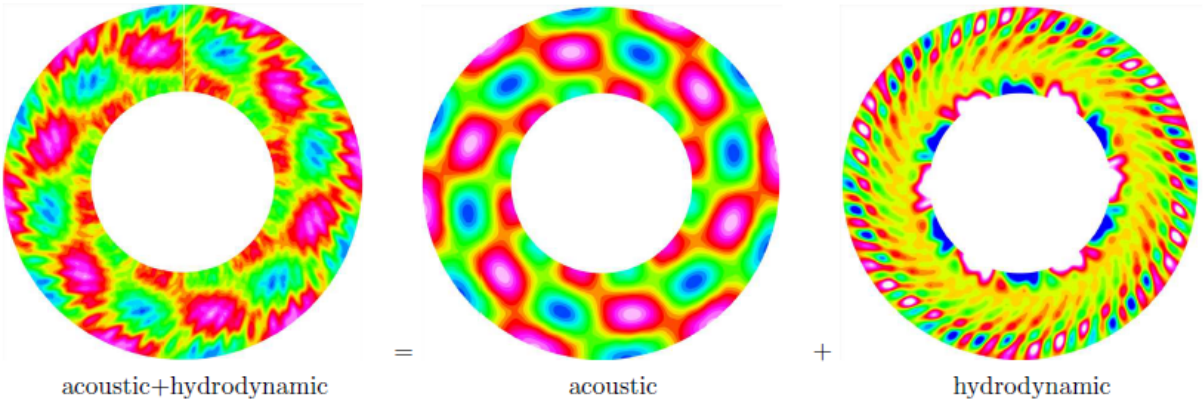

Figure 1.4: Fluctuating pressure field obtained through RANS methodology [3]

The figure 1.4 shows the fluctuating pressure field and illustrates the two distinct scales that coexists in the same system. That fact presents as ones of the main difficulties for the numerical simulation as the methods should be robust enough to represent small fluctuations as the acoustic scale and the hydrodynamic.

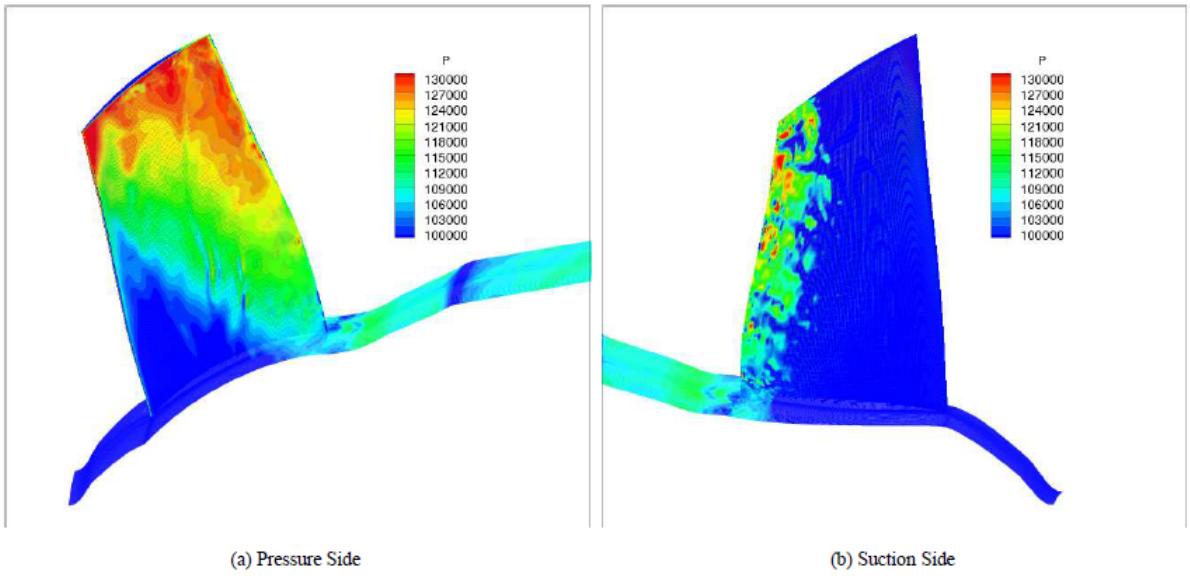

Figure 1.5: Fan pressure field obtained through the LES methodology [4]

The figure 1.5 its a great example of the interface of the CFD methods with the CAD/CAM technologies.

1.4.2 Lower Computational Cost Methodologies - Ducted Sound Propagation

In general, the perturbations due to the rotor and stator interaction are then propagated along the duct using linear equations, like the linearised Euler's equations and Pridmore-Bronwn Equations. However the methodology used, the problem is governed by differential equations and an variety of discretization methods are applied for their solution.

The boundary element method (BEM) is one of those discretization methods, the BEM attempts to use the boundary conditions to fit boundary values rather than values to all the domain defined by the partial differential equation and from that, an integral equation is used to numerically calculate the solution at any desired point in the solution domain, as done in the reference [28]. Another method broadly applied is the finite element method (FEM) which perform the subdivision of the domain into a large number of small elements with a specified format where the problem is solved, such approach is shown in the references [24] [29] [30][31]. The finite differences (FDM) methods are also implemented in such cases, the FD uses a discrete approximation of the derivatives transforming the ODE in an equation system which can be solved algebraically as the authors present in the reference [3].

1.5 Hybrid Approaches

Although this work presents a categorisation of the methods applied to the aerodynamic noise attenuation and propagation topic, the great majority of the works cited here don't restrict themselves to the usage of only one approach. Instead, due to the complex nature of the topic, the authors make use of hybrid approaches to optimise the methodology, in general, the authors approach the noise generation part of the problem, which is highly non-linear, with CFD/CAA methods and uses the linearised equations and methodologies in the sound propagation and attenuation part where they show greater effectiveness.

By using such approach, the computational costs are lowered without compromising the results, allowing a rapid development of the field and technologies that can not only be applied to the turbomachinery, the focus of this work, but also HVAC system ducts [32], or in automotive air induction systems [33].

1.6 Acoustic Liners

As the presence of tonal noise is penalised by the EPNL metric, one of the solutions adopted by turbine manufacturers was the use of passive control devices on the walls of the aeronautical engine. The acoustic treatment panels used are known as acoustic liners and are usually arranged in the turbofan as shown in the figure 1.6

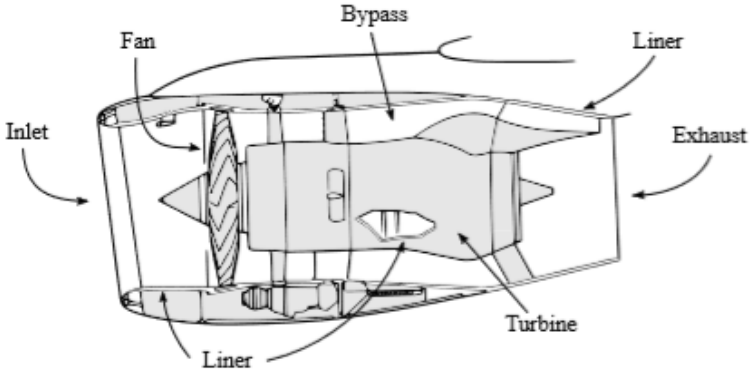

Figure 1.6: Schematic representation of liner positioning in high bypass ratio turbofans [2].

Commonly a locally reacting liner can be modelled as an array of Helmholtz resonators comprised of three elements. The first one is a face sheet with a regular pattern of holes (which will act as the neck of the resonator), the second is a structure in a honeycomb arrangement (which will act as the cavity of the resonator) and finally a rigid backplate. The main damping mechanism of the liner is attributed to the dissipation arising from the vortex shedding process at the holes of the perforated plate that forms the face sheet of the liner. The vortices convert the acoustic energy into rotational kinetic energy, and the resulting vortex is dissipated by the molecular viscosity. In cases where there is no shedding of vortices, attenuation occurs due to the viscous dissipation of the oscillatory flow that occurs at the face sheet inlet holes [34]

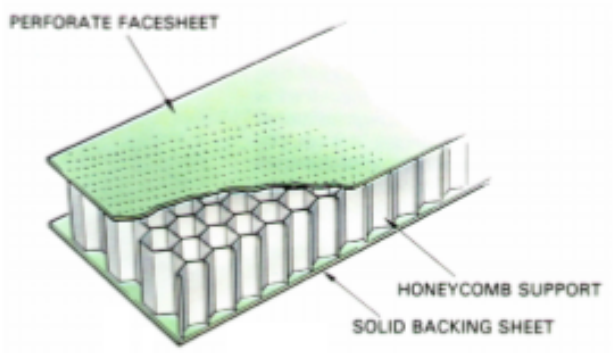

Figure 1.7: Acoustic liner scheme of a single perforated plate [5]

Depending on the frequency range for which the attenuation is required, one must choose the type of treatment applicable to the case. The most common types of liners are: one degree of freedom, two degrees of freedom and bulk absorber

The configuration aforementioned and shown in the figure 1.7 and also in figure 1.8 is known as a 1-degree-of-freedom acoustic liner as the air oscillating in the resonator neck can be modelled as a mass and the air in the cavity acts as a spring. However, other configurations with greater degrees of freedom can be built by adding an intermediary perforated sheet between the face sheet and

the backplate creating layers of the honeycomb structure as exemplified in the figure 1.9. Also, by changing the honeycomb arrangement to a porous material the attenuation device can be changed into a non-locally reacting liner as shown in the figure 1.10. Nevertheless, for any kind of liner, the fundamental idea in the design of a liner is to approximate the maximum attenuation frequency to the fundamental tone of the fan [35].

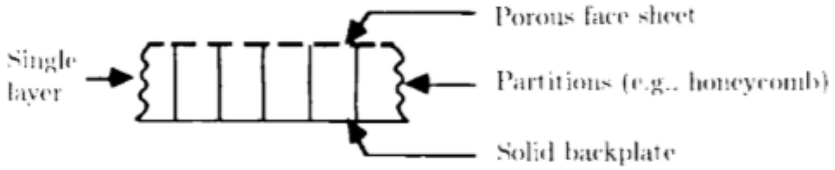

Figure 1.8: Schematic of a single degree of freedom liner [6]

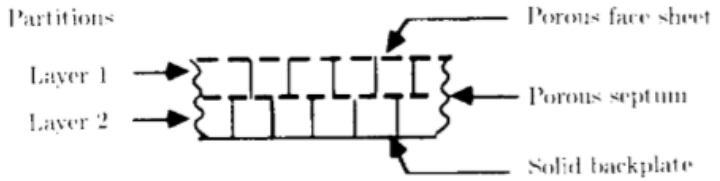

Figure 1.9: Schematic of a double degree of freedom liner [6]

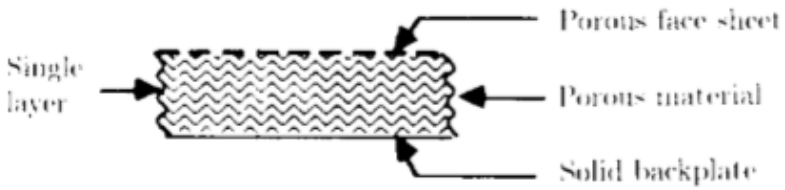

Figure 1.10: Schematic of a bulk attenuator [6]

The single-degree-of-freedom liner has the narrowest band attenuation, however, has a high attenuation in such a range and because of such characteristic is the most studied and widely implemented aircraft liner. The main mechanisms of attenuation of a single-degree-of-freedom liner are the acoustic wave damping at the walls of the holes and the one-quarter wavelength resonance at the cell[2].

In liners with two degrees of freedom the attenuated frequency range is larger but the maximum attenuation is smaller[6] when compared to the single-degree-of-freedom liner. The expansion of this concept to multiple degrees of freedom liner using several intermediate plates allows the desired attenuation configuration to be reached, however, due to space and weight restrictions in the turbofan nacelle, this option becomes unfeasible in commercial aviation.

A bulk attenuator has a wide attenuation range extending up to three octaves. Its attenuation parameters depend on the fibre diameter and density of the material used and the depth of the cavity, such relationships are especially impactful in the attenuation of high-frequency noise. Due to great difficulties in its commercial project, the bulk attenuator is rarely used in commercial aviation [6].

1.6.1 Acoustic impedance

For engineering purposes, it is an accepted practice to characterise an acoustically treated surface and its macroscopic effects using the acoustic impedance quantity Z. This is a convenient way of modelling the attenuation induced by acoustic liners. The acoustic impedance is defined as the ratio between the acoustic pressure and the particle velocity, the acoustic impedance is also a complex quantity, which consequently takes into account the attenuation and the phase shift promoted by the liner, or any other surfaces, on the sound waves[36].

$$Z(w) = \frac{p}{u} = R + iX. \tag{1.1}$$

The real part R is denominated reactance, such a quantity is related majorly to the energy on the perforated face sheet, and the imaginary part X is named resistance and is related to the inertial effects in the cavity of the resonator.

1.6.2 Impedance models

Liner performance is affected by operating conditions, flow velocity, and sound pressure level, among others. The usual way of approaching the problem of liners is by the acoustic impedance that can be related as a function of geometry, air temperature and flow velocity. Even though the liners have fixed geometry, the speed and sound pressure level conditions vary, especially in landing and take-off conditions, which leads to differences in acoustic impedance values. This fact must be taken into account during the design of the liners. Wave propagation is also affected by the presence of flow so the attenuation in the liner is also affected.

Once the impedance of a material is determined it is desirable to have a model that describes its behaviour throughout the frequency so the model can be implemented in computational or analytical analysis.

Some conditions should be met by an impedance model to be physically representable, those conditions were condensed by Rienstra in its *Theorem 1* [37], as

$$\begin{cases} Z(\omega) \text{ is analytic in } Im(\omega) < 0; \\ Z(\omega) \neq 0 \text{ in } Im(\omega) < 0; \\ Z(\omega) = Z^*(-\omega)\ \forall \omega \in \Re; \\ Re(Z(\omega)) \geq 0\ \forall \omega \in \Re. \end{cases} \tag{1.2}$$

The first three conditions expressed in the equation 1.2 are needed in order to satisfy the causality condition whereas the fourth one is needed in order to satisfy the passivity condition that is, the liner is an attenuator that absorbs energy at any frequency. Therefore, the acoustic intensity into the wall is positive which leads to $Re(Z(\omega)) \geq 0$ [37]. In the following sections, some of the relevant models that are used to describe the impedance in liners will be introduced.

1.6.2.1 Mass-Spring-Damper model

By making an analogy of a damped mechanical resonator, this model describes a frequency-dependent model given by:

$$Z(\omega) = R + id\omega - \frac{ib}{\omega}, \tag{1.3}$$

where d is the mass or density of the boundary, R is the damping constant (taking place as the reactance) and b is the spring constant representing the stiffness of the mechanical system. The model proposed by Tam and Ariault in 1996 [12] also known as the three-parameter model is equivalent to the mass-spring-damper model and is given by:

$$Z(\omega) = R(\omega) - i(X_{-1}/\omega + X_1\omega). \tag{1.4}$$

Some particularity of such a model is that the resistance is assumed constant in frequency, i.e., $R(\omega) = R$ as it does not vary much throughout the frequency, X_1 and X_{-1} are calibration parameters that are obtained experimentally.

1.6.2.2 Helmholtz Resonator Model

A liner which consists of an array of Helmholtz resonators can be modelled as:

$$Z(\omega) = Z_{fs} - icot(KL), \tag{1.5}$$

where, $K = \omega/c$ which is the free field wavenumber, Z_{fs} is the impedance of the face sheet that can be modelled using any semi-empirical models. The imaginary terms refer to the cavity reactance of a cell of depth L. It is worth mentioning that a cavity impedance is purely reactive [38], further mathematical demonstrations can be found in the appendix.

1.6.2.3 Double Degree of Freedom Model

A liner with a double degree of freedom or also known as the double array Helmholtz resonator model can be described by the following equation

$$Z(\omega) = Z_{fs} + \frac{Z_s cosh(-iKL_1)sinh(-iKL_2) + cosh(iKL)}{Z_s sinh(-iKL_1)sinh(-iKL_2) + sinh(iKL)}, \tag{1.6}$$

where Z_s is the septum's impedance, that is the impedance of the second perforated plate between the face sheet and the backplate, L_1 and L_2 are the depth of the first and second cavities respectively. The impedance value for Z_s and also Z_fs can be modelled by using a semi-empirical model.

The double degree of freedom model can also be represented by

$$Z(\omega) = Z_{fs} + \frac{\frac{Z_s cos(KL_1) sin(KL_2)}{sin(KL)} - icot(KL)}{1 + \frac{iZ_s cos(KL_1) sin(KL_2)}{sin(KL)}}. \tag{1.7}$$

Such representation can be found in the works done by Burd [14] and Eversman [31] in 2009 and 2010 respectively.

1.7 Semi-Empirical Impedance Models

Several impedance models emerged from the studies of the effects of the perforated plates, and resonant cavities. Those models are in the vast majority semi-empirical models which in general are composed of different parcels that take into account different effects. One part which takes into consideration the linear part of the impedance behaviour dependent on the liner geometry, frequency and fluid viscosity, such parcel is also known as the viscous and mass impedance Z_ν. The other part takes into account the non-linear effects given the acoustic velocity and radiation effects Z_{NL} and Z_R. The impedance of the backing plate Z_B is also considered and coupled to the semi-empirical models. Also, operational conditions such as the flow velocity and excitation frequency have a great impact on the values of the impedance and are also considered in the models [39][2].

The models presented in this section are named semi-empirical as part of their components are analytically modelled from the physical characteristics of the given problem. Other parts, mainly the non-linear effects, are modelled from empirical results. Therefore the impedance of a liner can be dependent on several factor and expressed as

$$Z = Z(\rho, c, \nu, \omega, M, u_0, d, t, L, \sigma), \tag{1.8}$$

where ρ is the specific mass of the air, c, the sound velocity, ν is the kinematic viscosity of the air, M the Mach Number, u_0 is the particle acoustic velocity, d the diameter of the cavity, t the thickness of the face sheet, L is the depth of the cavity and σ is the percentage of the open area of the face sheet.

1.7.1 Guess Model

In 1975, one of the first models for the general impedance for a single degree of freedom liner (an array of Helmholtz resonators) was proposed by Guess [40]. The main goal of the work done by Guess was to use the methodology published to find the geometrical characteristics of a liner given an impedance value however, it is perfectly possible to use the same methodology to calculate the

impedance value given the geometrical features of the passive device. The methodology proposed by Guess considers an only one frequency of excitation, therefore, there are no non-linearities given the interaction between tones, also the face sheet thickness, the cavity diameter and the space between each hole have to have values inferior to the acoustic wavelength.

The expression for the viscous and mass effects considered in Guess's work was derived by Kinsley and Frey [41] in their book in 1950, and it is the impedance of a single tube of short length and it is given by

$$Z_\nu = -i\rho\omega t\left(\frac{4J_1(K_s d/2)}{K_s d J_0(K_s d/2)} - 1\right), \tag{1.9}$$

where $K_s = -i\omega/\nu$ is the Stokes's number, J_0 and J_1 are the Bessel functions of the first kind of 0 and first order respectively. By multipliyng the equation1.9 by $1/\sigma\rho c$ and considering that $|K_s d/2| > 10$ an approximated expression for an array of short length tubes, i.e. a perforated plate, can be obtained.

$$z_\nu \approx \frac{\sqrt{8\nu\omega}t}{\sigma c d} + i\left(\frac{\omega t}{\sigma c} + \frac{\sqrt{8\nu\omega}t}{\sigma c d}\right), \tag{1.10}$$

it is worth mentioning that the consideration for the Stokes's number is valid for general operational conditions of liners in aircraft engines.

For the radiation impedance, Guess obtained the expression following the derivation done by Morse and Ingard [42] in their book in 1968 and assuming $\omega d/c < 1/2$ in addition to interaction effects between adjacent holes, along with airflow and sound amplitude effects[40] the radiation impedance can be written as

$$z_R = \frac{\pi^2}{2\sigma}\left(\frac{\omega d}{c}\right)^2 + i\frac{\omega\delta}{\sigma c}, \tag{1.11}$$

where orifice end correction δ is given by

$$\frac{8d(1-0.7\sqrt{\sigma})}{3\pi(1+305M^3)}\left(\frac{1+5\cdot 10^3 M_o^2}{1+10^4 M_o^2}\right). \tag{1.12}$$

The last term in parenthesis is an attempt developed by Guess in order to account for the effects of the sound amplitude with M_o being the Mach number at the orifice of the perforated plate. The factor $1-0.7\sqrt{\sigma}$ accounts for the orifice interactions proposed by Ingard [43]. The factor $1+305M^3$ accounts for the steady airflow effects [44].

The non-linear effects resulting from the high sound amplitude and grazing flow are given by the expression

$$z_{NL} = \frac{1-\sigma^2}{\sigma}\left[\frac{|u_o|+|v|}{c}\right], \tag{1.13}$$

where $|v|$ is an estimate of the magnitude of the turbulent velocity fluctuation due to a turbulent boundary layer. This expression was developed by Ingard and Ising [45] in 1967.

And as aforementioned the impedance of a cavity with a rigid back plate is given by

$$z_B = -icot(KL). \tag{1.14}$$

Therefore the sum of all the effects described in the present section leads to Guess expressions for the reactance and resistance. However, it is also possible to determine an expression for the perforated face sheet which is given by

$$R = \frac{\sqrt{8\nu\omega}}{\sigma c}(1 + t/d) + \frac{1}{8\sigma}\left(\frac{\omega d}{c}\right)^2; \tag{1.15}$$

$$X = \frac{\omega}{\sigma c}\left(t + \frac{8d}{3\pi}(1 - 0.7\sqrt{\sigma}) + \sqrt{\frac{8\nu}{\omega}}(1 + t/d)\right). \tag{1.16}$$

If the presence of a uniform flow is considered that the equations can be written as

$$R = \frac{\sqrt{8\nu\omega}}{\sigma c}(1 + t/d) + \frac{1}{8\sigma}\left(\frac{\omega d}{c}\right)^2 + \frac{1 - \sigma^2}{\sigma}; \tag{1.17}$$

$$X = \frac{\omega}{\sigma c}\left(t + \frac{1}{1 + 305M^3}\frac{8d}{3\pi}(1 - 0.7\sqrt{\sigma}) + \sqrt{\frac{8\nu}{\omega}}(1 + t/d)\right). \tag{1.18}$$

Those expressions can be used in order to calculate the necessary values for the face sheet impedance and septum impedance.

1.8 Objectives

The main objective of this work is to propose an analytical investigation of the acoustic modes resulting from the rotor-stator iteration in lined ducts with mean flow. This is then used to discuss the attenuation performance of different models for liners in terms of the wave dispersion curve.

1.9 Methodology

In order to achieve the proposed aims, the following methodology is proposed. The Muller's method is proposed as a numerical scheme for root-finding of the analytical transcendental equations. Numerical validation of the implemented methodology is proposed using results from the literature. Then, three different models for liners are investigated, the *Tam and Auriault* model, the single degree of freedom and the two degrees of freedom Helmholtz resonator models. The evolution of the radial mode shapes along the frequency is also shown and discussed. In addition, the physical interpretation of the obtained dispersion curves for the different liners' models is discussed.

1.10 Organisation of the dissertation

Chapter 1 presents the context and relevance of aircraft noise reduction and the use of acoustic liners in one of the main noise sources. It also briefly reviews some of the literature's model of

liners in terms of acoustic impedance. This chapter also presents the dissertation objectives and methodology. Chapter 2 presents e equations that analytically govern the phenomena of generation and propagation of waves in pipelines. The theory is described from the governing equations of fluid mechanics. The equations that govern the phenomenon are highly nonlinear due to the presence of advective terms, thus its linearized version is used. The rotor-stator interaction for tonal noise generation is presented. Chapter 3 presents the general boundary conditions for a softwall case and the analytical wave equation and corresponding modal solution for an annular duct with finite wall impedance under mean flow. Chapter 4 presents a validation of the implemented methodology. Chapter 5 presents the numerical results of the investigation of the attenuation performance of the lined ducts under mean flow. A parametric analysis of the two-degree freedom liner model is also presented. Finally, Chapter 6 presents the conclusion and suggestions for further work.

Chapter 2

Noise Generation and Propagation in Ducts

In this chapter, the equations that analytically govern the phenomena of generation and propagation of waves in pipelines are reviewed and presented. The theory is described from the governing equations of fluid mechanics. In an aeroacoustic problem, the principles used are the conservation of mass, the change in momentum (newton's second law), and the energy equation (first law of thermodynamics).

Using the Reynolds Transport Theorem it is possible to obtain the differential form for the three principles since the Reynolds Transport Theorem leads to an integral relationship of any conserved quantity of a control volume, where the flow of this quantity is accounted for at the surface as well as the transformation of this property given the phenomenon that occurs within the control volume. Evaluating the three principles, we have more variables than equations, so constitutive relations are necessary that allow us to obtain the solution of the system. The constitutive equations used are Fourier's law for thermal conductivity, the ideal gas law, since the fluid for the case studied is the air that can be characterised as ideal under the circumstances, Newtonian and calorically perfect, and also Southerland's law. for viscosity.

The equations that govern the phenomenon are highly nonlinear due to the presence of advective terms, this situation makes the solution of these equations extremely difficult. A great example of this is the equation of variation of the momentum, also known as the Navier-Stokes equation, which has been known for over 100 years and has no proof of solution or uniqueness for all real situations.

Mathematically developing the conservation of mass equation, also known as the continuity equation, we have that

$$\frac{\partial \rho}{\partial t} + \nabla \cdot (\rho \mathbf{u}) = 0. \tag{2.1}$$

In index notation, we have

$$\frac{\partial \rho}{\partial t} + \frac{\partial \rho u_i}{\partial x_i} = 0. \tag{2.2}$$

Applying the product rule

$$\frac{\partial \rho}{\partial t} + \rho \frac{\partial u_i}{\partial x_i} + u_i \frac{\partial \rho}{\partial x_i} = 0, \tag{2.3}$$

and defining the material derivative as

$$\frac{D}{Dt} = (\frac{\partial}{\partial t} + \mathbf{u} \cdot \nabla), \tag{2.4}$$

we have that the continuity equation takes the form

$$\frac{D\rho}{Dt} + \rho \nabla \cdot \mathbf{u} = 0. \tag{2.5}$$

Applying the momentum variation principle for a fluid particle, we have

$$\frac{\partial \rho \mathbf{u}}{\partial t} + \nabla \cdot (\mathbf{P} + \rho(\mathbf{uu})) = \mathbf{f}. \tag{2.6}$$

Rewriting the equation in index notation and working it algebraically, we have:

$$\rho \frac{\partial u_i}{\partial t} + u_i \frac{\partial \rho}{\partial t} + \frac{P_{ij}}{\partial x_i} + \rho u_i \frac{\partial u_j}{\partial x_i} + u_j (\rho \frac{\partial u_i}{\partial x_i} + u_i \frac{\partial \rho}{\partial x_i}) = f_i. \tag{2.7}$$

Evaluating the terms multiplied by the velocity, we observe that the sum of these results in the continuity equation which then result in zero. So, the equation takes the following form

$$\rho \frac{\partial \mathbf{u}}{\partial t} + \nabla \cdot (\mathbf{P}) + \rho \mathbf{u} \cdot \nabla \mathbf{u} = \mathbf{f}, \tag{2.8}$$

where $\mathbf{P}$ is given by

$$\mathbf{P} = p\mathbf{I} - \tau. \tag{2.9}$$

The term p is related to the pressure field and the tensor τ is the viscous stress tensor, therefore by applying the Stokes hypothesis, we have that

$$\tau = \mu(\nabla \mathbf{u} + (\nabla \mathbf{u})^T) - \frac{2}{3}\mu((\nabla \cdot \mathbf{u})\mathbf{I}), \tag{2.10}$$

where μ is the dynamic viscosity of the fluid Taking the divergent of $\mathbf{P}$, we have that

$$\nabla \cdot \mathbf{P} = \nabla \cdot (p\mathbf{I} + \tau) = \nabla \cdot (p\mathbf{I}) + \nabla \cdot (\tau) \tag{2.11}$$

and operating the first term of the equation, results in

$$\nabla \cdot (p\mathbf{I}) = \nabla p. \tag{2.12}$$

Therefore, assuming that the source term is equal to zero, that is, $\mathbf{f}$=0, and neglecting the viscous diffusion terms, $\tau = \mathbf{0}$, we obtain the following equation for the change in momentum of the fluid body

$$\rho \frac{\partial u}{\partial t} + \nabla \cdot (\rho \mathbf{u} \otimes \mathbf{u}) = -\nabla p, \tag{2.13}$$

which is denominated Navier-Stokes equation without the source term

Applying the Reynolds Transport Theorem to the total energy of the system and performing the required operations, we obtain the following equation:

$$\frac{\partial \rho e_t}{\partial t} + \nabla \cdot (\rho e_t u) = -\nabla \cdot (p\mathbf{I} \cdot \mathbf{u}) + \nabla \cdot (\tau \cdot \mathbf{u}) + \nabla \dot{q}, \tag{2.14}$$

where

$$e_t = (e + \frac{u^2}{2}). \tag{2.15}$$

Diffusive effects will be neglected for this analysis ($\tau = 0$ and $\dot{q} = 0$) since, in principle, they do not contribute to noise generation. Therefore, the following form of the energy variation equation is obtained,

$$\rho\frac{\partial e_t}{\partial t} + e_t\frac{\partial \rho}{\partial t} + \underbrace{\nabla \cdot (\rho \mathbf{u} e_t)}_{1} = -\nabla \cdot (P\mathbf{I} \cdot \mathbf{u}). \tag{2.16}$$

By expanding the term "1" 2.16, we have that

$$\nabla \cdot (\rho \mathbf{u} e_t) = e_t \nabla \cdot (\rho \mathbf{u}) + \rho \mathbf{u} \cdot \nabla(e_t). \tag{2.17}$$

Thus, obtaining the following expression

$$\rho\frac{\partial e_t}{\partial t} + \underline{e_t\frac{\partial \rho}{\partial t} + e_t \nabla \cdot (\rho \mathbf{u})} + \rho \mathbf{u} \cdot \nabla e_t = -\nabla \cdot (p\mathbf{I} \cdot \mathbf{u}). \tag{2.18}$$

The underlined terms result in the continuity equation therefore such sum is equal to zero . Then the energy equation takes the following form:

$$\rho\frac{\partial e_t}{\partial t} + \rho \mathbf{u} \cdot \nabla(e_t) = -\nabla \cdot (p\mathbf{I} \cdot \mathbf{u}). \tag{2.19}$$

Thus, applying the definition of material derivative, we have that

$$\rho\frac{De_t}{Dt} = -\nabla \cdot (p\mathbf{I} \cdot \mathbf{u}). \tag{2.20}$$

Using the index notation expanding the form of the energy equation given by 2.20 using the relation 2.15 we have that

$$\rho(\frac{D}{Dt}(e + \frac{1}{2}u_i u_i)) = -\frac{\partial p u_i}{\partial x_i}. \tag{2.21}$$

By applying the chain rule to the equation 2.21, we have that

$$\rho(\frac{De}{Dt} + u_i\frac{Du_i}{Dt}) = -p\frac{\partial u_i}{\partial x_i} - u_i\frac{\partial p}{\partial x_i}. \tag{2.22}$$

Applying the definition of material derivative to the equation 2.13, in index notation, one arrives at

$$.\rho\frac{Du_i}{Dt} = -\frac{\partial p}{\partial x_i}. \tag{2.23}$$

Substituting the equation 2.23 into the equation 2.22, logo

$$\rho(\frac{De}{Dt} - \frac{u_i}{\rho}\frac{\partial p}{\partial x_i}) = -u_i\frac{\partial p}{\partial x_i} - p\frac{\partial u_i}{\partial x_i}. \tag{2.24}$$

Simplifying the equation 2.24

$$\rho\frac{De}{Dt} = -p\frac{\partial u_i}{\partial x_i}. \tag{2.25}$$

The flow considered is totally subsonic for low compressibility levels, therefore, the discontinuities in the flow variables due to shock waves will not exist. The dissipative effects of heat transfer

and viscosity are also disregarded. Thus, the fundamental law of thermodynamics can be used for a reversible process that advocates that

$$Tds = de + pd(\rho^{-1}). \tag{2.26}$$

Further developing the term $d(\rho^{-1})$ of the equation 2.26 it is observed that

$$d\rho^{-1} = \frac{1}{\rho^2}d\rho. \tag{2.27}$$

Substituting the development of the equation 2.27 into the equation 2.26 it is obtained that

$$de = Tds - \frac{P}{\rho^2}d\rho. \tag{2.28}$$

Therefore, from equation 2.24 combined with the relation 2.28, we have that

$$\rho T\frac{Ds}{Dt} = -p(\frac{1}{\rho}\frac{D\rho}{Dt} + \rho\frac{\partial u_i}{\partial x_i}). \tag{2.29}$$

Analysing the equation 2.29, it is possible to see that the rigth-handed side of the equation is equal to the continuity equation which implies being equal to zero, thus

$$.\frac{Ds}{Dt} = 0 \tag{2.30}$$

The equation 2.30 implies that the phenomenon is isentropic hence, for a subsonic regime, without viscous stresses or heat transfer, the energy equation is decoupled from the others, becoming independent.

2.1 Linearization of the Governing Equations

The linearization of the governing equations will be given based on the decomposition of the variables of the governing equations system 2.1 and 2.13 into mean value terms and acoustic fluctuation terms. Thus, for a given property ϕ we have that

$$\phi = \phi_0 + \phi', \tag{2.31}$$

where ϕ_0 is the mean value given by

$$\phi_0 = \frac{1}{T}\int_t^{t+T} \phi dt, \tag{2.32}$$

and ϕ' is the acoustic fluctuation value.

The main hypothesis for linearization considers that the values of the fluctuations are much smaller than the mean values of the properties, hence it is known that the equations obtained from such considerations will only be valid in regions where the phenomenon has these characteristics. It is also known that most aeroacoustic phenomena have large regions of nonlinearity and that determining from where the linearization of the event occurs is very difficult. Illustrating this situation, we consider the case of noise generated in an airfoil, 2.1.

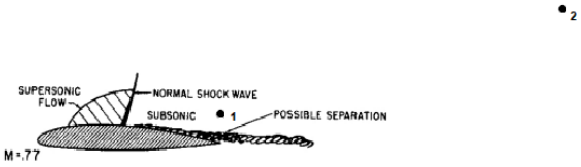

Figure 2.1: Exemplification of non-linear and linear regions in airfoil [7]

The region of point 1 of the figure 2.1 is a region where the presence of a shock wave and a wake of vortices can be perceived, this implies in a region where the fluctuations of the properties are of the order of the average value of these, such a region is characterised as highly nonlinear. On the other hand, the region of point 2 finds itself sufficiently distant from the source, causing the fluctuations of the properties to be much smaller than the mean values of the properties. Applying the decomposition 2.31 to the continuity equation at the form of the equation 2.1 we have that,

$$\frac{\partial(\rho_0 + \rho')}{\partial t} + \nabla \cdot [(\rho_0 + \rho')(\mathbf{u}_0 + \mathbf{u'})] = 0, \tag{2.33}$$

expanding, one has that

$$\frac{\rho_0 + \rho'}{\partial t} + \nabla \cdot [(\rho_0 \mathbf{u}_0 + \rho_0 \mathbf{u'} + \rho' \mathbf{u}_0 + \rho' \mathbf{u'})] = 0. \tag{2.34}$$

As the fluctuations of the properties are much smaller than the mean values of the properties, the second order terms will be neglected, so we arrive that

$$\frac{\rho_0 + \rho'}{\partial t} + \nabla \cdot [(\rho_0 \mathbf{u}_0 + \rho_0 \mathbf{u'} + \rho' \mathbf{u}_0] = 0. \tag{2.35}$$

Separating the terms, the equation assumes the following form

$$\frac{\partial \rho_0}{\partial t} + \frac{\partial \rho'}{\partial t} + \nabla \cdot (\rho_0 \mathbf{u'}) + \nabla \cdot (\rho_0 \mathbf{u}_0) + \nabla \cdot (\rho' \mathbf{u}_0) = 0. \tag{2.36}$$

By applying the same decomposition to a steady flow without fluctuations, the following equation is obtained

$$\nabla \cdot (\rho_0 \mathbf{u}_0) = 0. \tag{2.37}$$

Substituting the equation 2.37 into the equation 2.36 and expanding the relations, we have

$$\frac{\partial \rho'}{\partial t} + \rho_0 \nabla \cdot \mathbf{u'} + \mathbf{u'} \nabla \rho_0 + \rho' \nabla \cdot \mathbf{u}_0 + \mathbf{u}_0 \cdot \nabla \rho' = 0. \tag{2.38}$$

It is now assumed that the mean values of the properties do not vary with time or space, which results in a free stream solution for the mean flow. Such a hypothesis implies that the observation point is not influenced by the mean values of the properties, this situation can be illustrated as

the visualisation of a plane passing where the observer can hear it but the pressure field generated by such a phenomenon is not perceived. Therefore, we arrive at the final form of the linearised continuity equation

$$\frac{\partial \rho'}{\partial t} + \rho_0 \nabla \cdot \mathbf{u'} + \mathbf{u}_0 \cdot \nabla \rho' = 0. \tag{2.39}$$

The linearisation of the momentum variation equation 2.13 is given by following the same hypothesis and principles thus, applying the decomposition 2.31, we have that

$$\frac{\partial}{\partial t}[(\rho_0 + \rho')(\mathbf{u}_0 + \mathbf{u'})] + \nabla \cdot [(\rho_0 + \rho')(\mathbf{u}_0 + \mathbf{u'}) \otimes (\mathbf{u}_0 + \mathbf{u'})] = -\nabla(p_0 + p'). \tag{2.40}$$

Expanding and neglecting the second, or higher, order terms, we have that

$$\rho_0 \frac{\partial \mathbf{u'}}{\partial t} + \rho_0 \mathbf{u}_0 \cdot \nabla \mathbf{u}_0 + \rho_0 \mathbf{u}_0 \cdot \nabla \mathbf{u'} + \rho' \mathbf{u}_0 \cdot \nabla \mathbf{u}_0 + \rho_0 \mathbf{u'} \cdot \nabla \mathbf{u}_0 + \nabla p_0 + \nabla p^{'} = 0. \tag{2.41}$$

Once more, applying the decomposition to a steady flow without fluctuations, Newton's second law takes the following form

$$\rho_0 \mathbf{u}_0 \cdot \nabla \mathbf{u}_0 = -\nabla p_0. \tag{2.42}$$

Replacing the equation 2.42 into the equation 2.41 and assuming that the mean terms vary neither with time nor with space, we have that

$$\rho_0 \frac{\partial \mathbf{u'}}{\partial t} + \rho_0 \mathbf{u}_0 \nabla \cdot \mathbf{u'} = -\nabla p^{'}. \tag{2.43}$$

Hence, one arrives at the linearized governing equations given by the relations 2.39 and 2.43.

2.2 Wave Equation

To obtain the wave equation, the governing equations linearised in the previous section are used, firstly, taking the time derivative of the continuity equation 2.39 we arrive at

$$\frac{\partial^2 \rho'}{\partial t^2} + \rho_0 \frac{\partial}{\partial t}(\nabla \cdot \mathbf{u'}) + u_0 \frac{\partial}{\partial t}(\nabla \rho') = 0. \tag{2.44}$$

Now, taking the divergence of the equation of momentum variation 2.43 it is obtained that

$$\rho_0 \frac{\partial}{\partial t}(\nabla \cdot \mathbf{u'}) + \rho_0 \mathbf{u}_0 \cdot \nabla^2 \mathbf{u'} + \nabla^2 p' = 0. \tag{2.45}$$

Subtracting the equation 2.45 from the equation 2.44, it turns out that

$$\frac{\partial^2 \rho'}{\partial t^2} + \mathbf{u}_0 \frac{\partial}{\partial t}(\nabla \rho') \underline{-\rho_0 \mathbf{u}_0 \nabla^2 \mathbf{u'}} - \nabla^2 p' = 0. \tag{2.46}$$

The Laplacian of the velocity field can be replaced by

$$\nabla^2 \mathbf{u'} = \nabla(\nabla \cdot \mathbf{u'}) - \nabla \times (\nabla \times \mathbf{u'}). \tag{2.47}$$

Such a substitution can be proved by expanding the left-handed side of the following vector identity

$$\nabla \times (\nabla \times \mathbf{f}) = \nabla(\nabla \cdot \mathbf{f}) - \nabla \cdot (\nabla \mathbf{f}). \tag{2.48}$$

Expanding

$$\big(\hat{e}_i\frac{\partial}{\partial x_i}\big)\times\big(\big(\hat{e}_j\frac{\partial}{\partial x_j}\big)\times f_k\hat{e}_k\big)=$$

$$\frac{\partial^2 f_k}{\partial x_j\partial x_i}\hat{e}_m\delta_{jm}\delta_{ki}-\frac{\partial^2 f_k}{\partial x_j\partial x_i}\hat{e}_m\delta_{ji}\delta_{km}=\frac{\partial^2 f_i}{\partial x_j\partial x_i}\hat{e}_j-\frac{\partial^2 f_k}{\partial x_i\partial x_i}\hat{e}_k$$

$$\therefore \nabla\times(\nabla\times\mathbf{f})=\nabla(\nabla\cdot\mathbf{f})-\nabla\cdot(\nabla\mathbf{f}). \tag{2.49}$$

Therefore, by evaluating the terms of the equation 2.47, it is possible to conclude that the rotational term is null since the rotational o of the acoustic field velocity fluctuation is also null. Hence, the underlined term of the equation 2.46 takes the following form

$$-\rho_0\mathbf{u}_0\nabla^2\mathbf{u'}=\rho_0\mathbf{u}_0\nabla(\nabla\cdot\mathbf{u'}). \tag{2.50}$$

From the continuity equation, we have that

$$\nabla\cdot\mathbf{u'}=\frac{-1}{\rho_0}\big(\frac{\partial\rho'}{\partial t}+\mathbf{u}_0\nabla\rho'\big). \tag{2.51}$$

Substituting 2.50 and the equation 2.51 in the equation 2.46 and rearranging the terms, we have that

$$\frac{\partial^2\rho'}{\partial t^2}+2\mathbf{u}_0\frac{\partial}{\partial t}(\nabla\rho')+\mathbf{u}_0\cdot\nabla(\mathbf{u}_0\cdot\nabla\rho')-\nabla^2p'=0. \tag{2.52}$$

Now, applying the following vector relation

$$\nabla(\mathbf{f}\cdot\mathbf{g})=(\mathbf{f}\cdot\nabla)\mathbf{g}+(\mathbf{g}\cdot\nabla)\mathbf{f}+\mathbf{f}\times(\nabla\times\mathbf{g}). \tag{2.53}$$

And again, assuming the flow is irrotational and knowing that the curl of a gradient is always zero. One can combine the vector identity and the equation2.52 and considering again that the mean flow terms do not vary with space, we arrive at

$$\frac{\partial^2\rho'}{\partial t^2}+2\mathbf{u}_0\cdot\frac{\partial}{\partial t}(\nabla\rho')+\mathbf{u}_0\cdot((\mathbf{u}_0\cdot\nabla)\nabla\rho')-\nabla^2(p')=0. \tag{2.54}$$

The equation 2.30 preconises that the entropy of the particle remains constant, which is a consequence of neglecting the heat transfer in the flow of a frictionless gas. Heat transfer and momentum transfer are phenomena governed by the same molecular collision process, so one of the most used equations of state for this case is [46]:

$$c_0=\sqrt{\big(\frac{\partial p}{\partial\rho}\big)_s}. \tag{2.55}$$

Commonly for the case of wave propagation, 2.55is used in the following format

$$p'=c_0\rho'. \tag{2.56}$$

Combining the equation 2.54 with the relation given by the equation 2.56 , the general form of the wave equation with mean flow over time and space is arrived at

$$\frac{1}{{c_0}^2}\frac{\partial^2p'}{\partial t^2}+\frac{2\mathbf{u}_0}{{c_0}^2}\cdot\frac{\partial}{\partial t}(\nabla p')+\frac{\mathbf{u}_0}{{c_0}^2}(\mathbf{u}_0\cdot\nabla)\nabla p'-\nabla^2p'=0. \tag{2.57}$$

2.3 Solution of the Wave Equation

The case considered consists of an approximate cylindrical geometry of a turbofan where the presence of the rotor hub is also considered, as illustrated in the figure. 2.2. Thus, the coordinate system that best represents such a configuration is the cylindrical coordinates system. The flow is defined as uniform in the direction x (axial). The rotor-stator set is considered as a point source in the direction, and the origin of the system is defined at the position where such set is located.

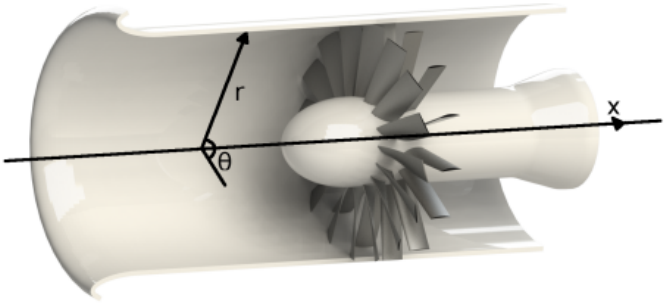

Figure 2.2: Turbofan scheme considered for the solution of the wave equation [8].

Defining $\mathbf{u}_0 = U\hat{\mathbf{i}}$ and reducing the first three terms of the equation 2.57, the final form of the wave equation to be solved for the case studied can be obtained.

$$\frac{1}{c_0^2}\left(\frac{\partial^2}{\partial t^2} + U\frac{\partial}{\partial x}\right)^2 p' - \nabla^2 p' = 0. \tag{2.58}$$

Defining the operator ∇^2 in cylindrical coordinates we have that

$$\nabla^2 = \frac{\partial^2}{\partial r^2} + \frac{1}{r}\frac{\partial}{\partial r} + \frac{1}{r^2}\frac{\partial^2}{\partial \theta^2} + \frac{\partial^2}{\partial x^2}. \tag{2.59}$$

Therefore, the wave equation in cylindrical coordinates is given by

$$\frac{1}{c_0^2}\left(\frac{\partial}{\partial t} + U\frac{\partial}{\partial x}\right)^2 p' - \left(\frac{\partial^2}{\partial r^2} + \frac{1}{r}\frac{\partial}{\partial r} + \frac{1}{r^2}\frac{\partial^2}{\partial \theta^2} + \frac{\partial^2}{\partial x^2}\right)p' = 0. \tag{2.60}$$

The Mach number in the axial direction is defined as

$$M_0 = \frac{U}{c_0}. \tag{2.61}$$

Then, expanding the equation 2.60 and substituting the Mach number relation given by 2.61, it turns out that

$$\frac{1}{c_0^2}\frac{\partial^2 p'}{\partial t^2} + \frac{2M_0}{c_0}\frac{\partial}{\partial t}\frac{\partial p'}{\partial x} + M_0^2\frac{\partial^2 p'}{\partial x^2} = \frac{\partial^2 p'}{\partial r^2} + \frac{1}{r}\frac{\partial p'}{\partial r} + \frac{1}{r^2}\frac{\partial^2 p'}{\partial \theta^2} - \frac{\partial^2 x}{\partial x^2}. \tag{2.62}$$

The equation 2.62 it is a partial differential equation with four variables and its solution will be obtained by the method of separation of variables. Therefore, the solution will have the following format

$$p'(x,r,\theta,t) = X(x)R(r)\Theta(\theta)T(t). \tag{2.63}$$

So, the equation takes the following form

$$\frac{1}{c_0^2}(XR\Theta)T'' + \frac{2M_0}{c_0}(R\Theta)X'T' + M_0^2(R\Theta T)X'' = (X\Theta T)R'' + \frac{1}{r}(X\Theta T)R' - \frac{1}{r^2}(XRT)\Theta'' + (RT\Theta)X'. \tag{2.64}$$

Dividing the equation 2.64 by $XR\Theta T$ and rearranging the terms, it follows that

$$\frac{1}{c_0^2}\frac{T''}{T} + \frac{2M_0}{c_0}\frac{X'T'}{XT} + (M_0^2 - 1)\frac{X''}{X} = \frac{R''}{R} + \frac{1}{r}\frac{R'}{R} + \frac{1}{r^2}\frac{\Theta''}{\Theta}. \tag{2.65}$$

In order to obtain the solution for the separation of variables, first, the mean flow is considered to be zero; later, the effects of its introduction in the solution found will be evaluated. As we first consider $M_0 = 0$, the equation to be solved has the format expressed by

$$\frac{1}{c_0^2}\frac{T''}{T} - \frac{X''}{X} = \frac{R''}{R} + \frac{1}{r}\frac{R'}{R} + \frac{1}{r^2}\frac{\Theta''}{\Theta}. \tag{2.66}$$

Taking this consideration into account, we arrive at four linear differential equations. The solution of three of these is well known, and for the last one, although complex, the solution can also be obtained. Considering

$$\frac{T''}{T} = -K_t^2, \tag{2.67}$$

$$\frac{X''}{X} = -K_x^2, \tag{2.68}$$

$$\frac{\Theta''}{\Theta} = -K_\theta^2, \tag{2.69}$$

$$\frac{R''}{R} + \frac{1}{r}\frac{R'}{R} + \frac{1}{r^2}\frac{\Theta}{\Theta} = -K_r^2, \tag{2.70}$$

for each of the equations the term K^2 corresponds to the wave number, which is also the separation constant. Solving first the equation that depends on θ, that is, the equation 2.69, it is a second order differential equation with constant coefficients, i.e.

$$\Theta'' + K_\theta^2\Theta = 0. \tag{2.71}$$

The problem of wave propagation in a turbofan duct is a cyclic problem. Thus, despite the existence of other solutions such as decay or exponential amplification, the solution of interest to the problem has an oscillatory nature, advocating a wave signal travelling in the direction of the analysed variable. The decays or amplifications arise naturally from the oscillatory solutions that govern the propagation along the duct. In view of this fact, one of the possible solutions to the equation 2.71 is $\Theta = e^{g\theta}$ so, one has that:

$$\Theta = e^{g\theta} \therefore$$
$$\Theta'' = g^2 e^{g\theta} \tag{2.72}$$

Substituting the relations of 2.72 in the equation 2.71, we have that:

$$g^2 e^{g\theta} + K_\theta^2 e^{g\theta} = 0 \therefore$$
$$e^{g\theta}(g^2 + K_\theta^2) = 0 \tag{2.73}$$

So for the solution of the equation 2.73, the term in parentheses is zero since the other term of the multiplication is exponential, which intrinsically is always different from zero. Thus, one obtains

$$g^2 + K_\theta^2 = 0 \therefore g = \pm iK_\theta. \tag{2.74}$$

On the principle of superposition, the linear combination of the solutions obtained in the equation is also a solution for 2.69, that is

$$\Theta = Ae^{iK_\theta\theta} + Be^{-iK_\theta\theta}. \tag{2.75}$$

The constants A and B can be found from the boundary conditions in the problem. Boundary conditions and source characterization allow finding relationships for the wavenumber of the coordinate θ and for the coordinate t. The continuity between the angles $\theta = 0$ and $\theta = 2\pi$, since they physically represent the same point, allows obtaining a relationship for the wave number of the angular coordinate

$$\Theta(0) = \Theta(2\pi). \tag{2.76}$$

Substituting into the solution presented in the equation 2.75 we have that

$$Ae^{iK_\theta(2\pi)} + Be^{-iK_\theta(2\pi)} = Ae^{iK_\theta(0)} + Be^{-iK_\theta(0)}. \tag{2.77}$$

So, applying Euler's formula, we get that

$$Acos(K_\theta 0) + Bcos(K_\theta 0) + Aisen(K_\theta 0) - Bisen(K_\theta 0) =$$
$$Acos(K_\theta 2\pi) + Bcos(K_\theta 2\pi) + Aisen(K_\theta 2\pi) - Bisen(K_\theta 2\pi). \tag{2.78}$$

The equality of the equation 2.78 is satisfied for all integer values of K_θ, so only integer-period waves are allowed in the solutions. This fact builds the first modal characteristic of the noise propagated in the duct. Thus, m is defined as the circumferential mode where m is a number belonging to positive or negative integers. So the general solution to the equation 2.69 is given by

$$\Theta(\theta) = \Theta_1 e^{im\theta} + \Theta_2 e^{-im\theta}. \tag{2.79}$$

Using the same principles aforesaid to the solution of the equation 2.69, one can obtain, considering the correct boundary conditions, the solution to the equations 2.67 and 2.68. The solution in the time variable is given by

$$T(t) = T_1 e^{i\omega t} + T_2 e^{-i\omega t} \tag{2.80}$$

Where ω is the angular frequency of the time oscillation of the noise generated by the rotor blades. For the axial coordinate the solution will be

$$X(x) = X_1 e^{iK_x x} + X_2 e^{-iK_x x} \tag{2.81}$$

The solution of the equation 2.70 is less trivial than the others, firstly, it is observed that it is directly related to the circumferential wavemodes, therefore, replacing the equation 2.69 in 2.70, the equation for the radial coordinate of the problems assumes the following format

$$\frac{R''}{R} + \frac{1}{r}\frac{R'}{R} + \left(K_r^2 - \frac{m^2}{r^2}\right) = 0, \tag{2.82}$$

which is, according to [47], the characteristic equation with the enginevalues K_r that can be obtained from the boundary conditions on the walls of the duct, [47] makes use of the substitution $x = K_r$ and $R(r) = y(\frac{x}{K_r})$ in order to suppress the eigenvalues of the equation. Thus one arrives at:

$$\frac{d^2y}{d(\frac{x}{K_r})^2} + \frac{1}{(\frac{x}{K_r})}\frac{dy}{d(\frac{x}{k_r})} + \left(K_r^2 - \frac{m^2}{(\frac{x}{k_r})}\right) = 0 \tag{2.83}$$

. Obtaining then the Bessel equation of order m

$$\frac{d^2y}{dx^2} + \frac{1}{x}\frac{dy}{dx} + (1 - \frac{m^2}{x^2})y = 0. \tag{2.84}$$

The equation 2.84 is a differential equation of variable coefficients that has a singular point so, its solution can be obtained through the Frobenius method because it is a long development until the recurrence relations are found, such a solution will be explained in the appendix of this work. The general solution of the equation 2.84 is given by:

$$R(r) = R_1 J_m(K_r r) + R_2 N_m(K_r r) \tag{2.85}$$

Such a solution is composed of the linear combination of Bessel and Neumann functions of order m. The order m of the functions that compose the solution is the same integer referring to the circumferential mode.

The boundary conditions to be applied to the equation 2.85 are related to the characteristics of the tube walls in the interaction with the acoustic wave. The most general case considered is a duct with the rotor hub present, thus forming a tube with an annular section as shown in the figure 2.3. In this way, the most usual boundary condition is considered, which is the rigid wall condition both in the duct nacelle and in the rotor hub wall, mathematically such condition preconizes that:

$$\frac{dp'}{dr}|_{r=R_i} = \frac{dp'}{dr}|_{r=R_0} = 0 \tag{2.86}$$

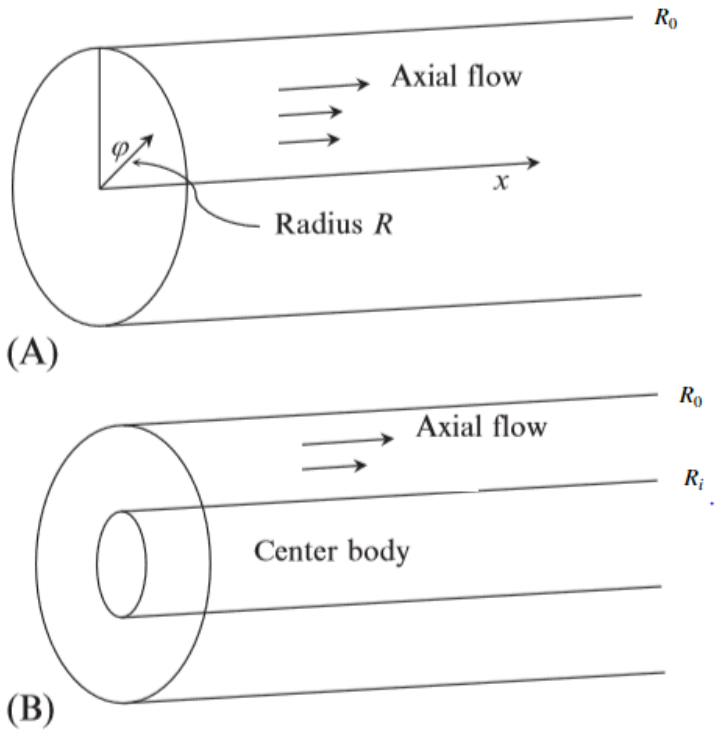

Figure 2.3: Ducts without and with the central body representing the absence or not of the rotor hub [9].

That is, the derivative of the pressure fluctuation on the walls is zero. The notation used in the boundary conditions considers the position of the nacelle and the rotor hub, which are respectively R_0 and R_i

For the case of a duct disregarding the presence of the rotor hub, only the part of the solution referring to $J_m(K_r r)$ is admissible since the Neumann function, $N_m(K_r r)$, is not finite in $r = 0$ so to solve this case we make $R_2 = 0$.

Defining then σ_{mn} as

$$\sigma_{mn} = K_r R_0, \tag{2.87}$$

then, σ_{mn} is the relationship between the eigenvalue K_r and the relative position where the boundary conditions are applied. The ratio between the innermost and outermost radius of the considered geometry is also defined as

$$\sigma = \frac{R_i}{R_0}, \tag{2.88}$$

where $\sigma = 1$ in the nacelle of the duct. Substituting the solution of the equation 2.85 and the relations of the equations 2.87 and 2.88 in the boundary conditions explained in 2.86, we arrive at

$$\begin{cases} R_1 J'_m(\sigma_{mn}\sigma) + R_2 N'_m(\sigma_{mn}\sigma) = 0 \\ R_1 J'_m(\sigma_{mn}) + R_2 N'_m(\sigma_{mn}) = 0 \end{cases} . \tag{2.89}$$

Isolating R_1 in the first equation of the linear system and substituting in the second, we arrive at

$$\frac{N'_m(\sigma_{mn}\sigma)}{J'_m(\sigma_{mn}\sigma)} - \frac{N'_m(\sigma_{mn})}{J'_m\sigma_{mn}} = 0. \tag{2.90}$$

Note that the roots of the equation 2.90 cannot be obtained analytically. Thus, the values of σ_{mn} that satisfy the relationship must be obtained numerically. Due to the oscillatory behaviour of the Bessel (J_m) and Neumann (N_m) functions, for each circumferential mode m there will be more than one root. Then, define the radial modes n that will be the roots of the equation 2.85 obtained numerically. Using the linear system of the equation 2.89 to relate R_1 and R_2, we arrive at the following form of the equation 2.85

$$R(r) = R_1[(J_m(K_r r) - \frac{J'_m(K_r R_0)}{N'_m(K_r R_0)} N_m(K_r r))] \tag{2.91}$$

	$R_i/R_o = 0.0$				$R_i/R_o = 0.5$			
$m\backslash n$	1	2	3	4	1	2	3	4
1	1.84118	5.331440	8.536320	11.70600	1.354670	6.564940	12.70642	18.94266
2	3.05424	6.706130	9.969470	13.17037	2.681200	7.062580	12.94941	19.10316
3	4.20119	8.015240	11.34592	14.58585	3.957750	7.840110	13.34760	19.36843
4	5.317550	9.282400	12.68191	15.96411	5.175230	8.836440	13.89228	19.73536
5	6.415620	10.51986	13.98719	17.31284	6.338890	9.985860	14.57363	20.20002
6	7.501270	11.73494	15.26818	18.63744	7.462160	11.22699	15.38192	20.75803
7	8.577840	12.93239	16.52937	19.94185	8.558630	12.50947	16.30771	21.40492
8	9.647420	14.11552	17.77401	21.22906	9.638210	13.79645	17.34065	22.13653
9	10.71143	15.28674	19.00459	22.50140	10.70710	15.06463	18.46709	22.94926
10	11.77088	16.44785	20.22303	23.76072	11.76886	16.30316	19.66825	23.84022
11	12.82649	17.60027	21.43085	25.00852	12.82556	17.51086	20.92081	24.80708
12	13.87884	18.74509	22.62930	26.24605	13.87842	18.69206	22.20008	25.84735
13	14.92837	19.88322	23.81939	27.47434	14.92818	19.85273	23.48394	26.95706
14	15.97544	21.01540	25.00197	28.69427	15.97535	20.99829	24.75601	28.12910

Figure 2.4: Values of σ_{mn} for a circular and annular duct [8]

Thus, substituting all the solutions found in the equation 2.63 we have:

$$\begin{aligned} p'(x,r,\theta,t) = (X_1 e^{iK_x x} + X_2 e^{-iK_x x})(\Theta_1 e^{im\theta} + \Theta_2 e^{-im\theta})(T_1 e^{i\omega t} + T_2 e^{-i\omega t}) \\ (R_1\left[J_m(K_r r) - \frac{J'_m(K_r R_0)}{N'_m(K_r R_0)} N_m(K_r r)\right]) \end{aligned} \tag{2.92}$$

Or yet,

$$p'(x,r,\theta,t) = X\Theta T e^{i(-\omega t + K_x x + m\theta)} R_1\left[J_m(K_r r) - \frac{J'_m(K_r R_0)}{N'_m(K_r R_0)} N_m(K_r r)\right] \tag{2.93}$$

We still have to find a relationship for the K_x wavenumber. For the no-flow case, one can relate the wavenumber K_x with the wavenumbers K_t and K_r through the relationship given by 2.66 given that:

$$\begin{aligned} \frac{1}{c_0^2}\frac{T''}{t} = \frac{-K_x^2}{c_0^2} = -\frac{-\omega}{c_0^2} \\ \frac{X''}{X} = -K_x^2 \\ \frac{R''}{R}\frac{1}{r}\frac{R'}{R} + \frac{1}{r^2}\frac{\Theta''}{\Theta} = -K_r^2 \end{aligned} \tag{2.94}$$

Therefore,substituting the relations of 2.94 in the equation 2.66, we have:

$$-K_t^2 + K_x^2 = -K_r^2 \therefore K_x^2 = -K_r^2 + K_t^2 \tag{2.95}$$

From this relation it is possible to define the an expression for the axial wavenumber

$$K_x = \sqrt{K_t^2 - K_r^2} \tag{2.96}$$

Considering now the presence of a uniform flow in the axial direction, and using the same idea of substituting the results obtained in the separation of variables, the remaining terms of the equation are evaluated 2.65, which are

$$\underbrace{\frac{2M_0}{c_0}\frac{X'T'}{XT}}_{1} + \underbrace{(M_0^2 - 1)\frac{X''}{X}}_{2} \tag{2.97}$$

Expanding term 2, we have that

$$(M_0 - 1)\frac{X''}{X} = (M_0^2 - 1)(-K_x^2) = (1 - M_0^2)K_x^2. \tag{2.98}$$

Analysing the dependent terms of the variable x, of term 1 of the equation 2.97 one has that:

$$\begin{aligned} X &= X_1 e^{iK_x x} + X_2 e^{-iK_x x} \\ X' &= iK_x(X_1 e^{iK_x x} + X_2 e^{iK_x x}) \\ \therefore \frac{X'}{X} &= iK_x \end{aligned} \tag{2.99}$$

Evaluating the dependent terms of t of term 1 of the equation 2.97

$$\begin{aligned} T &= T_1 e^{i\omega t} + T_2 e^{-i\omega t} \\ T' &= -i\omega(T_1 e^{i\omega t} + T_2 e^{-i\omega t}) \\ \therefore \frac{T'}{T} &= -i\omega \end{aligned} \tag{2.100}$$

Therefore, the equation 2.97 can be written as

$$\frac{2M_0}{c_0}(-i\omega i K_x) = \frac{2M_0}{c_0}\omega K_x \tag{2.101}$$

Combining the solutions of each of the separate coordinates using the equation 2.65, we have the following relationship for the wave number K_x for the case with the presence of a uniform flow,

$$-\frac{\omega^2}{c_0^2} + \frac{2M_0}{\omega}K_x + (1 - M_0^2)K_x^2 = -K_r^2, \tag{2.102}$$

which can be further rewritten in the following form:

$$K_r^2 + K_x^2 = \frac{\omega}{c_0^2} - \frac{2M_0}{c_0}\omega K_x + M_0^2 K_x^2, \tag{2.103}$$

Note that the right hand side is a notable product of type $(a - b)^2$, that is

$$K_r^2 + K_x^2 = (\frac{\omega}{c_0} - M_0 K_x)^2 \tag{2.104}$$

Thus,this relationship can be rewritten as

$$\pm K_x = \frac{\omega/c_0}{1-M_0^2}\left[-M_0 \pm \sqrt{1-(1-M_0^2)\left(\frac{K_r c_0}{\omega}\right)^2}\right]. \tag{2.105}$$

The sign of the wave number K_x indicates the positive or negative direction of the wave in the axial direction.

Thus, the following solution is obtained from the product of the solutions of each of the considered coordinates:

$$p'(x,r,\theta,t) = \sum_{m=-\infty}^{\infty}\sum_{n=1}^{\infty} P_{m,n}\left[J_m\left(\sigma_{mn}\frac{r}{R_0}\right) - \frac{J'_m(\sigma_{mn})}{N'_m(\sigma_{mn})}N_m\left(\sigma_{mn}\frac{r}{R_0}\right)\right]e^{-i(\omega t + K_x x + m\theta)} \tag{2.106}$$

Where $P_{m,n}$ is the product of all the amplitudes of the solutions of each one of the evaluated coordinates, related to the circumferential and radial mode.

2.4 Rotor-Stator Interaction's Noise

In addition to the rotor and stator generating noise independently, a large interaction between both parts occurs, contributing to the generation of noise, with the rotor-stator interaction being one of the biggest sources of noise in turbofans.

The main result of the rotor-stator interaction is the production of radial and circumferential modes also known as Tayler and Sofrin modes that compose the tonal noise. The Tayler and Sofrin modes are directly related to the frequency of passage of the rotor blades and their harmonics, the interaction between the rotor and the stator will generate a set of modes that, given certain circumstances, will propagate in the positive and negative axial direction.

Modelling the pressure field generated by only one rotor and using the solution to the wave equation developed in the previous section, we arrive at the equation 2.106.

Analysing the generated modes, only the temporal, radial and angular parts of the particular solution are considered, where the frequency ω and the circumferential mode m are values obtained from the rotor-stator interaction and the frequency of the passage of rotor blades:

$$p'(x,r,\theta,t) = P'(x,r)P_{m,n}e^{i(-\omega t + m\theta)} \tag{2.107}$$

Where $P'(x,r)$ is composed by the oscillatoy functions in the axial and radial directions. Considering now the passage of the rotor blades through a given fixed point. Near this point the blades will produce a perturbation in the pressure field that will remain constant, in certain conditions, if the same point rotates together with the rotor blades. From the wave equation solution the value for the pressure fluctuation amplitude is not calculated as it depends of several complex factors as the blades geometry the characterisation of the flow around them. Taking this things in consideration the time term from the wave equation solution, may be characterised for a fixed point in space [8], i.e.

$$\omega = hB\Omega, \tag{2.108}$$

where h represents the harmonics of the passing frequency of the blades, B is the number of rotor blades and $\Omega = 2\pi f$ where f is the rotation in RPS of the rotor.

Considering that the temporal solution for the pressure field is given by the sum of all harmonics of the rotor rotation frequency, we have that

$$p'(x,r,\theta,t) = \sum_{h=1}^{\infty} P'(x,r) P_{m,n,h} e^{i(-hB\Omega t + m\theta + \Phi_{m,h})}, \tag{2.109}$$

where $\Phi_{m,h}$ is the phase related to the rotor position and its respective harmonic. In general, the wave equation has a solution for any value of m. It is now considered that at time t the relative position of the rotor to the stator is θ, and that in such a situation a pressure fluctuation due to the interaction of the rotor with the stator equivalent to the equation 2.109 is produced. Considering also that the distance between two stator blades is given by

$$\Delta\theta = \frac{2\pi}{V}, \tag{2.110}$$

where V is the number of stator vanes. The time required for the initially generated pressure state to repeat itself (when the next rotor blade occupies the position of the previous one) is given by

$$\Delta T = \frac{2\pi}{V\Omega}. \tag{2.111}$$

So the pressure field will be the same in time t at position θ and in time $t + \Delta T$ in position $\theta + \Delta\theta$, therefore:

$$\sum_{h=1}^{\infty} P'(x,r) P_{m,n,h} e^{i(-hB\Omega t + m\theta + \Phi_{m,h})} = \sum_{h=1}^{\infty} P'(x,r) P_{m,n,h} e^{i(-hB\Omega (t+\Delta t) + m(\theta+\Delta\theta) + \Phi_{m,h})} \tag{2.112}$$

Rearranging:

$$\sum_{h=1}^{\infty} P'(x,r) P_{m,n,h} e^{i(-hB\Omega t + m\theta + \Phi_{m,h})} = \sum_{h=1}^{\infty} P'(x,r) P_{m,n,h} e^{i(-hB\Omega t + m\theta + \Phi_{m,h})} e^{i(-hB\Omega\Delta t + m\Delta\theta)} \tag{2.113}$$

hence,

$$e^{i(-hB\Omega\Delta t + m\Delta\theta)} = 1 \tag{2.114}$$

Possible solutions for2.114 are:

$$e^{i} 2\pi k = 1 \tag{2.115}$$

where k is any integer value. Substituting the definitions of the equations 2.110 and 2.111 we have that:

$$\begin{aligned} i(-hB\Omega\Delta t + m\Delta\theta) &= i2\pi k \\ \therefore i(-hB\Omega\frac{2\pi}{V\Omega} + \frac{m2\pi}{V}) &= i2\pi k \end{aligned} \tag{2.116}$$

Therefore, the circumferential mode m can be given by:

$$m = hB + kV \tag{2.117}$$

The m modes obtained from the equation 2.117 are the possible values related to the cyclic conditions of Δt and $\Delta\theta$. These modes are known as Tayler and Sofrin rotor-stator interaction modes, which are the modes obtained by the interaction of the rotor blades with the stator vanes, associated with the fundamental frequency of passage of the blades and their harmonics. The relationship for the Tayler and Sofrin modes has special cases such as when there is no presence of stator vanes causing the modes to be only multiples of the number of blades with only one mode per harmonic. Or even the case where there are no rotor blades, which despite being mathematically possible is physically inconsistent since there is no stator movement so there is no frequency associated with only the stator vanes.

Substituting the relation 2.117 in the solution of the wave equation obtained in the previous section 2.106 arrives at

$$\sum_{h=1}^{\infty}\sum_{m=1}^{\infty}\sum_{k=-\infty}^{\infty} P_{m,n}\left[J_m\left(\frac{\sigma_{mn}r}{R_0}\right) - \frac{J'_m(\sigma_{mn})}{N'_m(\sigma_{mn})}N_m\left(\sigma_{mn}\frac{r}{R_0}\right)\right]e^{i(-hB\Omega t+K_x x+\theta(hB+kV))}, \tag{2.118}$$

which represents the general solution for the tonal noise generated by the interaction of the rotor with the stator where the acoustic waves propagate in both the positive and negative directions axially. The selection of which of the generated circumferential modes will propagate is given by the Tyler and Sofrin rule. The amplitude of the circumferential modes must be obtained experimentally or numerically as they depend on the aerodynamic properties of the rotor and stator.

2.5 Tonal Noise Propagation in Ducts

Using the solution for the wave equation considering the convective effects introduced by the presence of the flow together with the rule of selection of the circumferential modes of Tayler and Sofrin, it is possible to characterise the propagation of the acoustic wave along the duct. Using the propagation theory, the set of modes that actually make up the tonal noise is reduced since only the generated and propagated modes will radiate out of the duct. The turbofan can be modelled as a uniform circular duct with a constant axial flow and, at first, a rigid wall condition, having two different parts one where there is no rotor hub and the other where there is. Thus, two different configurations of ducts can be evaluated, one of a simple duct and the other of an annular duct formed by the walls of the nacelle and the rotor hub. The Equation 2.105 is the relation that will give the modal behaviour given the flow conditions considered.

Analysing the equation2.118, if all the arguments of the spatial and temporal variables and of the exponential terms are real, the modes of a particular solution will propagate without changes in their amplitudes. This is valid for the wavenumbers of the temporal, circumferential and radial terms, considering that the eigenvalues of the Bessel and Neumann functions are real values. The wave number that is associated with the axial direction and its respective exponential term can be a complex number.

From the equation 2.105, it is worth mentioning that the variation of the sign of the wave number K_x implies the direction of the wave propagation in the axial direction. K_x. The square

root of the equation for the axial wavenumber can take on either real or imaginary values. The real values indicate a purely oscillatory solution, however, when complex these values indicate a decay or amplification effect with oscillation on the wave propagation.

In order to maintain thermodynamic coherence, it is observed that only complex arguments related to wave decay are permissible. Thus, isolating the square root term of the equation 2.105, we have the following conditions for modal propagation

$$(1-M_0^2)\left(\frac{K_r c_0}{hB\Omega}\right)^2 = \begin{cases} < 1 \text{ cut-on}, \\ = 1 \text{ valor crítico}, \\ > 1 \text{ cut-off} \end{cases} . \tag{2.119}$$

It is observed that when the term of the equation 2.119 is less than one, the square root of the expression 2.105 will be a real number, so there will be no attenuation in the wave propagation in the equation 2.118, therefore such mode is defined as cut-on. For values equal to one, the mode will be considered a critical mode but still a cut-on mode. For values greater than unity, the square root will have an imaginary value, so an exponential decay term will appear in the equation 2.118, and the modes that cover this case will be cut-off.

According to the equation 2.105, the factors that influence the propagation of the modes are the speed of sound, the Mach number of the axial flow, the number of rotor blades, and the rotation frequency of the rotor shaft and radius of the duct. That is, thermodynamic, operational and engine design factors. The circumferential mode m must be obtained numerically for a given radial mode n and then compared with a critical value. Substituting the relation given by the equation 2.87 in the critical condition of the equation 2.119, the critical value of the circumferential mode can be isolated.

$$\sigma_{mn,c} = \frac{R_0 \Omega h B}{c_0 (1-M_0^2)^{1/2}} \tag{2.120}$$

When performing a kinematic analysis it is possible to obtain a better understanding of the cut-on or cut-off of the generated modes due to the iteration of the rotor with the stator. Thus, analysing the exponential arguments of the equation 2.118 such that they define the phase

$$-hB\Omega t + K_x x + \theta(hB + kV) = \phi \tag{2.121}$$

Analysing the phase velocity in the θ direction, a point is fixed in space (thus, $x = \text{cte}$) and the time derivative of the equation 2.121 is taken. We choose $\phi = 0$, which implies the maximum amplitude since $Re(e^{\phi}) = cos(\phi) = 1$, so we have that:

$$(hB + kV)\frac{d\theta}{dt} + \frac{d(K_x x)}{dt} + hB\Omega = 0 \tag{2.122}$$

As the analysis is done for a fixed point in space, one arrives at:

$$(hB + kV)\frac{d\theta}{dt} = hB\Omega \tag{2.123}$$

Multiplying both sides of the above expression by the radius of the tube, the phase velocity is defined as:

$$R_0 \frac{d\theta}{dt} = U_m = \frac{hB\Omega R_0}{hB + kV} \tag{2.124}$$

defining the circumferential speed of the rotor pair tip as:

$$U_{R_0} = \Omega R_0 \tag{2.125}$$

so, one has that:

$$\frac{U_m}{U_{R_0}} = \frac{hB}{hB + kV} \tag{2.126}$$

The equation 2.126 represents the ratio between the circumferential velocity of the m mode and the circumferential velocity of the rotor blade tips. One of the consequences of this expression is that interaction modes that have a lower value than modes generated by the rotor alone have a higher circumferential phase velocity that can be greater than the speed of sound itself. [8].

Combining the equation 2.126 with the equation 2.119 for the critical case, we have

$$U_{m,c} = (1 - M_0^2)^{1/2} \frac{\sigma_{mn}}{m} c_0, \tag{2.127}$$

which preconizes the minimum phase circumferential velocity that the m mode must have in order for it to propagate. Simplifying the equation 2.127 for the case without flow $M_0 = 0$, observing that the ratio σ_{mn}/m approaches 1 for high values of m, the critical circumferential phase velocity can be approximated by

$$U_{m,c} = c_0, \tag{2.128}$$

that is, for a circumferential mode to propagate, its phase velocity must be at least sonic. This fact also implies that for the modes generated only by the rotor, the rotor blade tip must move at least at sonic speed. In the case of the rotor-stator, as we can evaluate by the equation 2.126, the rotor blades do not need sonic phase velocity to generate propagating modes, since some of the generated modes may have sonic phase velocity to maintain their respective harmonic frequency.

Now analyzing the phase velocity for the axial mode K_x, the same process is carried out, but now a point $\theta = \text{cte}$ is evaluated, hence the equation 2.122 takes the following form

$$K_x \frac{dx}{dt} = hB\Omega. \tag{2.129}$$

through the relation of the equation 2.108, the equation 2.129 can be written as:

$$\frac{dx}{dt} = \frac{\omega}{K_x} \tag{2.130}$$

from the equation 2.105 it is known that the axial wavenumber K_x can be positive or negative, indicating the propagation direction. Thus, substituting the relation 2.105 in equation 2.130, we have that

$$U_x = \frac{c_0(1 - M_0^2)}{-M_0 \pm \sqrt{1 - (1 - M_0^2)(\frac{K_r c_0}{\omega})^2}}. \tag{2.131}$$

For the equation 2.131 considering the case of a plane wave, that is, $m = n = 0$, we have that:

$$U_{x,00}^{\pm} = \frac{c_0(1 - M_0^2)}{-M_0 \pm 1} \tag{2.132}$$

that is, it is observed that the propagation speeds in the positive and negative axial direction are different. Rewriting it for both cases, using the remarkable product $(a^2 - b^2) =)(a + b)(a - b)$, we have that:

$$U^{+}_{x,00} = \frac{c_0(1 - M_0)(1 + M_0)}{1 - M_0} = c_0(1 + M_0) = c_0 + U,$$
$$U^{-}_{x,00} = \frac{c_0(1 - M_0)(1 + M_0)}{1 + M_0} = c_0(1 - M_0) = c_0 - U. \tag{2.133}$$

Thus, it is observed that the wave propagating in the positive axial direction, that is, in the same direction as the flow, propagates with the sum of the sound velocity and the flow velocity. For waves that propagate in the negative axial direction, the propagation velocity is the difference between the values of sound and flow velocity.

Chapter 3

General Boundary Condition for a Softwall Case

In this chapter, the derivation of appropriate boundary conditions for the disturbances of the base flow at the surface of a flexible wall is reviewed and presented. It considers a problem in which the vibration of the body generates an acoustic field given a small movement with respect to its mean or surface, and the reciprocal, where a given acoustic field generates the movement of the flexible wall. [48]

For years there has been a discussion about the general boundary condition for an acoustic field in the presence of a base flow. Especially in the area of acoustics in ducts, the apparent differences presented in the boundary conditions were addressed, given the considerations of inviscid or viscous media. As a result of such a scenario, it gradually became accepted that, in a flow treated as inviscid, the proper kinematic condition in an impenetrable contour of the acoustic field is physically expressed by the continuity of displacement of the acoustic particle [48]. That is, on a surface whose deformations generate an acoustic field or an acoustic field generates deformations on it, the displacement of the fluid particle in the normal direction of the undeformed surface must be equal to the normal displacement of this surface.

3.1 Derivation of the Boundary Condition

Considering a surface $S(t)$ that moves with respect to a frame of reference, this surface is assumed to be in contact with a fluid whose velocity $\mathbf{u}(x,t)$. From the continuum theory, one of the conditions that must be satisfied at each point on the surface, assuming impenetrability, is given by

$$\mathbf{u} \cdot \boldsymbol{\nu} = \mathbf{V} \cdot \boldsymbol{\nu} \tag{3.1}$$

where $\mathbf{V}$ is the velocity of the surface $S(t)$ with respect to the reference frame, and $\boldsymbol{\nu}$ is the unit vector normal to the surface $S(t)$.

Since the surface S can be spatially defined by

$$f(x,t) = 0 \tag{3.2}$$

so the normal vector $\boldsymbol{\nu}$ can be expressed as

$$\boldsymbol{\nu} = \frac{\nabla f(x,t)}{|\nabla(f)|} \text{ for } f = 0 \tag{3.3}$$

The normal vector $\boldsymbol{\nu}$ has positive values pointing away from the surface, that is, pointing towards fluid, and negative values towards the inside of the surface. As a point $\mathbf{x}$ always belongs to the surface S for any instant of time, we can derive the equation 3.2 with respect to time, obtaining that

$$\frac{\partial f}{\partial t} = \frac{\partial f}{\partial \mathbf{x}}\frac{\partial x}{\partial t} + \frac{\partial f}{\partial t} = \mathbf{V}\frac{\partial f}{\partial \mathbf{x}} + \frac{\partial f}{\partial t} = \mathbf{V}\cdot\nabla f + \frac{\partial f}{\partial t} = 0 \tag{3.4}$$

substituting the equation 3.3 in the equation 3.4 we have that

$$\boldsymbol{V}\cdot\boldsymbol{\nu}|\nabla f| + \frac{\partial f}{\partial t} = 0 \therefore \boldsymbol{V}\cdot\boldsymbol{\nu} = -\frac{1}{|\nabla f|}\frac{\partial f}{\partial t} \tag{3.5}$$

substituting the equation 3.5 into the equation 3.1 and using the relatioship given by 3.3, one can rewrite the impenetrability condition as

$$\boldsymbol{\nu}\cdot\boldsymbol{u}|\nabla f| + \frac{\partial f}{\partial t} = \boldsymbol{u}\cdot\nabla f = 0 \therefore \boldsymbol{u}\cdot\nabla f = -\frac{\partial f}{\partial t} \tag{3.6}$$

It is assumed that the surface S either generates an acoustic field in the fluid by vibration or is acoustically deformed in response to an acoustic field coming from the fluid. Thus, it is convenient to choose a coordinate system for $\boldsymbol{V}$ and $\boldsymbol{u}$ in which the motion of S is a perturbation on a stationary surface S_0 and the corresponding perturbation of velocity is a small perturbation of the steady flow velocity $\boldsymbol{U}(x)$. Thus, the use of a curvilinear orthogonal coordinate system appears to be a more general alternative for the description of such a situation. Thus, we define a fixed system S_0 composed of the coordinates

$$\alpha(\boldsymbol{x}), \beta(\boldsymbol{x}), \gamma(\boldsymbol{x}) \tag{3.7}$$

so that $\alpha(\boldsymbol{x}) = 0$ in S_0 and

$$\nabla\alpha\cdot\nabla\gamma = \nabla\alpha\cdot\nabla\beta = \nabla\beta\cdot\nabla\gamma = 0 \tag{3.8}$$

hat is, α is the normal coordinate and the others are the tangent coordinates of the defined system. Thus, $S(t)$ can be described, as proposed by [48], as

$$\alpha = \epsilon g(\beta,\gamma,t) + O(\epsilon^2), \tag{3.9}$$

and the speed as

$$\boldsymbol{u} = \boldsymbol{U} + \epsilon\boldsymbol{u}(x,t) + O(\epsilon^2), \tag{3.10}$$

where ϵ is a dimensionless parameter that characterises the magnitude of acoustic disturbances.

Thus, in terms of the curvilinear coordinates, 3.2 assumes the following format

$$\alpha - \epsilon g(\beta,\gamma,t) + O(\epsilon^2) = f(x,t) = 0 \tag{3.11}$$

therefore, the equation 3.6 can be rewritten as

$$\boldsymbol{u}\cdot\nabla f+\frac{\partial f}{\partial t}=(\boldsymbol{U}+\epsilon\boldsymbol{u}+O(\epsilon^2))\cdot\nabla(\alpha-\epsilon g+O(\epsilon^2))+ \\ \frac{\partial}{\partial t}(\alpha-\epsilon g+O(\epsilon^2))\text{ para }\alpha=\epsilon g+O(\epsilon^2). \tag{3.12}$$

The equation 3.6is satisfied for a steady flow without acoustic disturbances, such a case can be expressed by the equation 3.12 making $\epsilon=0$ which leads to

$$\boldsymbol{U}\cdot\nabla\alpha=0, \tag{3.13}$$

thus the flow $\boldsymbol{U}$ must be tangent to the stationary surface and not deformed S_0.

3.1.1 Linearisation of the Boundary Condition

Considering now the case where $\epsilon << 1$ will be evaluated what form will be assumed for the equation 3.6.

If $\boldsymbol{U}$ and $\boldsymbol{u}$ are functions of α, β, γ and that in $\alpha=0$ can be considered sufficiently smooth it is possible to expand the equation 3.12 n powers of ϵ. First, by rewriting the equation 3.12

$$\underbrace{\boldsymbol{U}\cdot\nabla\alpha}_{1}+\underbrace{\boldsymbol{U}\cdot\nabla(-\epsilon g)}_{2}+\underbrace{\epsilon\boldsymbol{u}\cdot\nabla\alpha}_{3}+\underbrace{\epsilon\boldsymbol{u}\cdot\nabla(-\epsilon g)}_{4}+ \\ \frac{\partial\alpha}{\partial t}-\frac{\partial(-\epsilon g)}{\partial t}+O(\epsilon^2)=0\text{ para }\alpha=\epsilon g+O(\epsilon^2) \tag{3.14}$$

as ϵ is constant, term four of the equation 3.14 will be a second-order term in ϵ that will be joined to the other second-order terms represented by $O(\epsilon^2)$. The time derivative of α is equal to zero as seen earlier.

By expanding term 1, we have that

$$\boldsymbol{U}\cdot\nabla\alpha|_{\alpha=\epsilon g+O(\epsilon^2)}=\boldsymbol{U}\cdot\nabla\alpha|_{\alpha=0}+\alpha(\frac{\partial}{\partial\alpha}(\boldsymbol{U}\cdot\nabla\alpha))|_{\alpha=0}+O(\epsilon^2) \tag{3.15}$$

substituting the equation 3.9 in the equation 3.15 and agglutinating the second-order terms in $O(\epsilon^2)$ we arrive at

$$\boldsymbol{U}\cdot\nabla\alpha|_{\alpha=\epsilon g+O(\epsilon^2)}=\boldsymbol{U}\cdot\nabla\alpha|_{\alpha=0}+\epsilon g(\frac{\partial}{\partial\alpha}(\boldsymbol{U}\cdot\nabla\alpha))|_{\alpha=0}+O(\epsilon^2). \tag{3.16}$$

Doing the same process for term 3 of the 3.14 equation, we first have that

$$\epsilon\boldsymbol{u}\cdot\nabla\alpha|_{\alpha=\epsilon g+O(\epsilon^2)}=\epsilon\boldsymbol{u}\cdot\nabla\alpha|_{\alpha=0}+\epsilon g(\frac{\partial}{\partial\alpha}(\epsilon\boldsymbol{u}\cdot\nabla\alpha))|_{\alpha=0}+O(\epsilon^2) \tag{3.17}$$

the second term on the right side of the equation 3.17 is of second order in ϵ so that:

$$\epsilon\boldsymbol{u}\cdot\nabla\alpha|_{\alpha=\epsilon g+O(\epsilon^2)}=\epsilon\boldsymbol{u}\cdot\nabla\alpha|_{\alpha=0}+O(\epsilon^2). \tag{3.18}$$

Thus, using the equation 3.13 athe condition given by the equation 3.12 can be rewritten as

$$\epsilon\left[\frac{\partial}{\partial\alpha}(\boldsymbol{U}\cdot\nabla\alpha)\cdot g+\boldsymbol{u}\cdot\nabla\alpha-\boldsymbol{U}\cdot\nabla g-\frac{\partial g}{\partial t}\right]|_{\alpha=0}+O(\epsilon^2)=0 \tag{3.19}$$

considering $\epsilon << 1$ the linearization will be done by neglecting the second order terms in ϵ, thus

$$\left(\frac{\partial}{\partial\alpha}(\boldsymbol{U}\cdot\nabla\alpha)\cdot g+\boldsymbol{u}\cdot\nabla\alpha-\boldsymbol{U}\cdot\nabla g-\frac{\partial g}{\partial t}\right)=0 \text{ for } \alpha=0. \tag{3.20}$$

Therefore,

$$\boldsymbol{u}\cdot\nabla\alpha=(\frac{\partial}{\partial t}+\boldsymbol{U}\cdot\nabla)g-g\frac{\partial}{\partial\alpha}(\boldsymbol{U}\cdot\nabla\alpha) \text{ for } \alpha=0. \tag{3.21}$$

The equation 3.21 is the linearized boundary condition that governs an acoustic perturbation of velocity $\boldsymbol{u}$ on an impermeable surface. As indicated, such a condition must be applied to the mean position S_0 of the surface that moves as is usual in linearized acoustics.

3.2 Linearized Boundary Condition Manipulation and Analysis

The derivation of the boundary condition represented by the equation 3.21 in the curvilinear orthogonal coordinates α, β, γ makes it more convenient to manipulate it in an easier way for shapes better interpretation and application. For this, it is necessary to apply some relations from the theory of orthogonal curvilinear coordinates that will be explained in the appendix of this work.

The unit vectors of the base coordinate system α, β, γ will be denoted, respectively, as $\hat{a}$, $\hat{b}$, $\hat{c}$. And the scale factors like: h_α, h_β, h_{h_γ}. Using the relation

$$\nabla\alpha=|\nabla\alpha|\hat{a}=\frac{1}{h_\alpha}\hat{a} \tag{3.22}$$

one can rewrite the equation 3.21 as

$$\boldsymbol{u}\cdot\hat{a}=h_\alpha(\frac{\partial g}{\partial t}+\boldsymbol{U}\cdot\nabla g)-g(\hat{a}\cdot\frac{\partial\boldsymbol{U}}{\partial\alpha}+\boldsymbol{U}\cdot\frac{\partial\hat{a}}{\partial\alpha}) \text{ for } \alpha=0, \tag{3.23}$$

putting the scale factor h_α into the material derivative we get

$$\boldsymbol{u}\cdot\hat{a}=(\frac{\partial}{\partial t}+\boldsymbol{U}\cdot\nabla)(gh_\alpha)-g\left[\hat{a}\frac{\partial\boldsymbol{U}}{\partial\alpha}+\boldsymbol{U}\cdot(\frac{\partial\hat{a}}{\partial\alpha}+\nabla h_\alpha)\right] \text{ para } \alpha=0 \tag{3.24}$$

Now introducing the following relation

$$\frac{\partial\hat{a}}{\partial\alpha}=-\frac{1}{h_\beta}\frac{\partial h_\alpha}{\partial\beta}\hat{b}-\frac{1}{h_\gamma}\frac{\partial h_\alpha}{\partial\gamma}\hat{c} \tag{3.25}$$

and also

$$\nabla h_\alpha=\frac{1}{h_\alpha}\frac{\partial h_\alpha}{\partial\alpha}\hat{a}+\frac{1}{h_\beta}\frac{\partial h_\alpha}{\partial\beta}\hat{b}+\frac{1}{h_\gamma}\frac{\partial h_\alpha}{\partial\gamma}\hat{c} \tag{3.26}$$

one can rewrite the last two terms of the equation 3.24 sing the relations 3.22, 3.25 and 3.26 as

$$g\boldsymbol{U}\cdot(1/h_\alpha)\hat{a}=-g(\partial h_\alpha/\partial\alpha)\boldsymbol{U}\cdot\nabla\alpha \tag{3.27}$$

thus, analysing the last two terms of the equation 3.24 in the form of the equation 3.27 it is observed that taking into account the equation 3.13 in $\alpha=0$ the terms are null. Thus, the equation 3.24 takes the following format

$$\boldsymbol{u}\cdot\hat{a}=(\frac{\partial}{\partial t}+\boldsymbol{U}\cdot\nabla)(gh_\alpha)-g\hat{a}\cdot\frac{\partial\boldsymbol{U}}{\partial\alpha} \text{ for } \alpha=0 \tag{3.28}$$

It can be observed that

$$\frac{\partial \boldsymbol{U}}{\partial \alpha} = h_\alpha \hat{a} \cdot \nabla \boldsymbol{U} \tag{3.29}$$

and that on the surface $\alpha = 0$ the unit vector $\hat{a}$ is simply the vector normal to S_0 directed to the fluid. This vector can be denoted as $\hat{n}$, and so the boundary condition expressed in the equation3.28 can be rewritten as

$$\boldsymbol{u} \cdot \hat{n} = (\partial/\partial t + \boldsymbol{U} \cdot \nabla)(g/|\nabla \alpha|) - (g/|\nabla \alpha|)\hat{n} \cdot (\hat{n} \cdot \nabla \boldsymbol{U}) \text{ em } S_0 \tag{3.30}$$

The result of the equation 3.30 is a specified boundary condition with no specific reference to the curvilinear coordinate system. The average surface S_0 is given by $\alpha(x) = 0$ and g can be considered as a function of time and space. These functions, as well as the normal vector $\hat{n}$, are known as long as S_0 and its movement after the perturbation is specified. The condition given in the equation 3.30 can also be applied on either side of an interface between different acoustic media. In this case, the right side of the equation 3.30 would be evaluated on each side of the interface given by $\alpha = 0$ and the two expressions would be equated to ensure the continuity of velocity in the normal direction along the interface. In this circumstance, a condition that expresses the continuity of pressure along the interface is also needed. The use of the two conditions together would allow the elimination of the unknown function g from the problem. Equation 3.30 is one of the major results of Myers in 1980 [48].

By the form of the 3.30 condition it is also simpler to derive an appropriate boundary condition for an acoustically absorptive boundary in which the acoustic impedance in the normal Z direction is known for harmonic motion. Within this context, the derivation of this case depends on the determination of the function $g/|\nabla \alpha|$ that represents the acoustic deformation of the contour. Considering the expression

$$\frac{\bar{p} - p_0}{\boldsymbol{V} \cdot \boldsymbol{\nu}} \tag{3.31}$$

Where $\bar{p}$ is the total pressure in the fluid, p_0 the ambient pressure and $\boldsymbol{V} \cdot \boldsymbol{\nu}$ the normal surface velocity. Proposing the following format for the numerator of the equation 3.31

$$\bar{p} - p_0 = \epsilon p + O(\epsilon^2) \tag{3.32}$$

and for the numerator using the relation 3.5 nd the format proposed in 3.9 we have that

$$\boldsymbol{V} \cdot \boldsymbol{\nu} = -\frac{1}{|\nabla f|}\frac{\partial f}{\partial t} = -\frac{1}{|\nabla(\alpha - \epsilon g)|}\frac{\partial}{\partial t}(\alpha - \epsilon g)|_{\alpha=0} + O(\epsilon^2) \tag{3.33}$$

Thus, substituting the equations 3.32 and 3.33 into the equation 3.31 and expanding the terms we have that

$$-\frac{\epsilon p \nabla \alpha - \epsilon p \nabla(\epsilon g)}{\frac{\partial \alpha}{\partial t} - \frac{\partial \epsilon g}{\partial t}}|_{\alpha=0} + O(\epsilon^2) \tag{3.34}$$

the second term of the numerator of the equation 3.34 will give rise to a term of the order of ϵ^2 and will be merged into $O(\epsilon^2)$, the temporal derivative of α is null . As $\epsilon << 1$ the second order terms will be neglected again. Therefore, the expression 3.31can be written as

$$\frac{\bar{p} - p_0}{\boldsymbol{V} \cdot \boldsymbol{\nu}} = \frac{p|\nabla \alpha|}{\partial g/\partial t}|_{\alpha=0}. \tag{3.35}$$

The equation 3.31 is the definition of acoustic impedance, which is the ratio between the pressure and the velocity of the particle. For a harmonic time dependence of the sound pressure of p and g, these are assumed to be quantities proportional to the complex exponential

$$p \sim e^{-i\omega t} \sim g \therefore \frac{\partial g}{\partial t} = -i\omega g e^{-i\omega t} \text{ e } p = pe^{-i\omega t} \tag{3.36}$$

Thus, the equation refDefinição Imped 2 can be rewritten as

$$Z = \frac{p|\nabla\alpha|}{\partial g/\partial t}|_{\alpha=0} = \frac{|\nabla\alpha|pe^{-i\omega t}}{-i\omega g e^{-i\omega t}}|_{\alpha=0} \therefore Z = -\frac{1}{i\omega g}|\nabla\alpha|p|_{\alpha=0} \tag{3.37}$$

In this way, from the expression given by the equation 3.37 we arrive at that

$$g = -(1/i\omega Z)(|\nabla\alpha|p)|_{\alpha=0} \tag{3.38}$$

Then the boundary condition given by 3.30 takes the form of

$$\boldsymbol{u}\cdot\hat{n} = -(p/Z) - (1/i\omega)\boldsymbol{U}\cdot\nabla(p/Z) + (p/i\omega z)\hat{n}\cdot(\hat{n}\cdot\nabla\boldsymbol{U}) \text{ em } S_0 \tag{3.39}$$

As the velocity is the basic quantity in an Eulerian description of the fluid motion, it is emphasised that the boundary condition given by the equation 3.39 represents the linearised version of the continuity of velocity in S_0. Such condition is true for any base flow whether it is viscous and must satisfy the no-slip condition or inviscid and must satisfy the impenetrability condition.

Now analysing the boundary condition, it is observed that the first term of the equation 3.30, given the relation 3.5, is the first approximation for normal velocity,direction $\boldsymbol{\nu}$, from a point on the surface S. The other two terms that evolve the base flow velocity $\boldsymbol{U}$ arise from the linearisation process and expression of the boundary condition in terms of $\hat{n}$ and S_0. The terms involving $\boldsymbol{U}\cdot\nabla g$ arise because the instantaneous normal vector and the normal vector S_0 at an angle of magnitude on the order of ϵ. Thus, the flow velocity $\boldsymbol{U}$ has a component in the direction of the instantaneous normal vector ($\boldsymbol{\nu}$) which is on the order of ϵ which is added to the acoustic velocity of the particle forming the total disturbance in the direction normal to S

It is now of interest to consider the implications of the boundary condition in terms of particle displacement. From the relation $\alpha = \epsilon g$ that defines the surface S in the linearized approximation, we have that the quantity $\epsilon g/|\nabla\alpha||_{\alpha=0}$ is the main approximation for the displacement of a point in S_0 in the direction normal to S_0 ($\hat{n}$). This quantity can be denoted as ξ_b. It is now convenient to use the boundary condition in the form 3.28 where the quantities $\boldsymbol{U}$, $\boldsymbol{u}$ and g are functions of the curvilinear system α, β, γ, thus being able to write the relation of the particle's velocity with its displacement with

$$\boldsymbol{u} = \frac{\partial\boldsymbol{\xi}}{\partial t} + \boldsymbol{U}\cdot\nabla\boldsymbol{\xi} \therefore \boldsymbol{u}\cdot\hat{a} = \hat{a}\cdot\frac{D\boldsymbol{\xi}}{Dt} \tag{3.40}$$

from the definition of ξ_b and the relation 3.22 we have

$$\xi_b = \frac{g}{|\nabla\alpha|}|_{\alpha=0} \therefore g = |\nabla\alpha|\xi_b = \frac{1}{h_\alpha}\xi_b \tag{3.41}$$

using the equation 3.41 one can rewrite the equation 3.28 as

$$\hat{a}\cdot\frac{D\boldsymbol{\xi}}{Dt} = \frac{D\xi_b}{Dt} - (\frac{\xi_b}{h_\alpha})\hat{a}\cdot\frac{\partial\boldsymbol{U}}{\partial\alpha} \text{ para } \alpha = 0 \tag{3.42}$$

putting the unit vector $\hat{a}$ into the material derivative, we can rewrite the equation 3.42 as

$$\frac{D(\boldsymbol{\xi}\cdot\hat{a})}{Dt} - \boldsymbol{\xi}\cdot(\boldsymbol{U}\cdot\nabla\hat{a}) = \frac{D\xi_b}{Dt} - \frac{\xi_b}{h_\alpha}\hat{a}\cdot\frac{\partial \boldsymbol{U}}{\partial\alpha} \text{ para } \alpha = 0 \tag{3.43}$$

Using the derivatives for the normal vectors $\hat{a}$, $\hat{b}$, $\hat{c}$ and the relation 3.13 we arrive that

$$\frac{D(\boldsymbol{\xi}\cdot\hat{a})}{Dt} - \boldsymbol{\xi}\left[\frac{\boldsymbol{U}_\beta}{h_\alpha h_\beta}\frac{\partial h_\beta}{\partial\alpha}\hat{b} + \frac{\boldsymbol{U}_\gamma}{h_\alpha h_\gamma}\frac{\partial h_\gamma}{\partial\alpha}\hat{c}\right] = \frac{D\xi_b}{Dt} - \frac{\xi_b}{h_\alpha}\left[\frac{\partial \boldsymbol{U}_\alpha}{\partial\alpha} + \frac{\boldsymbol{U}_\beta}{h_\beta}\frac{\partial h_\alpha}{\partial\beta} + \frac{\boldsymbol{U}_\gamma}{h_\gamma}\frac{\partial h_\alpha}{\partial\gamma}\right] \tag{3.44}$$

where $\boldsymbol{U}_\alpha$, $\boldsymbol{U}_\beta$, $\boldsymbol{U}_\gamma$ are the components of $\boldsymbol{U}$ in the α, β, γ directions of the curvilinear coordinates.

Considering that the base flow is inviscid, it is observed that the second term of both sides of the equation 3.44 is not null in general. So, in such cases the equation 3.44 shows that the boundary condition given by 3.39 is not equivalent to the displacement of the acoustic particle in the form

$$\boldsymbol{\xi}\cdot\hat{n} = \xi_b \text{ em } S_0 \tag{3.45}$$

On the other hand, for a viscous fluid, and a flow that satisfies the no-slip condition $\boldsymbol{U}_\alpha$, $\boldsymbol{U}_\beta$, $\boldsymbol{U}_\gamma$ are all null in $\alpha = 0$. Using the steady-state continuity equation

$$\rho\nabla\cdot\boldsymbol{U} + \boldsymbol{U}\cdot\nabla\rho = 0 \tag{3.46}$$

logo

$$\nabla\cdot\boldsymbol{U} = 0 \tag{3.47}$$

The tangential derivatives of $\boldsymbol{U}$ are also zero at $\alpha = 0$ since the velocity on the contour is zero for any point on it. Thus, from the continuity equation and the relations for curvilinear coordinates, explained in the appendix of this work, we have

$$\frac{\partial}{\partial\alpha}(h_\beta h_\gamma \boldsymbol{U}_\gamma) =\therefore \frac{\boldsymbol{U}_\alpha}{\partial\alpha}|_{\alpha=0} = 0 \tag{3.48}$$

Therefore, the equation 3.30 assumes the following format

$$\boldsymbol{u}\cdot\hat{n} = (1/\nabla\alpha)\partial g/\partial t \text{ em } S_0 \tag{3.49}$$

Thus, for a viscous base flow, the continuity of the particle displacement is recovered in its traditional format. Using the relation 3.35 we get that

$$\boldsymbol{u}\cdot\hat{n} = -\frac{p}{Z} \text{ em } S_0 \tag{3.50}$$

In the present work the flow considered is inviscid in this way, the appropriate shape of the boundary condition to be used will be the case expressed by the equation 3.39.

3.3 Wave Equation Solution for a Duct with Finite Acoustic Impedance in the Wall

In a duct whose walls do not have liners, the contours are considered rigid. In chapter three, the solution to the wave equation was developed in a case of a duct with rigid walls, that is, with

infinite acoustic impedance. The consideration of the presence of liners on the walls of the duct implies the existence of a finite impedance in these contours, such a scenario directly impacts the shape of the solution of the radial component derived in chapter 3.

The intention of this chapter is the derivation of the radial part, considering now the absorptive effects of the liner present in the contour given its impedance and also evaluating the effects of the inviscid and uniform flow in such a scenario.

3.3.1 Boundary Condition for a Locally Reactive Liner in a Duct unde Uniform Mean Flow

Considering a duct with a liner, it is assumed that the liner is locally reactive in the sense that the pressure at a point on its surface is related only to the normal velocity of the acoustic field at that point. Reintroducing the definition of acoustic impedance in terms of pressure p' and normal velocity $\boldsymbol{u} \cdot \hat{n}$ we have

$$Z(x, \omega) = \frac{p}{\boldsymbol{u} \cdot \hat{n}} = R + iX \tag{3.51}$$

where the real part R is called resistance and the imaginary part X reactance.

Evaluating the boundary condition derived in Chapter 5, we have that

$$\boldsymbol{u} \cdot \hat{n} = -(p/Z) - (1/i\omega)\boldsymbol{U} \cdot \nabla(p/Z) + \underline{(p/i\omega z)\hat{n} \cdot (\hat{n} \cdot \nabla \boldsymbol{U})} \text{ em } S_0 \tag{3.52}$$

as $\boldsymbol{U}$ is the velocity of a uniform flow in the axial direction x the underlined term is equal to zero and so the boundary condition given in 3.52 takes the following form

$$\boldsymbol{u} \cdot \hat{n} = -\frac{p'}{Z} - \frac{1}{i\omega} U \frac{\partial}{\partial x}\left(\frac{p'}{Z}\right). \tag{3.53}$$

Given the format for pressure p' described in chapter 3, it is observed that it can be rewritten as

$$p' = P \cdot Re^{-i(\omega t + K_x x + m\theta)} \tag{3.54}$$

so the first derivative of the equation 3.54 with respect to x is given by

$$\frac{\partial p'}{\partial x} = -iK_x P \cdot Re^{-i(\omega t + K_x x + m\theta)} = -iK_x p' \tag{3.55}$$

therefore, the boundary condition for a duct with liners takes the form

$$\boldsymbol{u} \cdot \hat{n} = -\frac{p'}{Z} + \frac{1}{i\omega Z} U i K_x p' \therefore \boldsymbol{u} \cdot \hat{n} = -i(\omega - K_x U)\frac{p'}{i\omega Z} \tag{3.56}$$

The behaviour of a fluid is governed by the conservation of linear momentum and given that the flow is uniform in the axial direction, the component in the normal direction r, of the linear momentum variation equation can be written as

$$(i\omega + U\frac{\partial}{\partial x})u_n = \frac{1}{\rho}\frac{\partial p'}{\partial r} \tag{3.57}$$

thus, substituting the relationship given in the equation 3.56 n the equation 3.57, we have

$$(i\omega + U\frac{\partial}{\partial x})\left(- i(\omega - K_x U)\frac{p'}{i\omega Z}\right) = \left[\frac{1}{\rho}\frac{\partial p'}{\partial r}\right]_{R_i, R_0} \tag{3.58}$$

manipulating and using the relation given in the equation 3.55 one arrives that

$$\left[\frac{\partial p'}{\partial r}\right]_{R_i,R_0} = \frac{1}{i\omega z c_0}(\omega - K_x U)^2 p' \tag{3.59}$$

the equation 3.59 represents the boundary condition for the case of a duct with walls with finite impedance under the action of a subsonic flow in the axial direction, where z is the dimensionless impedance defined as

$$z = \frac{Z}{\rho c_0}. \tag{3.60}$$

It is observed that the condition given by the equation 3.59, when considering the case of rigid walls, that is, infinite impedance, takes the form

$$\left[\frac{\partial p'}{\partial r}\right]_{R_i,R_0} = 0 \tag{3.61}$$

the equation 3.61 hows that the boundary condition 3.59 recovers the result for the rigid wall case discussed in Chapter 3.

One can rewrite the equation 3.59 in a more convenient form using the Mach number M and the dimensionless axial wavenumber λ defined as

$$\lambda = \frac{K_x}{K} \tag{3.62}$$

where K is the wavenumber of the free acoustic field defined by

$$K = \frac{\omega}{c_0} \tag{3.63}$$

To obtain the boundary condition in terms of such parameters, the equation 3.59 is observed in the form

$$\left[\frac{\partial p'}{\partial r}\right]_{R_i,R_0} = \underline{\frac{1}{i\omega}(\omega - K_x U)^2}\frac{p'}{z c_0} \tag{3.64}$$

expanding the underlined term of the equation 3.64 one has that

$$\frac{1}{i\omega}(\omega - K_x U)^2 = \frac{\omega^2}{i\omega} - \frac{2\omega K_x U}{i\omega} + \frac{K_x^2 U^2}{i\omega} \tag{3.65}$$

substituting the relation 3.62 in the equation 3.65 we have

$$\frac{\omega^2}{i\omega} - \frac{2\lambda\omega^2 U}{i\omega c_0} + \frac{\omega^2 U^2 \lambda^2}{c_0^2 i\omega} = -\frac{\omega}{i}(1 - \lambda M)^2 = i\omega(1 - \lambda M)^2 \tag{3.66}$$

In this way, from the result of the equation 3.66, the following form is obtained for the boundary condition

$$\left[\frac{\partial p'}{\partial r}\right]_{R_i,R_0} = \frac{i\omega}{z c_0}(1 - \lambda M)^2 p' \tag{3.67}$$

writing the equation 3.67 in terms of the dimensionless admittance defined by

$$A = \frac{1}{z} \tag{3.68}$$

one has that the most usual final form of the boundary condition for a duct with walls with liners is given by

$$\left[\frac{\partial p'}{\partial r}\right]_{R_i,R_0} = iKA(1 - \lambda M)^2 p'. \tag{3.69}$$

3.3.2 Analytical Modal Solution for an Annular Duct with Finite Wall Impedance under Uniform Mean Flow

Considering now the final form of the boundary condition given by the equation 3.69 one can again derive the solution in the radial direction in a similar way as done in Chapter 3, given the present scenario of an annular duct with walls with liners.

As the acoustic impedance depends only on the pressure in the normal direction, that is, in the radial direction r, we have that as

$$p'_r = R(r) \tag{3.70}$$

we obtain the following expression for the boundary condition

$$-R' + iKA(1-\lambda M)^2 R = 0 \tag{3.71}$$

Returning to the form of the R function expressed in chapter 3 in 2.85

$$R(r) = R_1 J_m(K_r r) + R_2 Nm(K_r r) \tag{3.72}$$

in this way, for the walls R_o and R_i, in the same way as done in chapter 3, a system of equations can be assembled from the boundary condition expressed in 3.71 with the following format

$$\begin{cases} (R_1 K_r J'_m(K_r R_i) + R'_2 K_r N'_m(K_r R_i)) + iKA(1-\lambda M)^2 (R_1 J_m(K_r R_i) + R_2 N_m(K_r R_i)) = 0 \\ (R_1 K_r J'_m(K_r R_o) + R'_2 K_r N'_m(K_r R_o)) + iKA(1-\lambda M)^2 (R_1 J_m(K_r R_o) + R_2 N_m(K_r R_o)) = 0 \end{cases}. \tag{3.73}$$

Isolating R_2 in the first equation of the system 3.73 we have:

$$R_2 = \frac{-R_1(-K_r J'_m(K_r R_i) + iKA(1-\lambda M)^2 J_m(K_r R_i))}{(-K_r N'_m(K_r R_i) + iKA(1-\lambda M)^2 N_m(K_r R_i))} \tag{3.74}$$

Thus, defining Q as the following term

$$Q = -\frac{(-K_r J'_m(K_r R_i) + iKA(1-\lambda M)^2 J_m(K_r R_i))}{(-K_r N'_m(K_r R_i) + iKA(1-\lambda M)^2 N_m(K_r R_i))} \tag{3.75}$$

Substituting the relation for R_2 found in the equation 3.74 in the second equation of the system 3.73 and using the relation from the equation 3.75 we arrive at

$$(K_r J'_m(K_r R_o) + Q K_r N'_m(K_r R_o)) + iKA(1-\lambda M)^2 (J_m(K_r R_o) + Q N_m(K_r R_o)) = 0 \tag{3.76}$$

as expressed earlier, it is defined

$$\sigma_{mn} = K_r R_o \text{ e } \sigma = \frac{R_i}{R_o} \tag{3.77}$$

so we can rewrite the equation 3.75 as

$$Q = -\frac{(-\frac{\sigma_{mn}}{R_o} J'_m(\sigma_{mn}\sigma) + iKA(1-\lambda M)^2 J_m(\sigma_{mn}\sigma))}{(-\frac{\sigma_{mn}}{R_o} N'_m(\sigma_{mn}\sigma) + iKA(1-\lambda M)^2 N_m(\sigma_{mn}\sigma))} \tag{3.78}$$

thus obtaining the following final form of the equation 3.76

$$\frac{\sigma_{mn}}{R_o}(J'_m(\sigma_{mn}) + QN'_m(\sigma_{mn})) + iKA(1-\lambda M)^2(J_m(\sigma_{mn}) + QN_m(\sigma_{mn})) = 0 \tag{3.79}$$

Thus, by numerically solving the transcendental equation 3.79, we arrive at the possible σ_{mn} for the case of an annular duct with subsonic flow in lined walls. The equation 3.79 must be solved iteratively since it is dependent on the radial and axial wavenumber, it is known from the derivative equation 2.105, that the axial wavenumber is also dependent on the radial wave number. In this way, you must use an initial value for K_x and search for the roots of the equation 3.79 iteratively until the values converge. Dado o comportamento oscilatório das funções de Bessel (J_m) e Neumann(N_m) novamente para cada modo circunferencial m.

Therefore, using the system to relate R_1 and R_2, the following form is obtained for the solution in the radial direction from the equation 3.72

$$R(r) = R_1[J_m(K_r r) - QN_m(K_r r)] \tag{3.80}$$

Chapter 4

Validation of the Implemented Methodology

In this chapter, a validation of the implemented methodology using data available from the literature is proposed. First, all analyses depend on the calculation of the roots of the equation 3.79, which is a transcendental equation in complex numbers and must be solved numerically and iteratively, since it also depends on the axial wavenumber K_x which in turn depends on the root of the equation 3.79.

The solution of such an equation is complex since it depends on the Bessel and Neumann functions as well as their derivatives, with these arguments being complex numbers, which restricts the number of numerical methods to search for roots that can be used. Graphical methods could be used, however, the process becomes very manual which limits the number of roots that can be found. In this way, the Muller method was used to solve it.

Muller's method is an interpolation method that uses a second-order interpolation. A complex root is located using a parabola that passes through three values in the vicinity of the initial estimation point [49]. Thus, for the application of this method, it is necessary to have a previous estimate of the location of the roots. It is expected that the values of the roots do not greatly differ from the values found for the rigid wall case. To confirm this hypothesis, an analysis of the function was performed, evaluating the surface generated by it in a mesh of complex numbers as well as its contour lines. Despite the presence of several local minima, it is possible to manually track the position of some roots and observe that their real parts are values close to the values found for the case of rigid walls. Thus, for the initial estimate, the values of roots independent of the frequency of the hardwall case are used.

To calculate the roots, the numerical method was implemented and a routine was written in MATLAB that calculates the roots for the hardwall case and uses them as initial estimates both for the roots themselves and for the axial wavenumber inside of an iterative process that is repeated until the change in the axial wavenumber K_x is on the order of 10^{-6}.

To validate the methodology used, the results obtained for the dimensionless axial wave number

λ were compared with the results found by [50] in the case of evaluation of the circumferential mode $m = 2$ for a circular duct with walls with dimensionless acoustic impedance $A = 0.72 + 0.42i$ at a dimensionless frequency (Helmholtz number) $He = 1$ and a subsonic uniform flow with Mach number $M = 0.5$

Table 4.1: Comparison between the dimensionless axial wave numbers λ positive direction

λ	[50]	Present
λ_0^+	0.6195 - 5.0139i	-
λ_1^+	-5.8195 - 3.8968i	-0.6195 + 5.0139i
λ_2^+	0.4453 - 9.1868i	-0.4453 + 9.1868i
λ_3^+	0.4539 - 13.062i	-0.4539 +13.0615i
λ_4^+	0.4795 - 16.822i	-0.4795 +16.8217i
λ_5^+	0.5029 - 20.531i	-0.5029 +20.5307i
λ_6^+	0.5220 - 24.213i	-0.5220 +24.2131i
λ_7^+	0.5376 - 27.8802	-0.5375 +27.8799i
λ_8^+	0.5502 - 31.5372	-0.5502 +31.5370i
λ_9^+ [50] λ_{13}^+(Present)	0.5891 - 49.754i	-0.5891 +49.7543i

Table 4.2: Comparison between the dimensionless axial wave numbers λ negative direction

λ	[50]	Present
λ_0^+	0.4101 + 1.2904i	-
λ_1^+	1.2595 + 6.0852i	-1.2595 - 6.0852i
λ_2^+	1.1457 + 9.6679i	-1.1457 - 9.6679i
λ_3^+	1.0218 + 13.315i	-1.0218 -13.3150i
λ_4^+	0.9425 + 16.977i	-0.9425 -16.9768i
λ_5^+	0.8908 + 20.635i	-0.8908 -20.6353i
λ_6^+	0.8549 + 24.288i	-0.8549 -24.2884i
λ_7^+	0.8288 + 27.937i	-0.8288 -27.9368i
λ_8^+	0.8089 + 31.581i	-0.8089 -31.5815i
λ_9^+ [50] λ_{13}^+(Present)	0.7547 + 49.7722	-0.7547 -49.7722i

As can be seen from the results presented in the tables 4.1 e 4.2 the implemented MATLAB script obtained values very similar to those found by [50] and by [51] before him. The difference presented in the signs is due to the convention used for the temporal term, so the results obtained are similar, simply by multiplying one of the columns by minus one, that is, inverting the convention used. In the table 4.1 there is a significant difference for the value found for λ_1^+ where the value obtained via the Muller method, used in the present work, converges to the value found for the λ_0^+ found by [50]. However, evaluating the value found for this dimensionless axial wavenumber, it can be seen that it strongly disagrees with the others, raising the possibility that it is the value

for a spurious mode that does not appear when evaluating the results in the negative direction of propagation 4.2, there is also the possibility that it is a surface mode or a hydrodynamic mode, for the verification of any of these possibilities a deeper analysis must be done. Another point analysed is that the ninth value found by [50], which refers to the ninth root of the 3.79 equation, was only found by the methodology used in the present work for the thirteenth root calculated. Analysing the tabulated values, it is observed that from λ_8 to λ_9 the variation was more abrupt than the previous values had preconized, which corroborates the idea of the existence of more roots between the eighth and ninth values found by [50], as delivered by the MATLAB algorithm.

The implemented code deals with a general formulation for a case of an annular duct, however, when using a very small radius ratio, the routine recovers the case of a circular duct without a central body and delivers satisfactory results as analysed in the tables 4.1 and 4.2.

Table 4.3: Eigenvalues calculated for a circular duct if $He = 1$, $M = 0.5$, $A = 0.72 + 0.42i$,$m = 2$

n	σ_{mn}
1	4.4930 - 0.0394i
2	8.0394 - 0.1897i
3	11.3704 - 0.1833i
4	14.6137 - 0.1616i
5	17.8176 - 0.1415i
6	21.0009 - 0.1251i
7	24.1723 - 0.1117i
8	27.3363 - 0.1007i
9	30.4952 - 0.0917i
10	33.6506 - 0.0840i
11	36.8035 - 0.0776i
12	39.9544 - 0.0720i
13	43.1040 - 0.0672i

A further validation of the methodology used in this present work was performed by drawing comparisons with the results obtained by Maldonado [10], where their method to solve for the wavenumbers and eigenvectors includes a Finite Difference (FD) approach applied on the linearized compressible Euler equations under isentropic plugged flow. In this case, an annular duct with a unitary outer radius and an inner radius $R_i = 0.3$ under uniform mean flow is considered. The parameters assumed are a Helmholtz Number 10, Mach number $M_0 = 0.5$ and an admittance of the lined wall $a = 0.4 + 0.2i$. Cases with both walls lined, only the outer wall lined and only the inner wall lined were considered.The modes evaluated are $m = 0$ and $m = 5$. The comparison was performed in the first ten wavenumbers for positive and negative directions, shown in Figures 4.1 to 4.7.

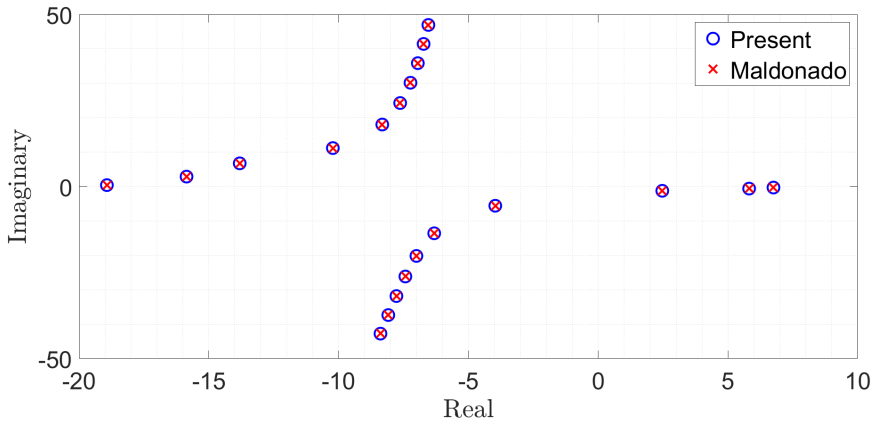

Figure 4.1: Axial wavenumber complex plane obtained from the present work and by Maldonado[10], assuming both walls lined and $m = 0$

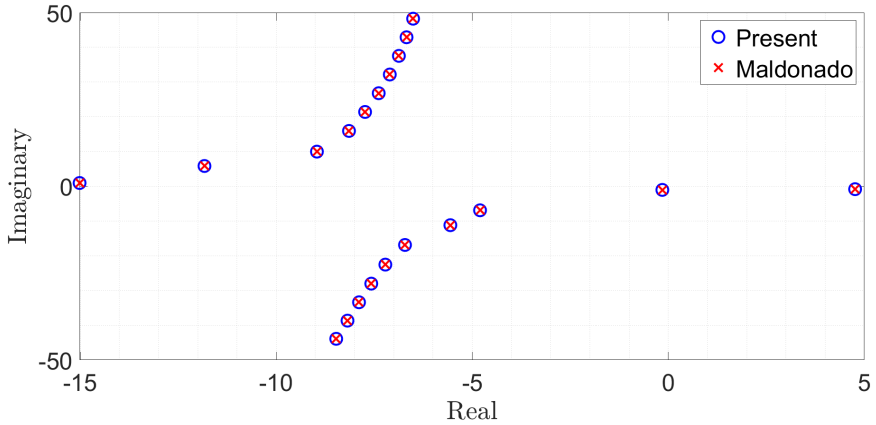

Figure 4.2: Axial wavenumber complex plane obtained from the present work and by Maldonado[10], assuming both walls lined and $m = 5$

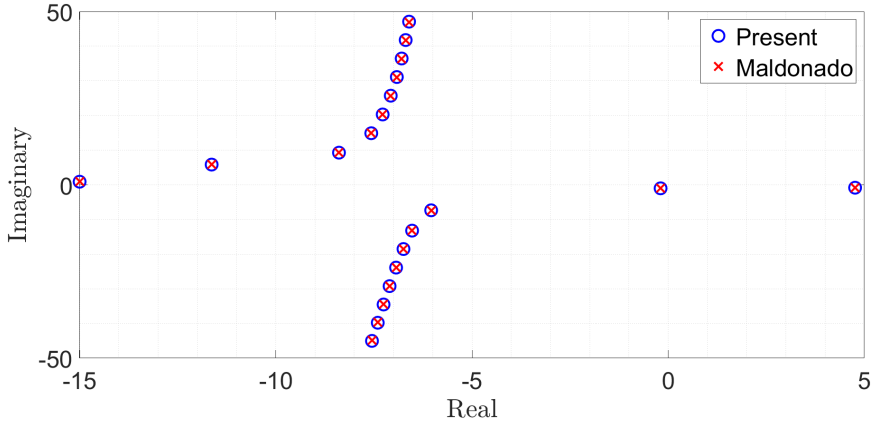

Figure 4.3: Axial wavenumber complex plane obtained from the present work and by Maldonado[10], assuming only the outer wall lined and $m = 5$

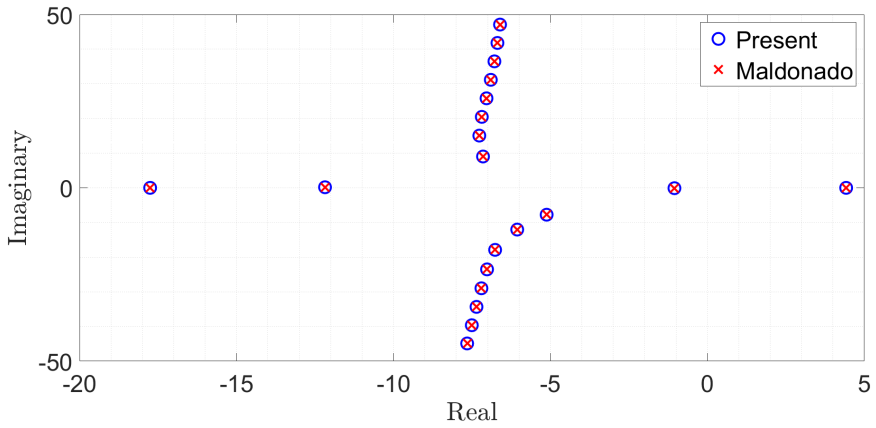

Figure 4.4: Axial wavenumber complex plane obtained from the present work and by Maldonado[10], assuming only the inner wall lined and $m = 5$

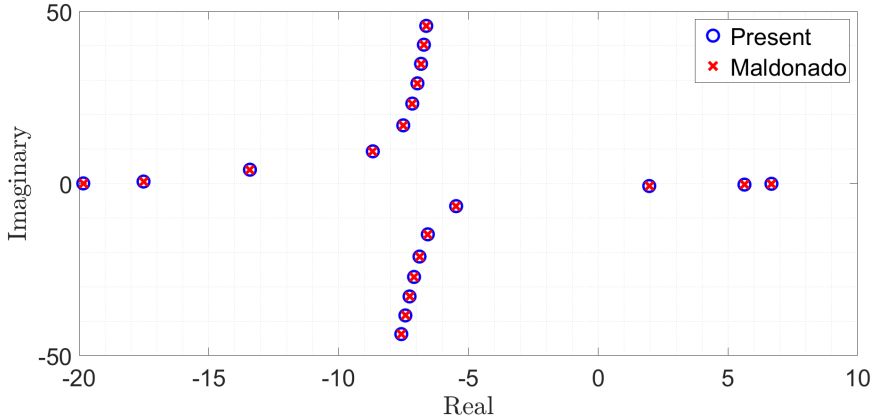

Figure 4.5: Axial wavenumber complex plane obtained from the present work and by Maldonado[10], assuming only the inner wall lined and $m = 0$

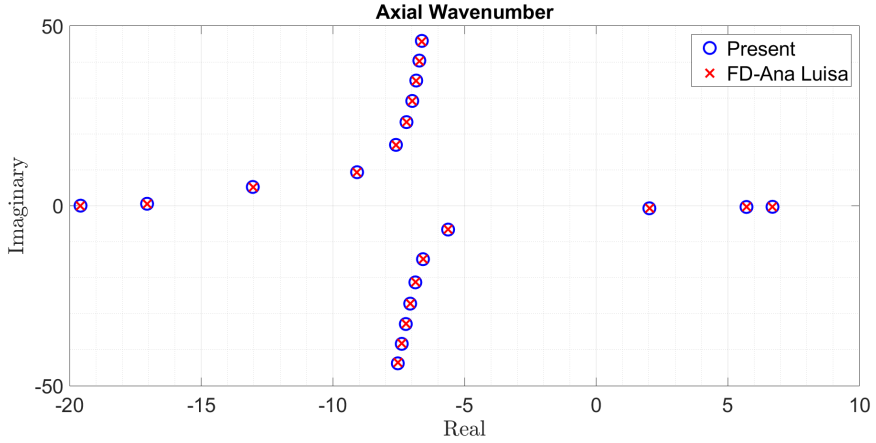

Figure 4.6: Axial wavenumber complex plane obtained from the present work and by Maldonado[10], assuming only the outer wall lined and $m = 0$

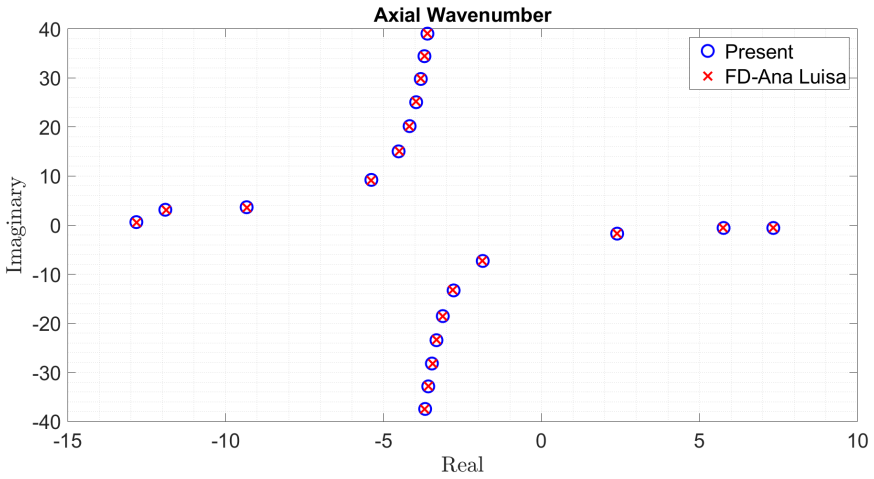

Figure 4.7: Axial wavenumber complex plane obtained from the present work and by Maldonado[10], assuming both walls lined and $m = 2$ and $\sigma = 0.25$

In all seven cases, there was an outstanding agreement between the presented wavenumbers and the published results, including the upstream and downstream acoustic modes. Either considering the a finite impedance on both walls, shown in the figures 4.1,4.2 and 4.7 or only on the outer or inner wall, presented on the figures 4.3 to 4.6 the algorithm lead to satisfactory convergence of the results. Therefore, the methodology proposed in the present work show itself to be robust enough to be used in further evaluations of the present theme.

Chapter 5

Liner Effects on the Acoustic Wave Propagation

In this chapter, the effects of the liner on the propagation of the acoustic wave will be demonstrated, given the theory discussed in the previous chapters. Comparisons will be made between cases with impedance in the nacelle wall and the case of rigid walls, within the same geometric and flow conditions.

The geometry and flow conditions considered for all the results presented in this chapter are based on the technical aspects of the Advanced Noise Control Fan located in AeroAcoustic Propulsion Laboratory at NASA Glenn Research Centre, Figure 5.1. The Advanced Noise Control Fan is a highly flexible fundamental test bed where it is possible to mount multiple rotor-stator configurations. It is equipped with a $1.219\,m$ diameter ducted fan with a low, variable, speed motor. Its hub-to-tip ratio is $\sigma_i n = 0.375$ for the intake region and $\sigma_e x = 0.5$ for the exhaust region. The Mach Number considered in the cases with the flow will equal to $M_0 = 0.12$ [11]. In order to analyse the liner effects in different modes a set of modes was chosen to be evaluated, the modes $m = 0$, $m = 5$ and $m = 20$

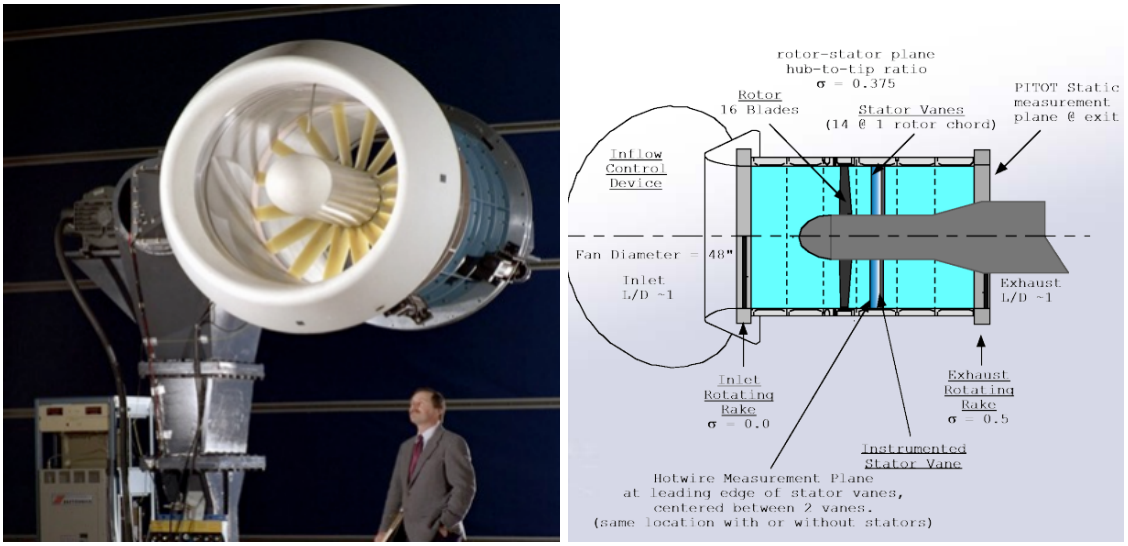

(a) Advanced Noise Control Fan Picture (b) Advanced Noise Control Fan features scheme

Figure 5.1: Advanced Noise Control Fan. [11]

5.1 Root locus for the axial wavenumbers

In this section, by analysing the real and imaginary components of the axial wavenumber K_x (equation 2.105) for a given operational condition the effects of the duct's wall impedance and also effects of the presence of a uniform flow will be evaluated.

The cases evaluated consist of the axial wave number for the circumferential modes of order $m = 0$, $m = 5$, $m = 20$, as aforementioned, the dimensionless acoustic impedance considered both at the walls of the outermost radius as in the walls of the central body was $A = 0.4 + 0.2i$, shown in Figures 5.2 to 5.4. The geometric characteristics considered were those of the Advanced Noise Control Fan, for each of the cases the first 10 radial modes were considered in an operational condition where the dimensionless frequency was $He = 15$. For such circumstance the critical values for σ_{mn} are

$$\begin{cases} \sigma_{mn,c} = 15 \text{ for } M_0 = 0 \\ \sigma_{mn,c} = 15.1717 \text{ for } M_0 = 0.15 \end{cases} \tag{5.1}$$

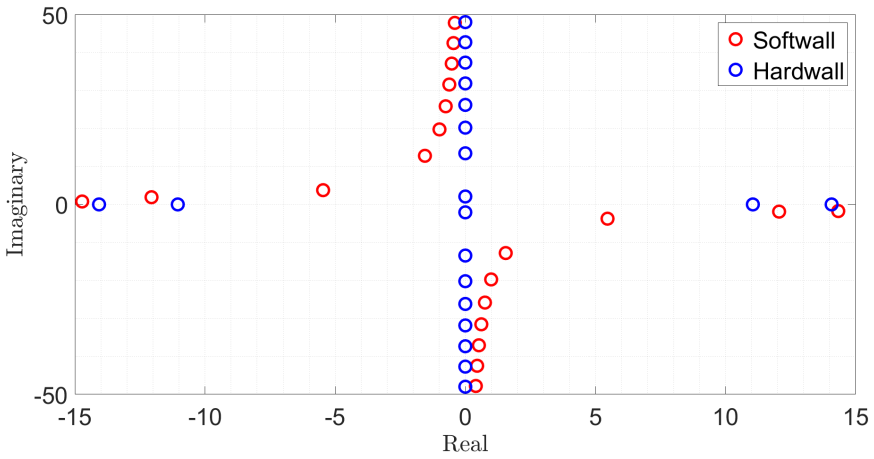

Figure 5.2: Axial wavenumber complex plane assuming both walls lined, $m = 0$, $M_0 = 0$

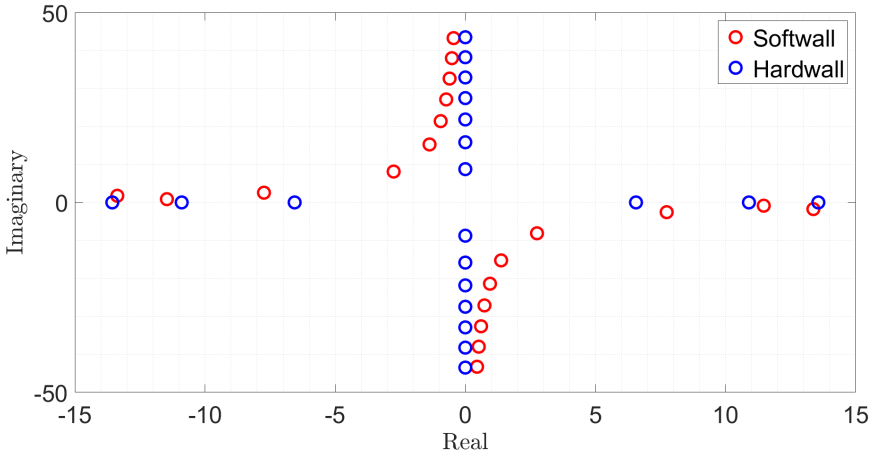

Figure 5.3: Axial wavenumber complex plane assuming both walls lined, $m = 5$, $M_0 = 0$

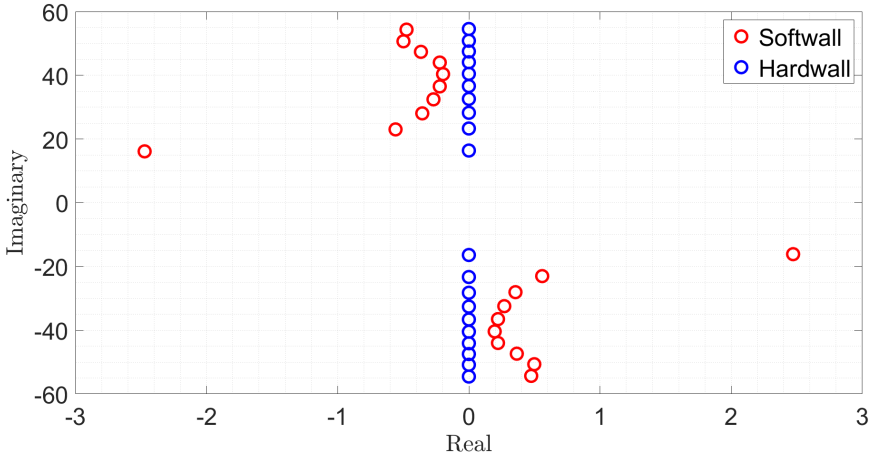

Figure 5.4: Axial wavenumber complex plane assuming both walls lined, $m = 20$, $M_0 = 0$

By analysing the figures 5.2, 5.3 and 5.4 it is observed that for the case of rigid walls, the axial wavenumbers for the propagating modes (cut-on) are purely real and for the non-propagating

modes (cut-off) the axial wavenumbers are purely imaginary. From the moment that the walls are considered to have a finite impedance, it is observed that even for modes that propagate the wave number K_x has an imaginary part even if small. Such a component indicates the attenuation that is introduced into the system by the presence of the liner. The cut-off modes are also no longer purely imaginary and start to have a real component. Therefore, the axial wavenumbers stop being purely real or purely imaginary and become complex numbers due to the effects of the wall's impedance. It is also worth mentioning that for the cases without a uniform mean flow, symmetry with respect to the origin of the complex plane is perceived.

Evaluating the propagating modes for the hardwall it is possible to observe that only 2 radial modes propagate for the circumferential mode $m = 0$, three for $m = 5$ and none for $m = 20$, that is only the radial modes which $\sigma_{mn} \leq \sigma_{mn,c}$. However, for the softwall case, some of the modes gain a significant real part and lose some of the imaginary part, which can lead to propagation with decay for the given operational condition. Such circumstance can be observed in the figure 5.2.

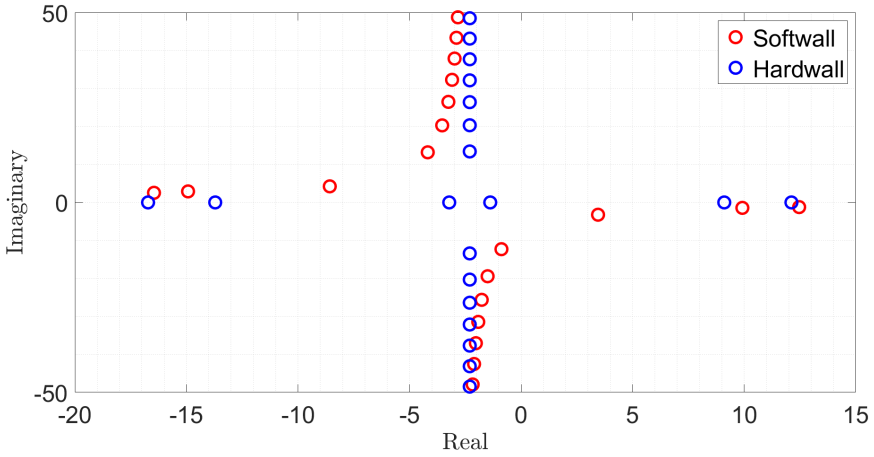

Figure 5.5: Axial wavenumber complex plane assuming both walls lined, $m = 0$, $M_0 = 0.15$

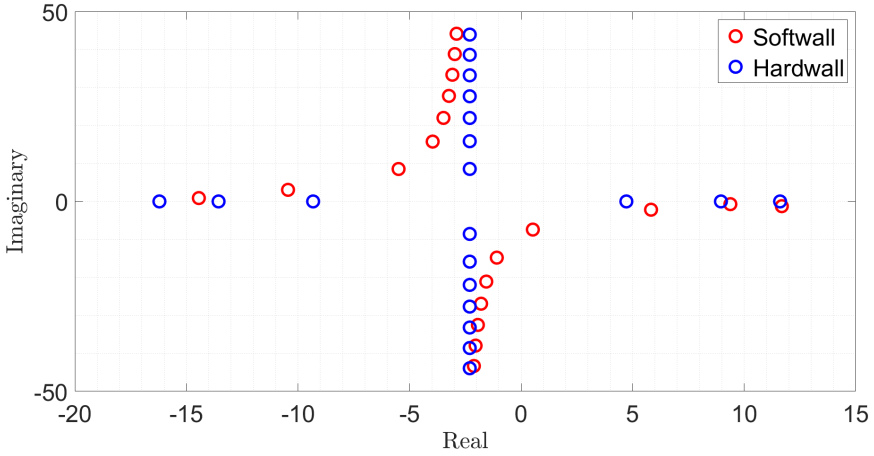

Figure 5.6: Axial wavenumber complex plane assuming both walls lined, $m = 5$, $M_0 = 0.15$

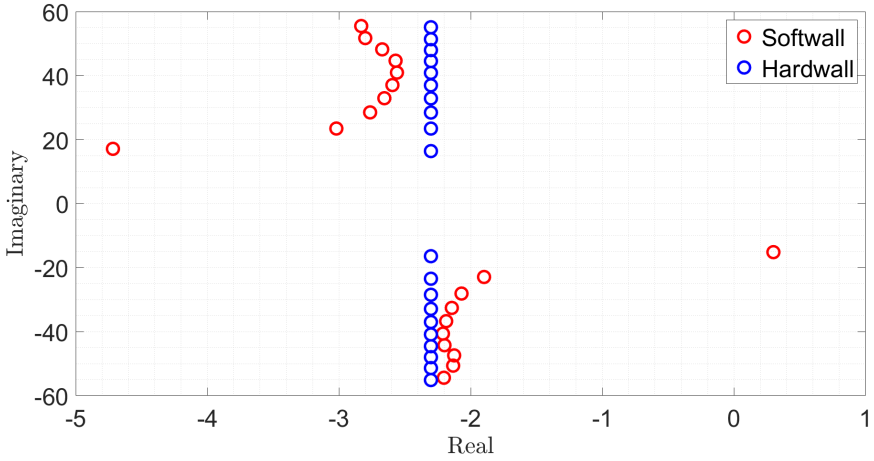

Figure 5.7: Axial wavenumber complex plane assuming both walls lined, $m = 20$, $M_0 = 0.15$

By analysing the figures 5.5, 5.6 and 5.7, it is possible to observe that the presence of a positive uniform mean flow in the axial direction displaces K_x wavenumbers complex plane to the left, the diagram also suffers a stretch in the direction of the positive axial wavenumbers, from such features presented in the diagram it is possible to constatate that the positive wavenumbers have its propagation aided by the flow. Also, it is important to note that even for the hardwall case some non-propagating modes start to propagate due to the presence of the mean flow, such fact is consistent with the values presented in the equation 5.1 where the presence of the flow increases the value for the $\sigma_{mn,c}$, which implies saying that the flow decreases the cut-on frequency.

5.2 Dispersion curves for the axial wavenumber

In this subsection, a dispersion analysis is presented. The axial wavenumber K_x is assessed to how it behaves with the change of the fundamental blade passing frequency for a given circumferential mode m coupled with a radial mode n. In the engineering sense this type of analysis makes sense of the fact that turbomachinery may operate at several flow regimes, for example, at some stages of flight, the flow velocity M_0 may remain the same but the needed thrust may vary, with the change of the fundamental frequency and its harmonics. Therefore, the lining performance must be at a given frequency interval. Considering the aforementioned operational conditions of the Advanced Noise Control Fan the dispersion curves for the first four radial wavenumbers are generated around the corresponding cut-on frequency of the given circumferential mode. Their frequency behaviour is investigated in terms of the cut-on frequency, operational conditions and effect of the liner treatment on the walls.

5.2.1 Hardwall case

For the hardwall case, the admittance considered for the duct walls is null, therefore they are considered rigid surfaces. Such case has great importance as it is the base of comparison in order to evaluate the effects of the presence of the liner.

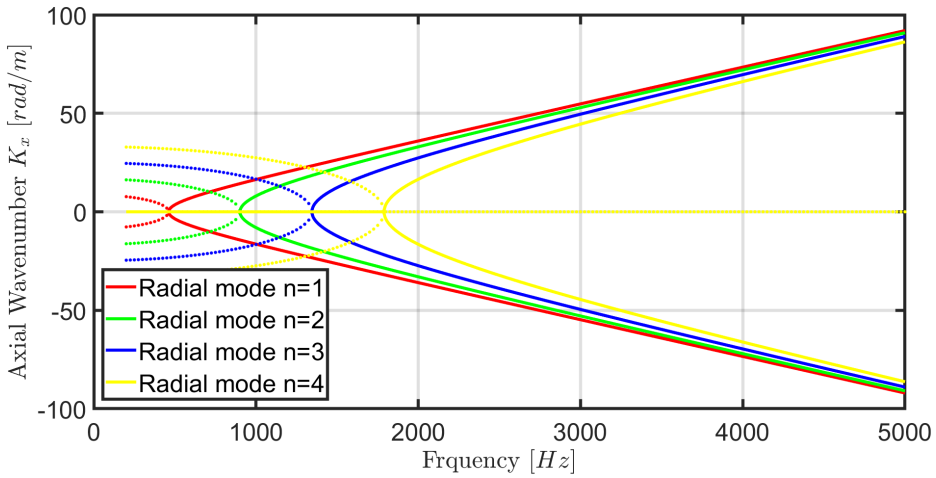

(a) Case considering the absence of uniform mean flow $M_0 = 0$

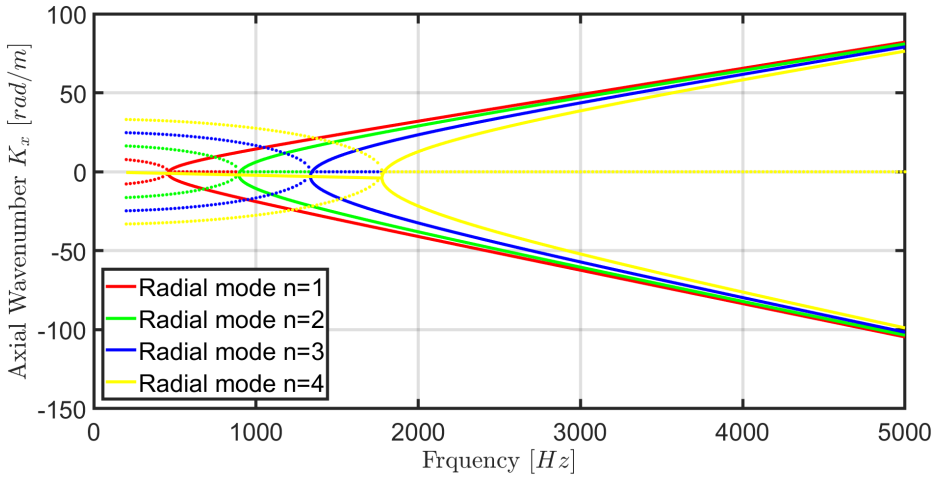

(b) Case considering the presence of uniform mean flow $M_0 = 0.12$

Figure 5.8: Dispersion curve for the hardwall case for the circumferential mode $m = 0$ and radial modes $n = 1, 2, 3, 4$

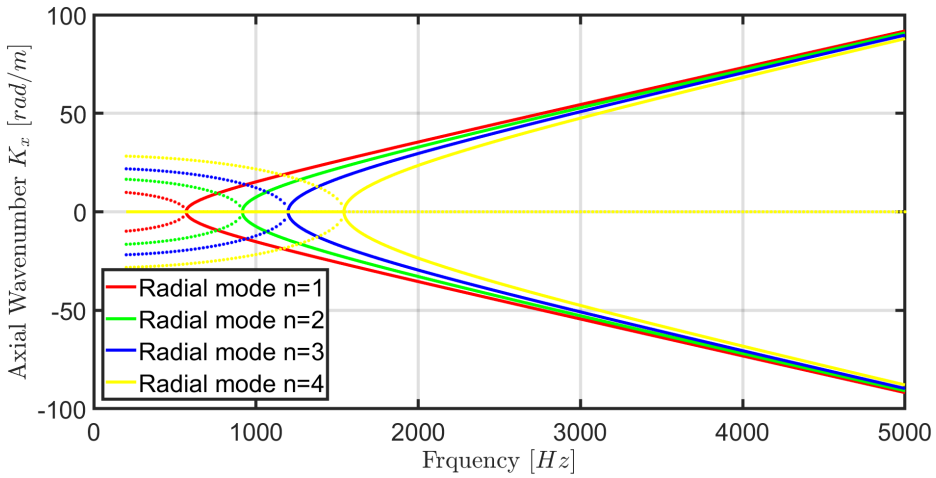

(a) Case considering the absence of uniform mean flow $M_0 = 0$

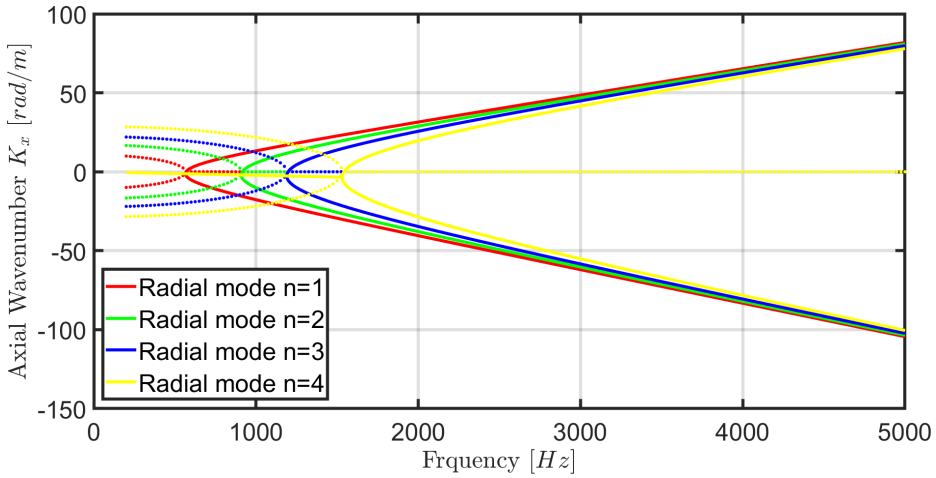

(b) Case considering the presence of uniform mean flow $M_0 = 0.12$

Figure 5.9: Dispersion curve for the hardwall case for the circumferential mode $m = 5$ and radial modes $n = 1, 2, 3, 4$

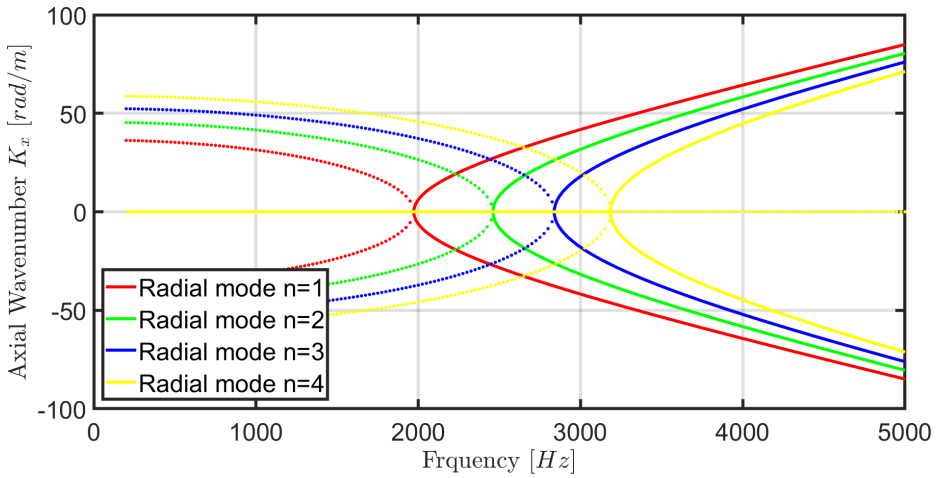

(a) Case considering the absence of uniform mean flow $M_0 = 0$

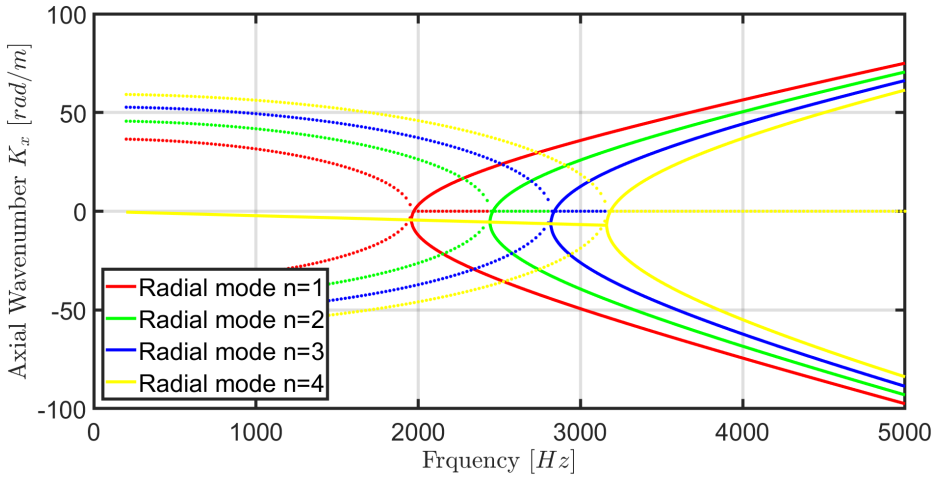

(b) Case considering the presence of uniform mean flow $M_0 = 0.12$

Figure 5.10: Dispersion curve for the hardwall case for the circumferential mode $m = 20$ and radial modes $n = 1, 2, 3, 4$

It can be observed in the dispersion curves presented in figures 5.8 to 5.10 that the axial wavenumber K_x is a purely imaginary number in frequencies in which the mode does not propagate, as soon as the cut-on frequency is reached the axial wavenumber becomes a purely real number. Such behaviour preconises a typical characteristic for the hardwall case, as there is no attenuation considered there is no imaginary part for the cut-on modes as they do not decay and no real part for the cut-off modes as they do not propagate. Also, it is worth mentioning that the higher the mode order, the higher the cut-on frequency. Such fact is true whether comparing the radial modes for the same circumferential mode or comparing different circumferential modes.

Another interesting characteristic is the symmetry about the frequency axis observed in the cases without a uniform flow, in which the dispersion curves for the modes propagating in the positive and negative direction have the same absolute value and opposing signals. Such a fact signals that the positive and negative modes have the same propagation speed. However the presence of the flow breaks this symmetry, and an inclination can be perceived for the real part

of the axial wavenumbers which implies that the propagation velocity is different for the positive-going and negative-going waves, which is a result that corroborates the statement presented in the equation 2.133.

5.2.2 Softwall - Single-Degree-of-Freedom Models

5.2.2.1 Tam and Auriault model

For this section analysis, the liner model proposed by Tam and Auriault [12] was used, where the resistance is taken as almost constant throughout the frequency and the reactance is given by equation 1.4. Based on the experimental data obtained by Motsinger and Kraft[6], a mean-least-square fit was performed using Matlab and consequently, the calibration constants X_{-1} and X_1 were obtained. The obtained reactance model parameters are presented in table 5.1. The values found for the X_{-1} and X_1 are slightly different from those found by Tam and Auriault [12] due to the data set used for the mean-least-square fitting[6]. As the model proposed by Tam and Auriault [12] considers the absence of flow, the results for this section will consider only the case without a uniform axial flow.

Table 5.1: Three parameter values obtained from the literature [6, 12].

Parameter	Value
R	0.72000
X_{-1}	-13.52000
X_1	0.06765

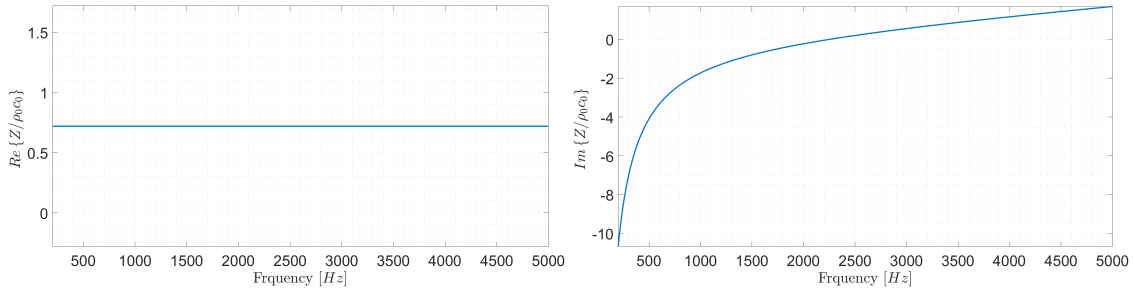

(a) Single degree of freedom Tam and Auriault model reactance

(b) Single degree of freedom Tam and Auriault model resistance

Figure 5.11: Single degree of freedom (a) real and (b) imaginary impedance profiles for the model proposed by Tam and Auriault [12]

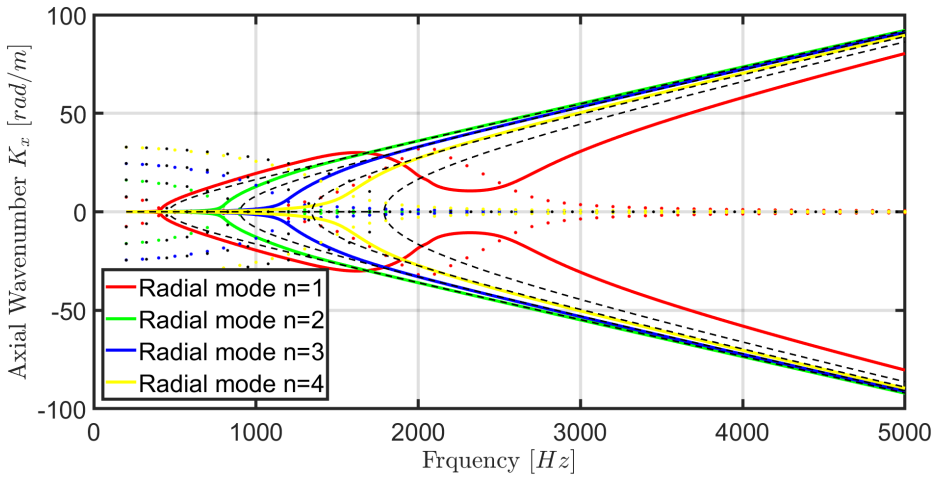

Figure 5.12: Dispersion curve for a finite impedance case for the circumferential mode $m = 0$ and radial modes $n = 1, 2, 3, 4$, $M_0 = 0$, considering the Tam and Auriault model [12]

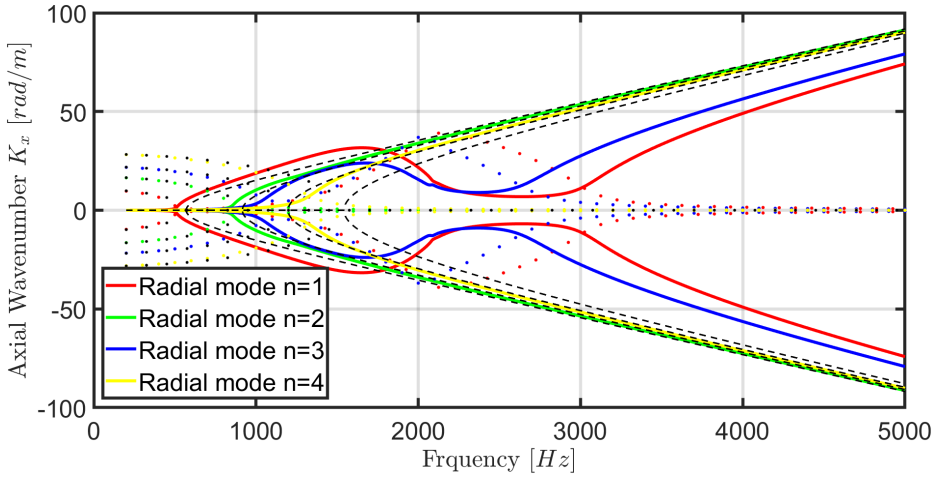

Figure 5.13: Dispersion curve for a finite impedance case for the circumferential mode $m = 5$ and radial modes $n = 1, 2, 3, 4$, $M_0 = 0$, considering the Tam and Auriault model [12]

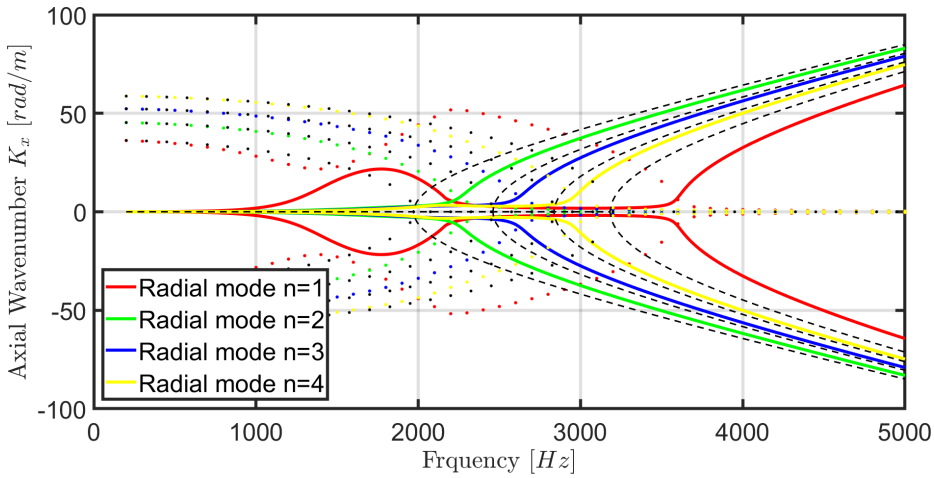

Figure 5.14: Dispersion curve for a finite impedance case for the circumferential mode $m = 20$ and radial modes $n = 1, 2, 3, 4$, $M_0 = 0$, considering the Tam and Auriault model [12]

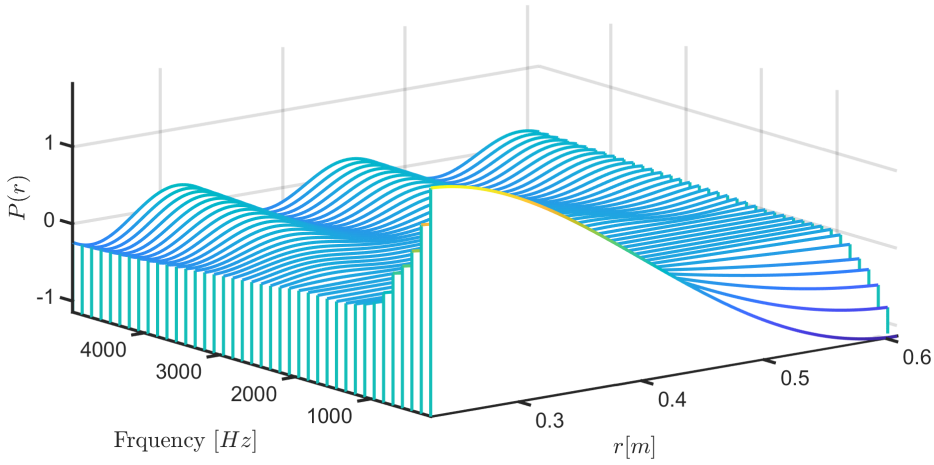

Figure 5.15: Radial mode shape (radial pressure fluctuation) throughout the frequency for mode $m = 0$ $n = 1$, $M_0 = 0$, considering the Tam and Auriault model [12]

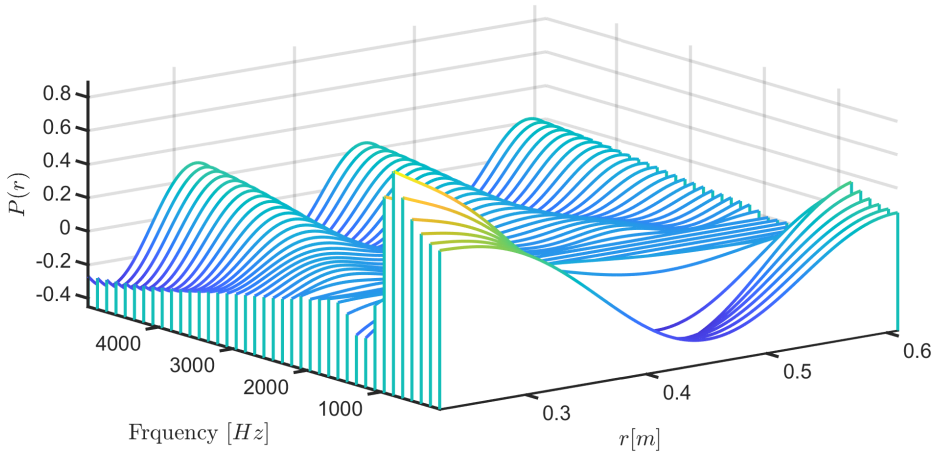

Figure 5.16: Radial mode shape (radial pressure fluctuation) throughout the frequency for mode $m = 0$ $n = 1$, $M_0 = 0$, considering the Tam and Auriault model [12]

One of the most remarkable characteristics present on the dispersion curves considering a duct with a finite impedance on the walls is the fact that both propagating or non-propagating modes are complex numbers, where the cut-off modes have a great imaginary parcel and little real part and the cut-on modes have a great real part and small imaginary part. Therefore the dispersion curves are smooth with the values for K_x progressing gradually with the increment of the frequency in comparison to the hardwall case, where once the cut-on frequency is reached the mode passes from purely imaginary to purely real.

Also, it is possible to observe that the cut-on frequency is lower for the softwall case as the dispersion curves are all shifted to the left in comparison to the dashed black lines which represent the hardwall case.

The model proposed by Tam and Auriault impact different modes differently as can be observed for the modes $m = 0$, $n = 1$ in the figure 5.12, $m = 5$, $n = 1$ and $n = 3$ in the figure 5.13 and for the mode $m = 20$, $n = 1$ in the figure 5.14 where they suffer a great attenuation in the band between $2000\,Hz$ and $3000\,Hz$. This is can be attributed to a strong wave coupling due to gyroscopic effects on the duct wall, known as wave locking [52] For those cases by analysing the radial modal shapes in the figures 5.15 and 5.16 it is possible to see that the mode shapes gradually change until a certain frequency, the same where the attenuation begins in the dispersion curves, from that frequency on the radial pressure fluctuation does not oscillate and remains with an almost constant value until it gradually starts oscillating again gaining the shape of another mode.

5.2.2.2 Helmholtz resonator model

For this section the analysis take as base the single degree of freedom impedance model. Such a model is described by the equation 1.5, which represents a Helmholtz resonator. The values for the geometrical parameters considered for the present analysis were presented by Busse [13] the values for the face sheet impedance Z_{fs} were calculated using the Guess model [40] for a perforated plate considering both cases, with and without flow. The magnitude of the axial flow considered was $M_0 = 0.12$ as it is one of the standard operational conditions for Advanced Noise Control Fan

Table 5.2: Single degree of freedom liner geometrical parameters

Parameter	Value
$\sigma_{opr,fs}$	0.043
t	$1\,mm$
d	1.5
L	$12.7\,mm$

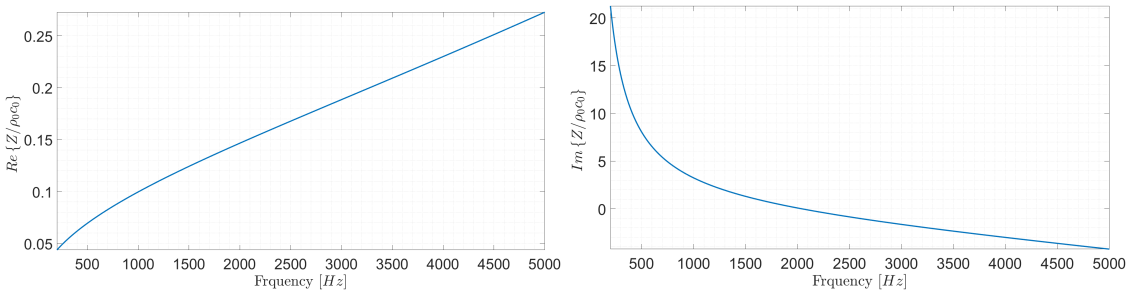

(a) Single degree of freedom model reactance

(b) Single degree of freedom resistance

Figure 5.17: Single degree of freedom (a) real and (b) imaginary impedance profiles for the liner parameters presented by Busse [13]

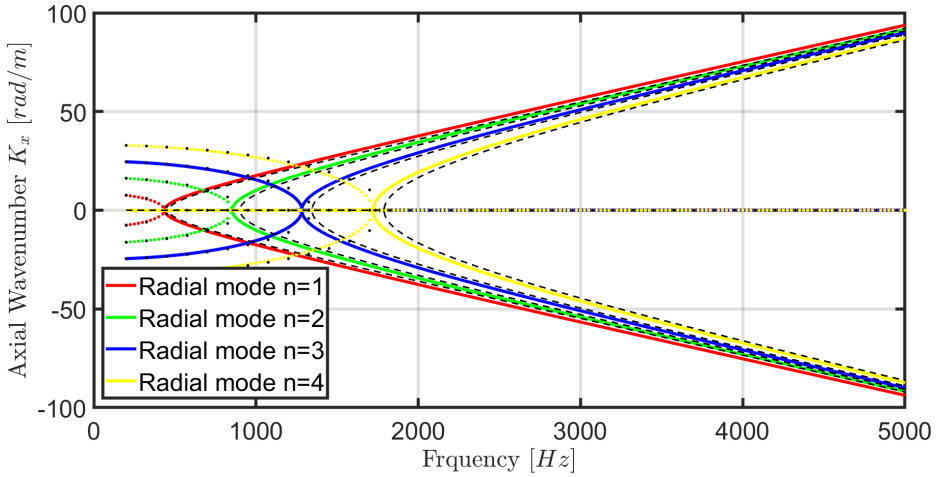

(a) Case considering the absence of uniform mean flow $M_0 = 0$

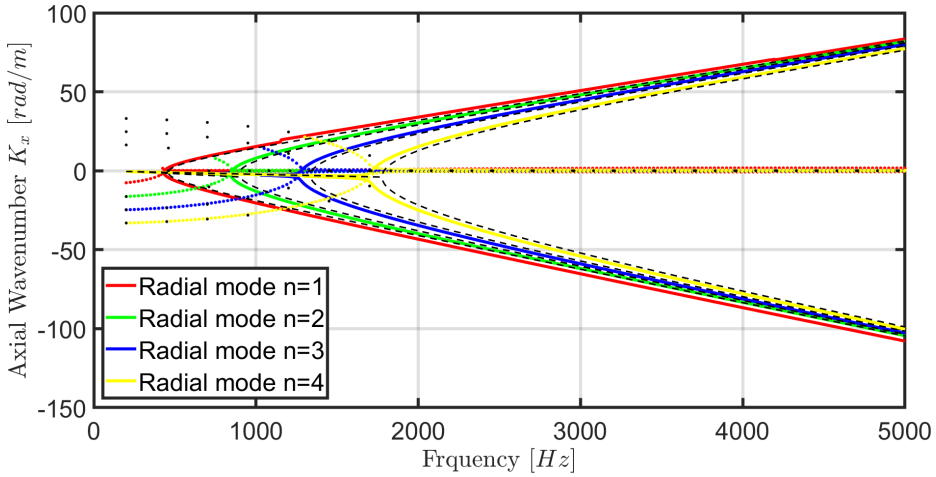

(b) Case considering the presence of uniform mean flow $M_0 = 0.12$

Figure 5.18: Dispersion curve for a finite impedance case for the circumferential mode $m = 0$ and radial modes $n = 1, 2, 3, 4$,considering the single degree of freedom model

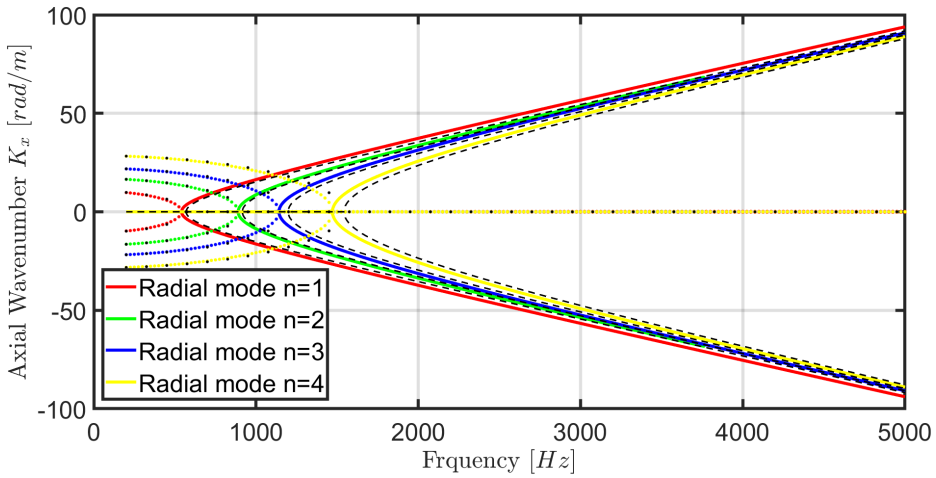

(a) Case considering the absence of uniform mean flow $M_0 = 0$

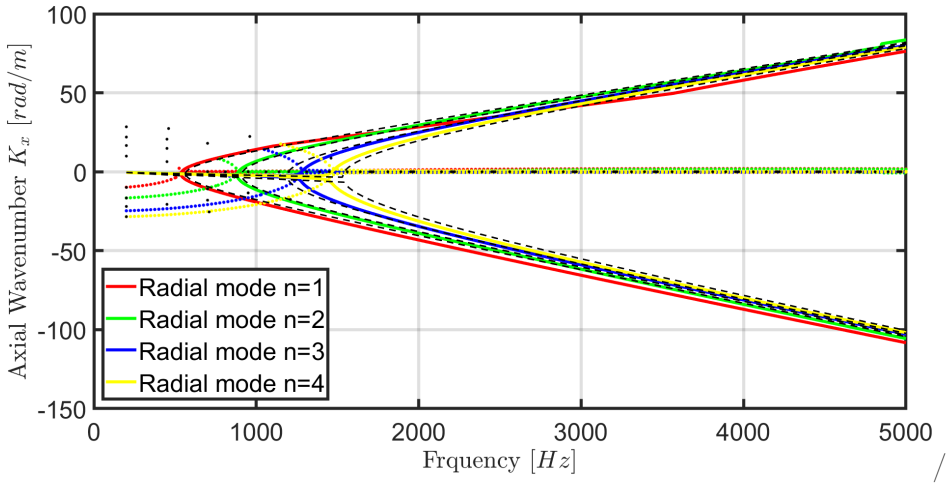

(b) Case considering the presence of uniform mean flow $M_0 = 0.12$

Figure 5.19: Dispersion curve for a finite impedance case for the circumferential mode $m = 5$ and radial modes $n = 1, 2, 3, 4$,considering the single degree of freedom model

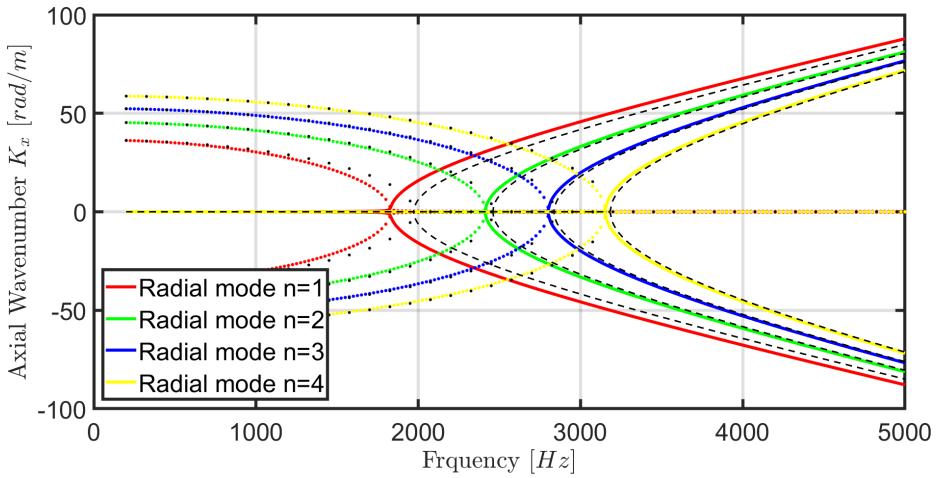

(a) Case considering the absence of uniform mean flow $M_0 = 0$

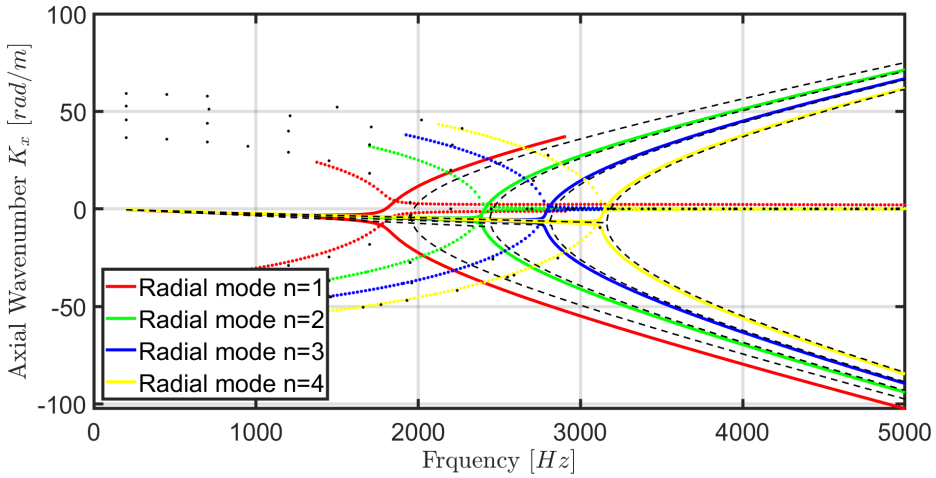

(b) Case considering the presence of uniform mean flow $M_0 = 0.12$

Figure 5.20: Dispersion curve for a finite impedance case for the circumferential mode $m = 20$ and radial modes $n = 1, 2, 3, 4$,considering the single degree of freedom model

Analysing the dispersion curves presented in the figures 5.18,5.19 and 5.20, again it is possible to note that the axial wavenumbers are complex numbers being propagating or non-propagating. Also, the cut-on frequency is lower for this case when compared to the hardwall case, as in all the figures the dispersion curves are displaced to the left.

The attenuation exerted by the liner with the geometrical characteristics proposed by Busse [13] is perceptibly lower than the attenuation evaluated in the previous case. None of the modes suffered great impacts as the attenuation of some modes analysed in the Tam and Auriault model. One of the reasons for such a difference is due to the values of reactance, the parameters used in Busse's work that lead to values that are less than half of the values found experimentally by Montsinger and Kraft [6] for reactance. As aforementioned the reactance is related to the energy absorption on the perforated face sheet, therefore it is possible to infer that energy absorption in the liner considered in the present case is lower than the absorption in the liner studied by Montsinger and Kraft. Obviously, these are studies done on different liners and different operational conditions

and such difference does not determine one liner as being more effective than the other.

In terms of the presence of the uniform mean flow it's possible to observe that in the cases with the flow the effects of the liner are a little less perceptible as the flow alters the values of the impedance of the face sheet. Also due to the asymmetry around the frequency axis that implies different propagation velocities for the waves heading in the positive and negative direction, the impedance has more impact on the waves travelling in the negative direction. Again the presence of a uniform mean flow introduces an inclination of the real part for the non-propagating modes

5.2.3 Softwall - Double degree of freedom Model

The analysis presented in this section is carried out based on the double degree of freedom impedance model. This model is described by the equation 1.6, and it can also be interpreted as liner mount that forms a double Helmholtz resonator. The values for the geometrical parameters used in the present analysis were presented by Burd [14], and the values for the face sheet impedance Z_{fs} and septum impedance Z_s were calculated using the Guess model [40] for a perforated plate. The magnitude of the axial flow considered for the pertinent cases was $M_0 = 0.12$ as it is one of the standard operating conditions for the Advanced Noise Control Fan.

Table 5.3: Double degree of freedom liner geometrical parameters[14]

Parameter	Value
$\sigma_{opr,fs}$	0.02
t	$1.016\,mm$
d	1.0922
$\sigma_{opr,s}$	0.009
d_s	0.2032
t_s	$0.7620\,mm$
L_1	$3.3020\,mm$
L_2	$28.1254\,mm$

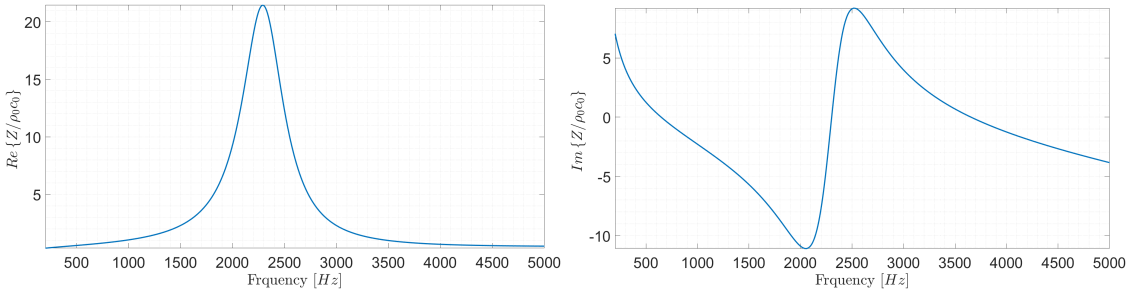

(a) Double degree of freedom model reactance (b) Double degree of freedom model resistance

Figure 5.21: Double degree of freedom (a) real and (b) imaginary impedance profiles for the liner parameters presented by Burd [14]

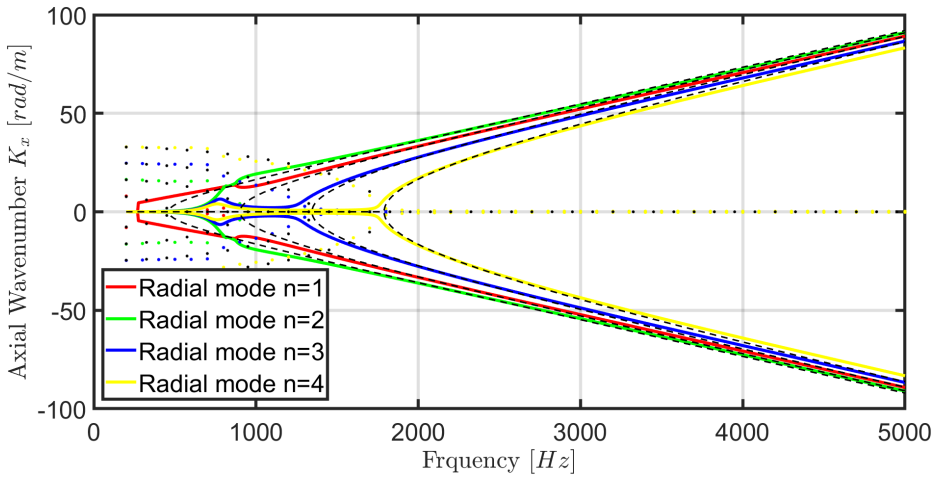

(a) Case considering the absence of uniform mean flow $M_0 = 0$

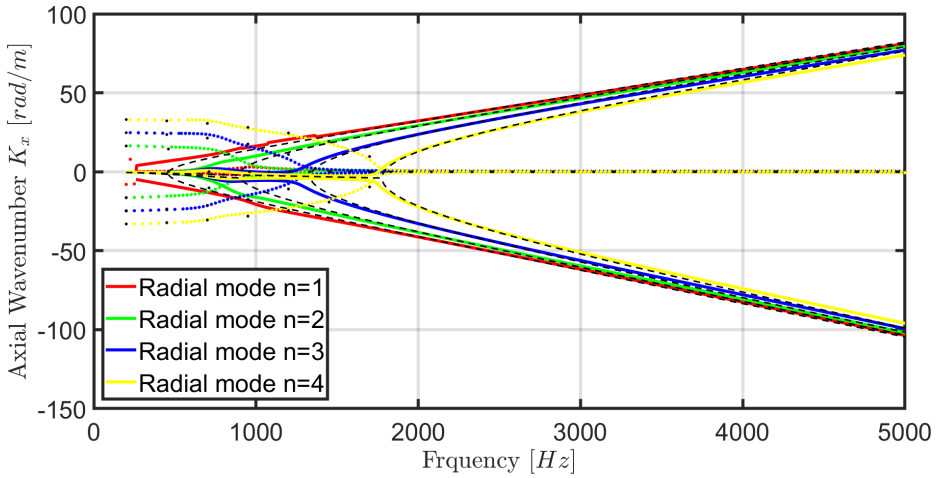

(b) Case considering the presence of uniform mean flow $M_0 = 0.12$

Figure 5.22: Dispersion curve for a finite impedance case for the circumferential mode $m = 0$ and radial modes $n = 1, 2, 3, 4$,considering two degrees of freedom model

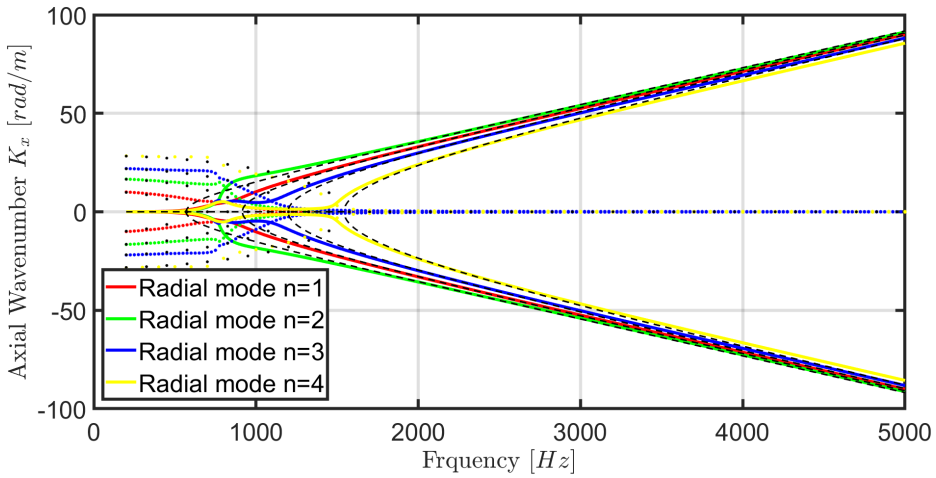

(a) Case considering the absence of uniform mean flow $M_0 = 0$

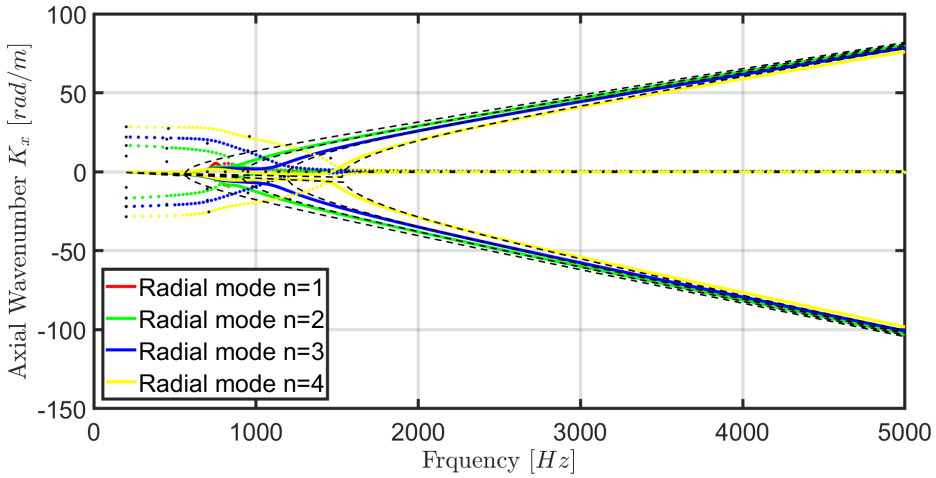

(b) Case considering the presence of uniform mean flow $M_0 = 0.12$

Figure 5.23: Dispersion curve for a finite impedance case for the circumferential mode $m = 5$ and radial modes $n = 1, 2, 3, 4$,considering two degrees of freedom model

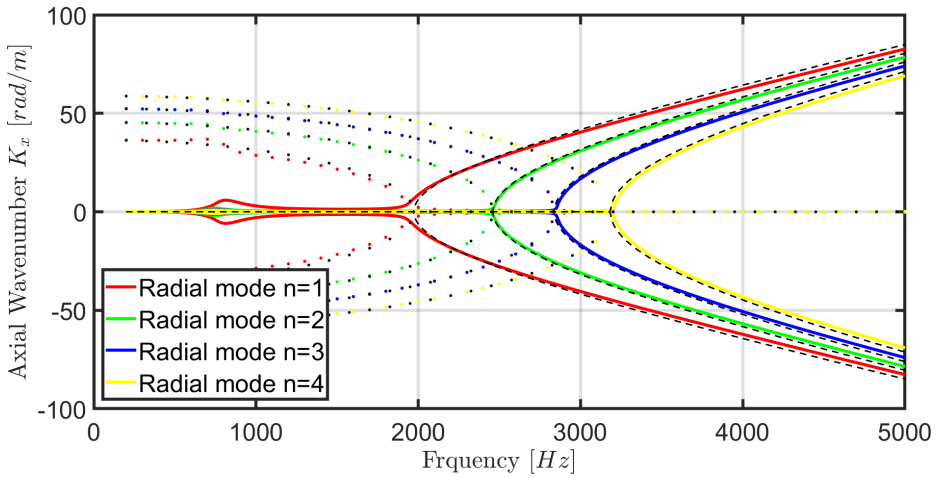

(a) Case considering the absence of uniform mean flow $M_0 = 0$

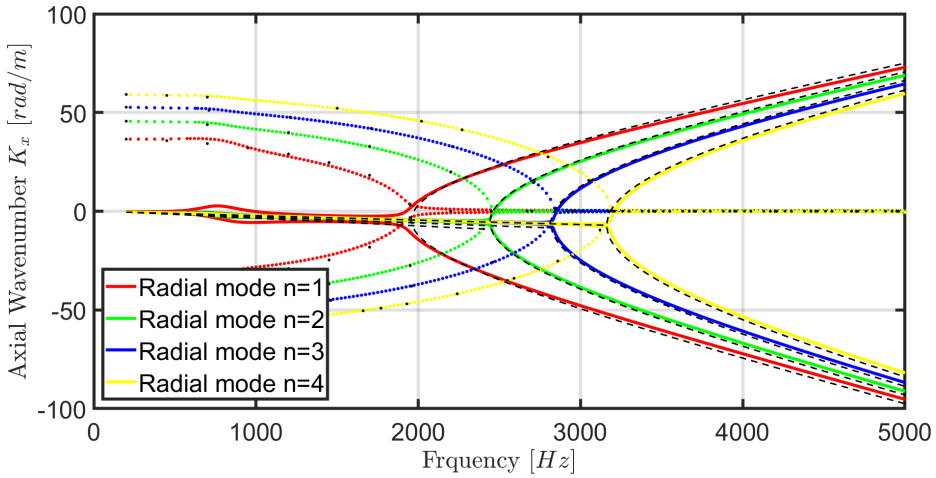

(b) Case considering the presence of uniform mean flow $M_0 = 0.12$

Figure 5.24: Dispersion curve for a finite impedance case for the circumferential mode $m = 20$ and radial modes $n = 1, 2, 3, 4$,considering two degrees of freedom model

Analysing the impedance profile for the 2 degrees of freedom case, it is clear that there is a resonant frequency where the value for the impedance is maxed, therefore it was expected locally resonant effects on the dispersion curves. However, as the impedance made all the axial wavenumbers become complex numbers, as it was analysed in the previous cases and shown in the figures 5.22 to 5.24, the locally resonant effect does not appear in the same frequency as the impedance profile in the figure 5.21 preconised. The cut-on frequency, as in the previous cases, decreased in comparison to the hardwall case.

The figures (b)'s from the figures 5.22 to 5.24 show that the introduction of the uniform mean flow again diminished the liner effects as well introduced the asymmetry about the frequency axis, aforementioned. It is possible to observe that the radial mode $n = 2$ is the one which suffered the greatest impact from the presence of the liner for this model as in the figures 5.23 (a) and (b) the mode had its cut-frequency greatly decreased and its imaginary parcel enhanced making such mode almost converging to the mode $n = 1$ as presented in figure 5.23 (b).

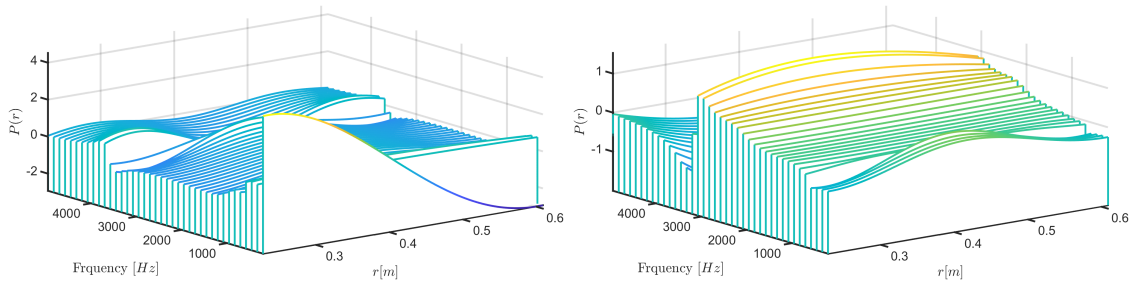

(a) Radial pressure fluctuation $n = 1$

(b) Radial pressure fluctuation $n = 2$

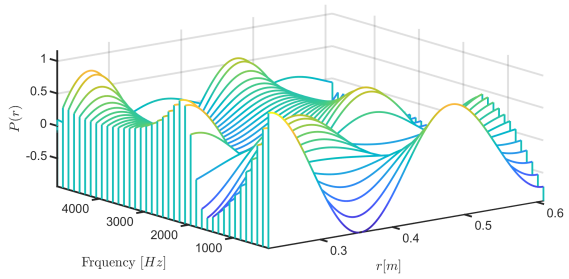

(c) Radial pressure fluctuation $n = 3$

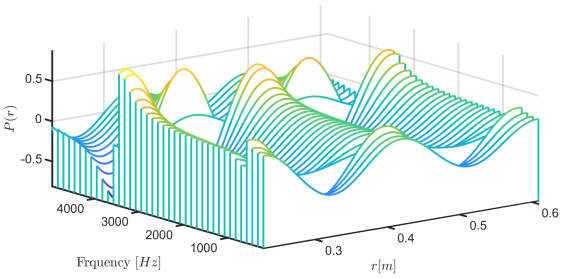

(d) Radial pressure fluctuation $n = 4$

Figure 5.25: Radial mode shape (radial pressure fluctuation) throughout the frequency for mode $m = 0$ $n = 1, 2, 3, 4$, $M_0 = 0$, considering the 2 degree of freedom model

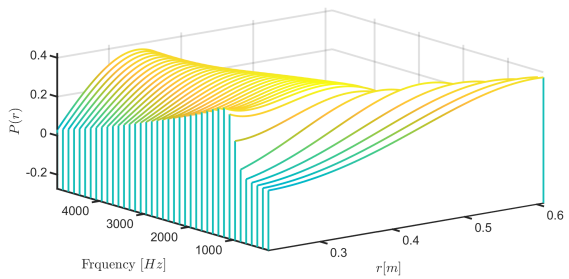

(a) Radial pressure fluctuation $n = 1$

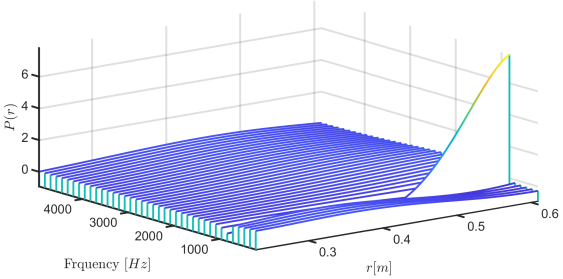

(b) Radial pressure fluctuation $n = 2$

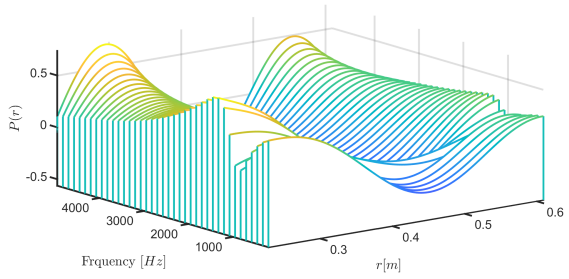

(c) Radial pressure fluctuation $n = 3$

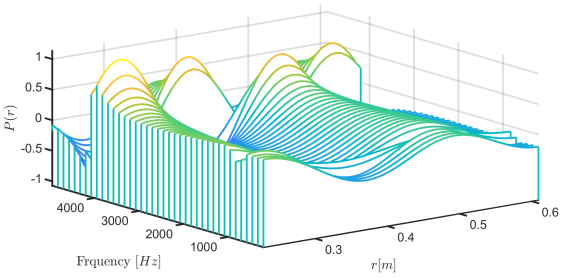

(d) Radial pressure fluctuation $n = 4$

Figure 5.26: Radial mode shape (radial pressure fluctuation) throughout the frequency for mode $m = 5$ $n = 1, 2, 3, 4$, $M_0 = 0$, considering the 2 degree of freedom model

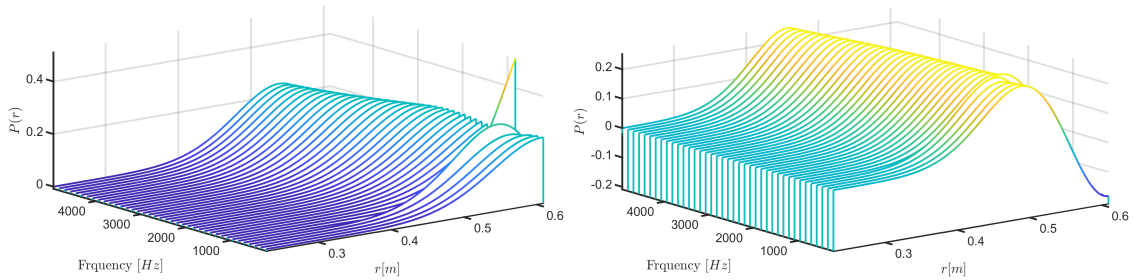

(a) Radial pressure fluctuation $n = 1$

(b) Radial pressure fluctuation $n = 2$

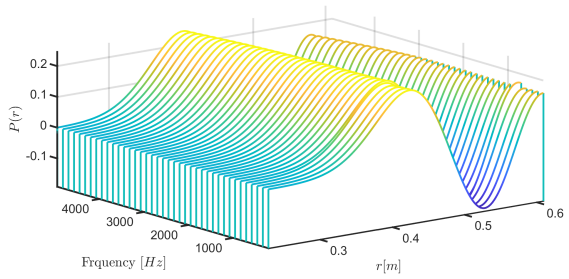

(c) Radial pressure fluctuation $n = 3$

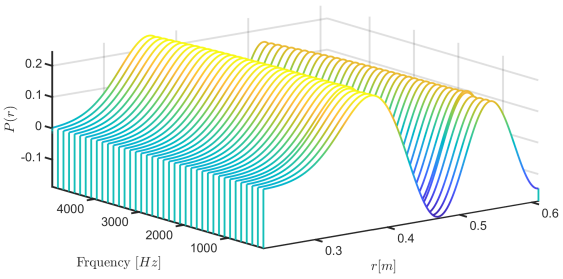

(d) Radial pressure fluctuation $n = 4$

Figure 5.27: Radial mode shape (radial pressure fluctuation) throughout the frequency for mode $m = 20$ $n = 1, 2, 3, 4$, $M_0 = 0$, considering the 2 degree of freedom model

All the cases analysed showed the presence of a little peak around the frequency of 800 Hz that is less perceptible for the cases with a uniform mean flow and also for higher-order modes. In order to clarify its presence, the radial modal shapes were evaluated for all the modes considered and as the figures from 5.25 to 5.27 show it may be differences in amplitude and phase throughout the frequency, however, the mode shape is preserved which leads to the conclusion that appearance of such a peak is an effect due to the liner model considered.

5.3 Parametric Analysis of the Two Degrees of Freedom Liner Model

In order to observe the effects of the changes in the geometrical parameters of the liner, the two degrees of freedom liner model was chosen in order to evaluate the effects of each parameter on the impedance profile. Such analysis is important in order to obtain an understanding of how can the liner parameters be tuned in order to obtain the necessary attenuation.

For this analysis, the parameters presented by Burd [14], summarised in the table 5.3 will be taken as base. Each parameter will be evaluated by varying it in a certain range while the other liner characteristics remain constant. The parameter evaluated will be the face sheet thickness, septum thickness, face sheet hole diameter, septum hole diameter, face sheet open area ratio, septum open area ratio, depth of the septum positioning and depth of the back plate positioning.

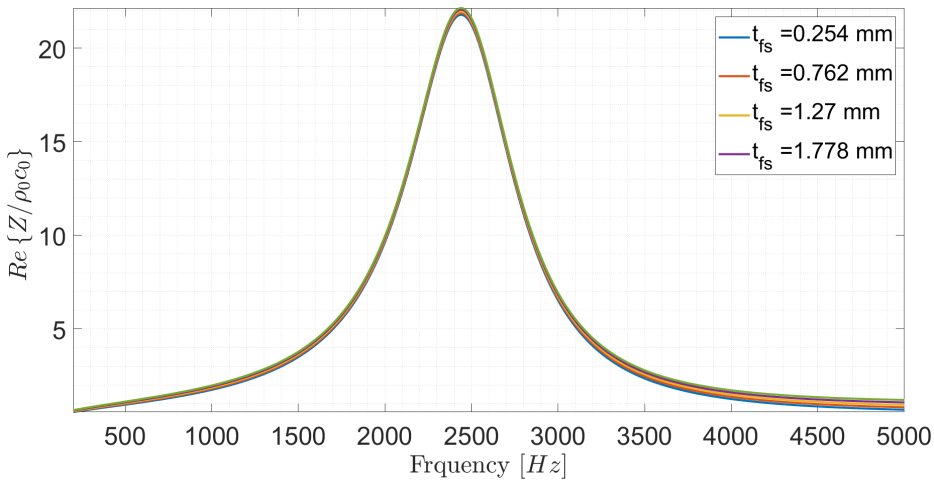

Figure 5.28: Effect of the variation of the liner face sheet thickness on the two degrees of freedom model reactance

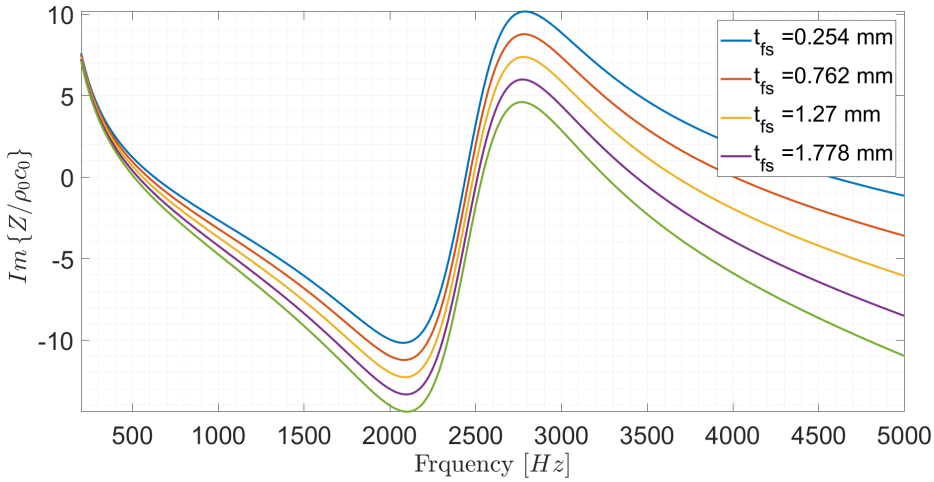

Figure 5.29: Effect of the variation of the liner face sheet thickness on the two degrees of freedom model resistance

It is possible to observe through the figures 5.28 and 5.29 that the values of the face sheet thickness have little impact on the reactance on the other hand the resistance decreases as the thickness of the face plate gradually increases. This is comprehensible as the resistance is related to the inertial effects on the cavity and neck of the resonator therefore changing values of the neck will affect the liner resistance.

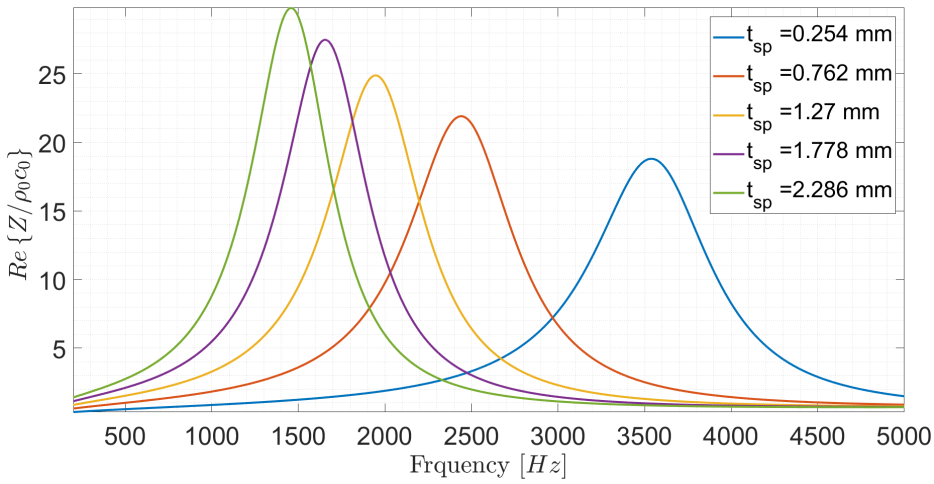

Figure 5.30: Effect of the variation of the liner septum thickness on the two degrees of freedom model reactance

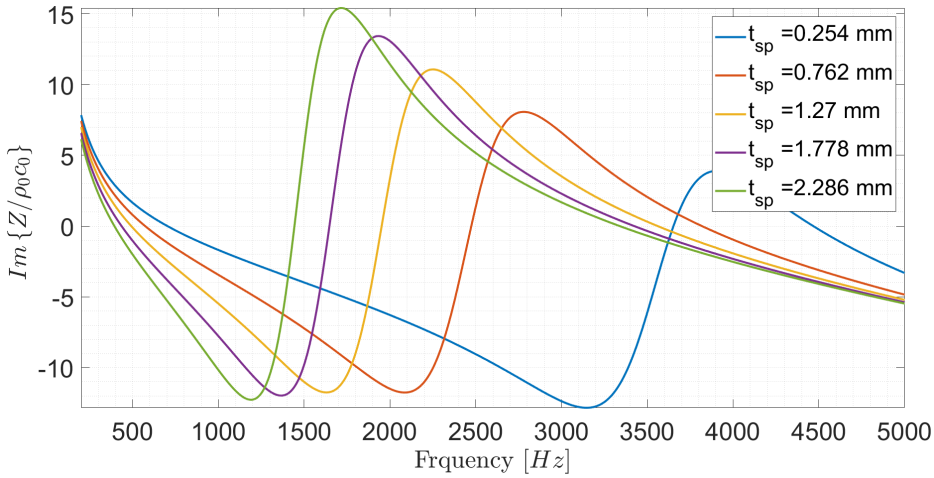

Figure 5.31: Effect of the variation of the liner septum thickness on the two degree of freedom model resistance

The thickness of the septum which is in general smaller than the thickness of the face sheet, also alters the values for the reactance however, the figures 5.30 and 5.31 shows that it has impacts on the reactance, changing its amplitude and resonance frequency where the thicker is the septum the lower is the resonance frequency and higher is the amplitude.

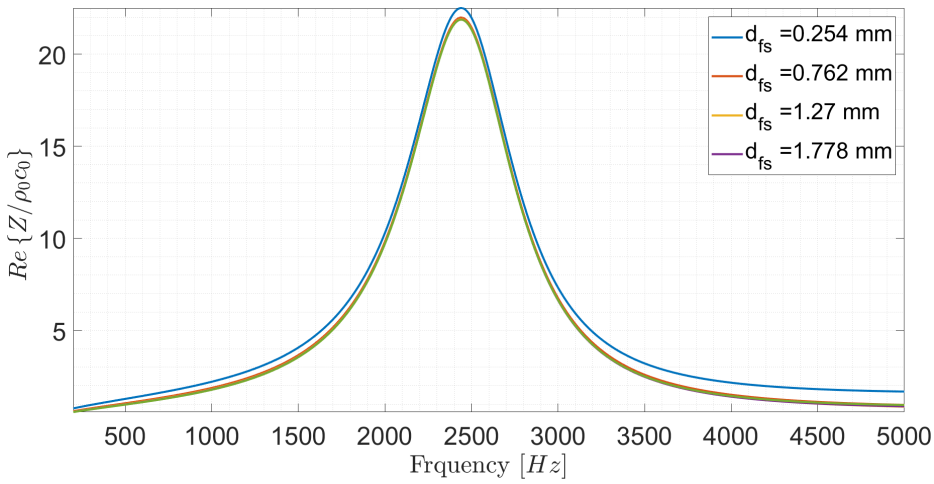

Figure 5.32: Effect of the variation of the liner face sheet holes diameter on the two degree of freedom model reactance

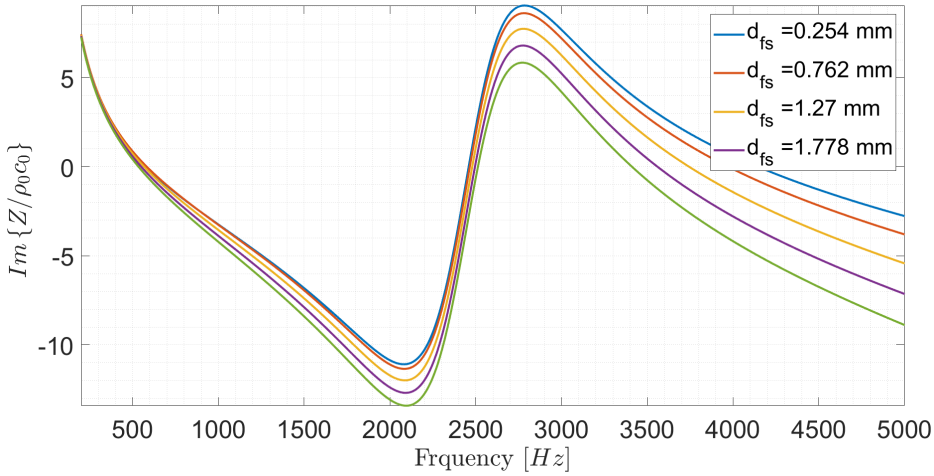

Figure 5.33: Effect of the variation of the liner face sheet holes diameter on the two degrees of freedom model resistance

The diameter of the holes present on the face sheet has similar effects as its thickness, having little impact on the reactance and leading to decay of the resistance as the diameter increases.

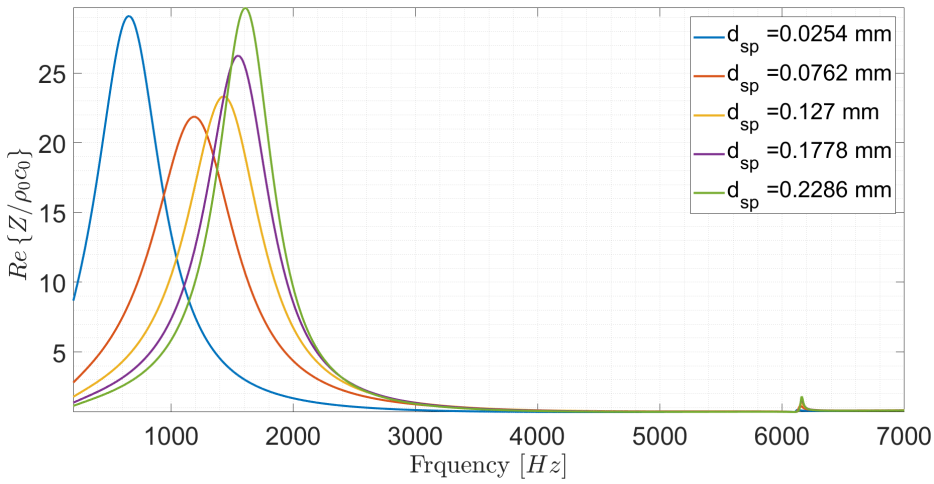

Figure 5.34: Effect of the variation of the liner septum holes diameter on the two degrees of freedom model reactance

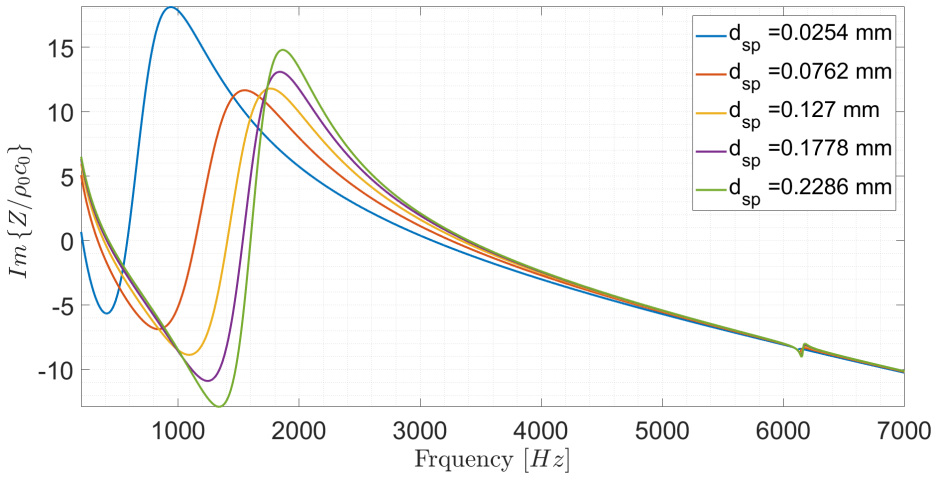

Figure 5.35: Effect of the variation of the liner septum holes diameter on the two degrees of freedom model resistance

The values for the septum holes lead to an increment in the resonant frequency however, there is no explicit relation to the amplitude. Therefore those parameters have a great influence when setting the liner operational frequency.

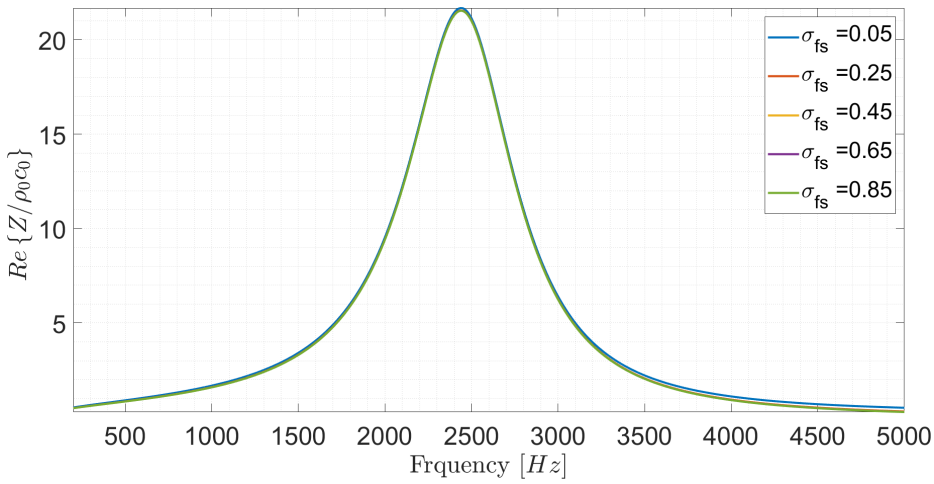

Figure 5.36: Effect of the variation of the liner face sheet open area ratio on the two degrees of freedom model reactance

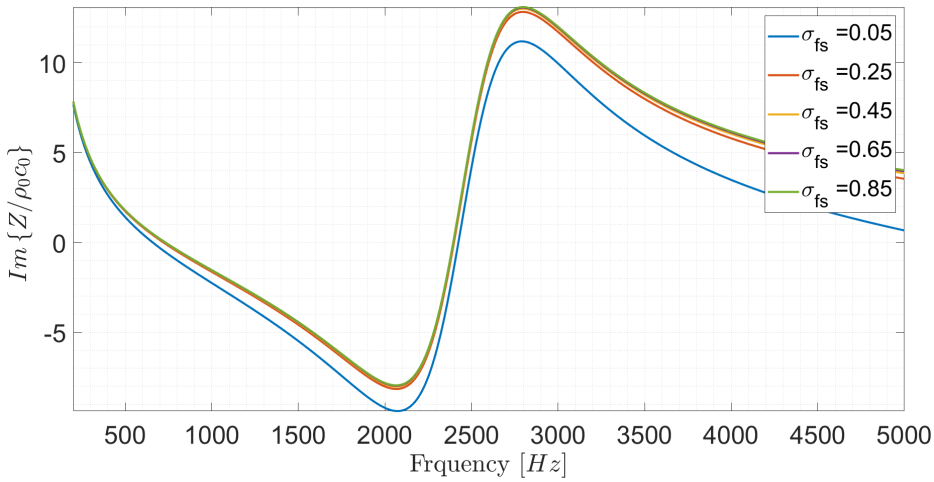

Figure 5.37: Effect of the variation of the liner face sheet open area ratio on the two degrees of freedom model resistance

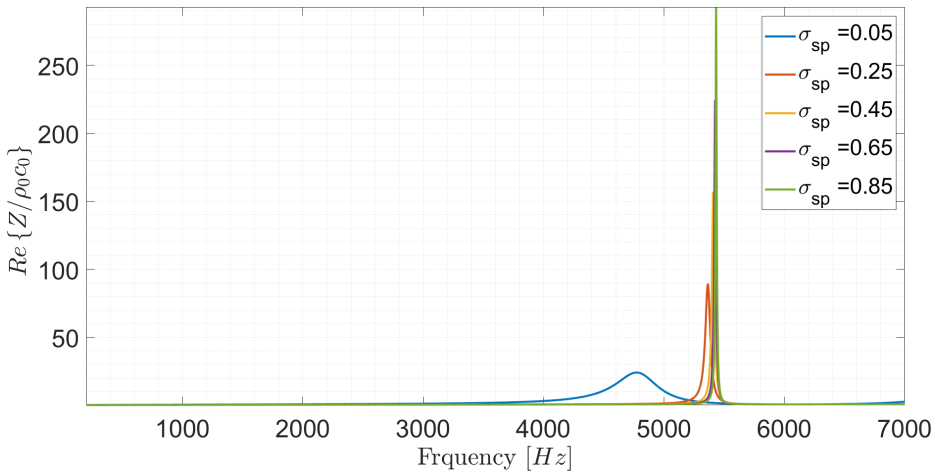

Figure 5.38: Effect of the variation of the liner face sheet open area ratio on the two degrees of freedom model reactance

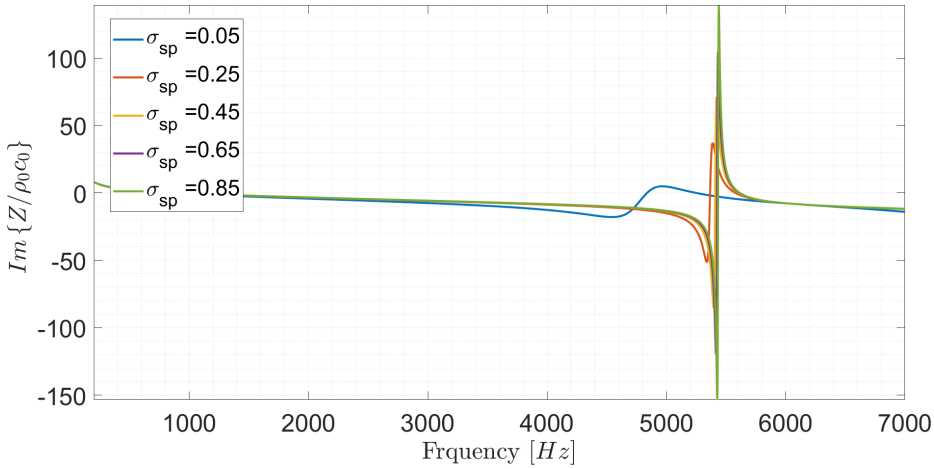

Figure 5.39: Effect of the variation of the liner face sheet open area ratio on the two degrees of freedom model resistance

The figures 5.36 to 5.39 present the effects of the variation in the open area ratio, by evaluating those effects for the face sheet and for the septum it is observed that increasing the number of holes in the face sheet has little impact on the impedance nevertheless, increasing the percentage of the open area for the septum decreases the bandwidth where the liner acts, therefore the effects can be more locally resonant the more open area ratio the septum has.

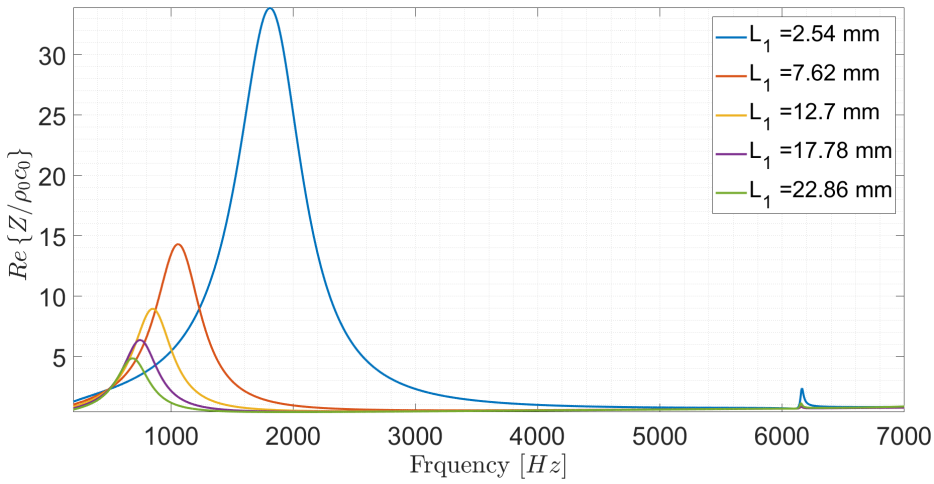

Figure 5.40: Effect of the variation of the depth of the septum positioning on the two degrees of freedom model reactance

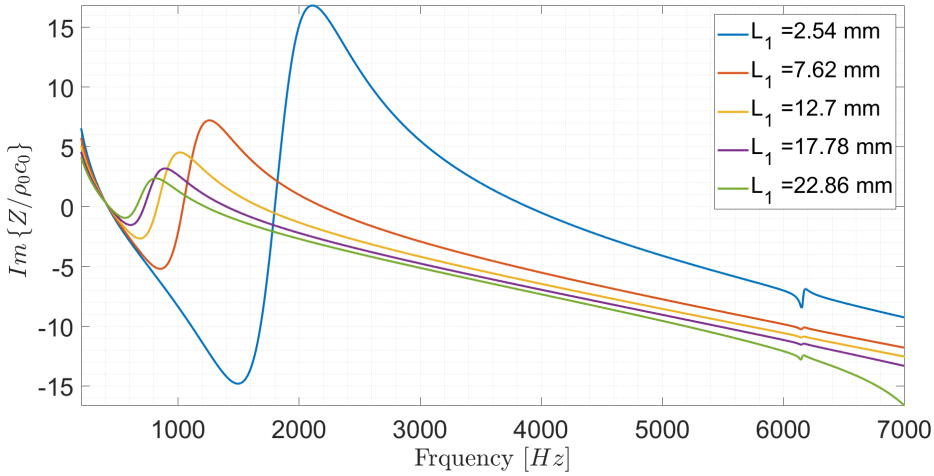

Figure 5.41: Effect of the variation of the depth of the septum positioning on the two degrees of freedom model resistance

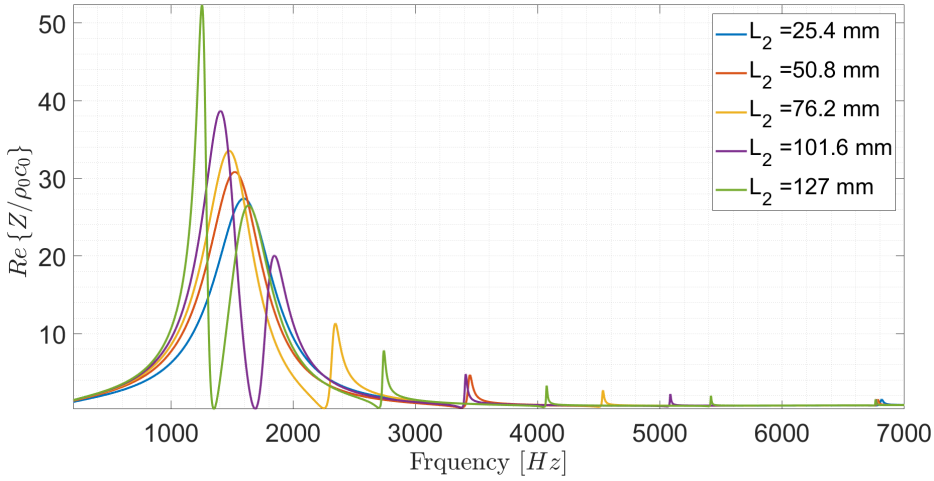

Figure 5.42: Effect of the variation of the depth of the back plate positioning on the two degrees of freedom model reactance

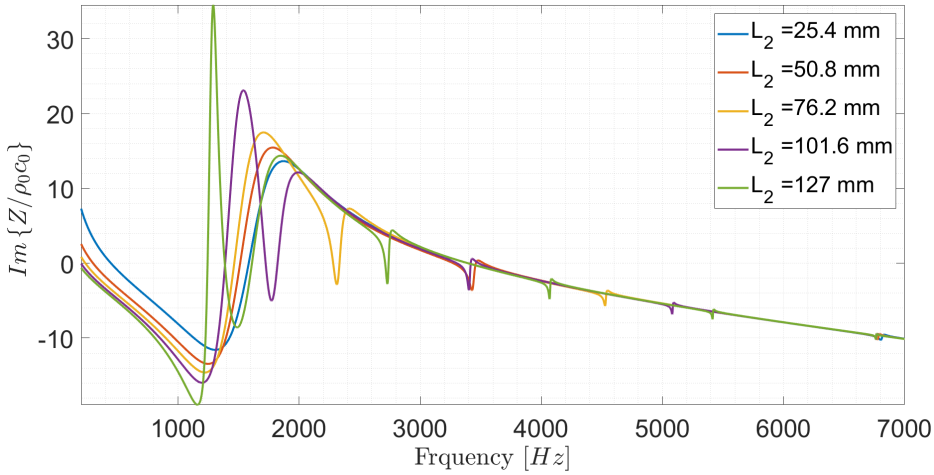

Figure 5.43: Effect of the variation of the depth of the back plate positioning on the two degrees of freedom model resistance

By analysing the figures 5.40 to 5.43 it is possible to infer that changing the position of the septum is the same as altering the length of the cavity of the first Helmholtz resonator therefore the inertial effects on the cavity also changes leading to impacts on the impedance. For the septum positioning, the greater the length of the cavity lower the resonant frequency, also the amplitude and the bandwidth for the reactance and resistances decays with the depth increment. The positioning of the back plate follows the same idea however as the depth of the back plate is usually significantly greater than the depth of the septum its effects are also greater, as the depth increases the bandwidth decays and the resonant first resonant frequency decays however, smaller peaks start appearing on greater frequencies.

Hence, by evaluating the effects of each parameter on the impedance profile it is possible to tune those values to attain a specific characteristic to attenuate more certain modes excited by the operational conditions. Also, it is possible to observe that the values related to the septum

characteristics have a great impact on the two degrees of freedom model therefore altering it can be one of the most efficient ways to attain the desired impedance values.

As an example, the values present in Burd's work were altered in order to obtain a different attenuation. The idea is to reduce the bandwidth of the reactance while increasing its amplitude as a consequence the same is expected to happen with the resistance. In order to attain the desired result, only the septum characteristics were modified the values considered are presented in the table 5.4

Table 5.4: Double degree of freedom liner geometrical parameters modified

Parameter	Value
$\sigma_{opr,fs}$	0.02
t	$1.016\,mm$
d	1.0922
$\sigma_{opr,s}$	0.25
d_s	0.2032
t_s	$0.7620\,mm$
L_1	$3.3020\,mm$
L_2	$53.5254\,mm$

By considering an open area ratio for the septum of $\sigma_{sp} = 0.25$ and the depth of the back plate as approximately $53.5\,mm$ the bandwidth of the reactance was decreased and the its frequency tuned around $2700\,Hz$ therefore the impedance profile in the figure 5.44 was obtained.

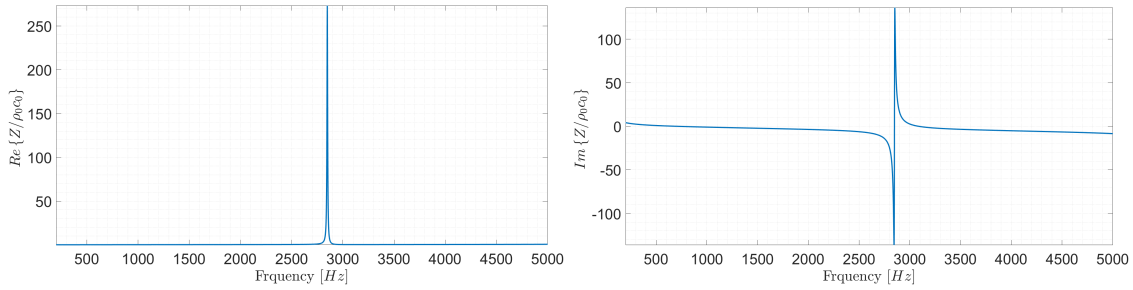

(a) Double degree of freedom model reactance (b) Double degree of freedom model resistance

Figure 5.44: Double degree of freedom (a) real and (b) imaginary impedance profiles for the modified parameters

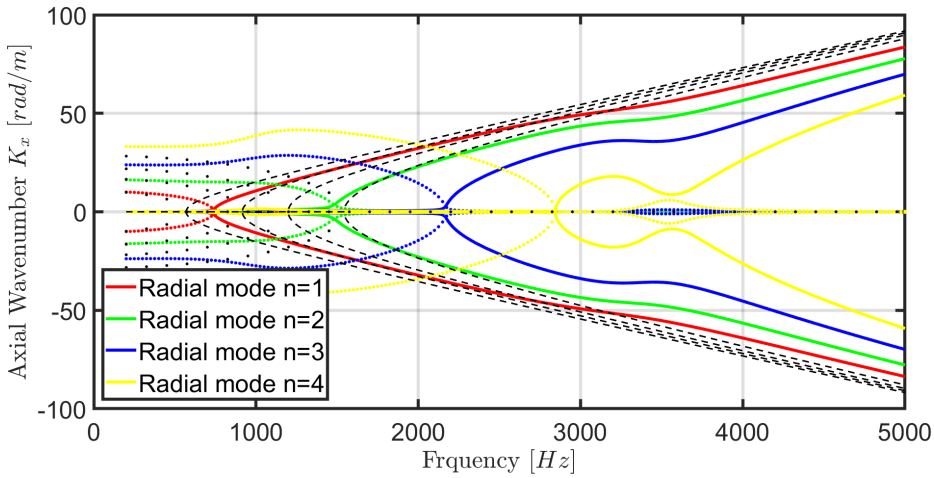

Figure 5.45: Dispersion curves for the mode $m = 5$, $n = 1, 2, 3, 4$ for the modified double degree of freedom parameters

In order to evaluate the effects of the impedance profile obtained, the dispersion curves for the circumferential mode $m = 5$ were generated. The figure 5.45 shows the effect of the considered liner on the first four radial wavenumbers. It is possible to observe that the cut-on frequency was increased as the curves are displaced to the right when compared to the hardwall reference lines. Each mode obtained a great imaginary parcel and it is possible to observe that from $2700\,Hz$, which is the resonant frequency for the obtained impedance profile, all the modes are attenuated and at some point, the derivatives of the curves become null indicating that the modes do not propagate as their group velocity is zero.

Chapter 6

Conclusions

In the present work, a semi-analytical investigation of the acoustic modes in annular lined ducts resultant of the rotor-stator interaction was proposed. Based on the theory of noise generation and propagation in ducts and analysing the shapes of the modes, it can be seen that with the exception of a plane wave all modes propagate in the form of helical waves, that is, they are rotating modes. The radial modes are propagated only if their phase velocity in the circumferential direction at the wall of the duct is greater than the speed of sound. There is a reduction in the cut-on frequency given the presence of flow where, the acoustic modes are propagated only above this frequency that depends on the flow velocity, the speed of sound in the medium and rotor parameters such as the number of blades and the rotor rotation frequency.

It was shown that in the presence of a liner in the duct wall, modelled by a finite impedance that varies as a function of the operational conditions and frequency, the radial modes gain an imaginary part that is not present for the hard wall case. Such fact implies modifications in the behaviour of the axial wavenumber as they pass to be a complex number even for propagating modes, thus adding an attenuation component that comes from the presence of the liner. The consideration of a duct with a liner drastically increases the complexity of the problem where the roots that dictate the circumferential modes become dependent of the frequency, flow velocity and boundary impedance. As the impedance of a liner also varies with frequency, the calculation of σ_{mn} must be performed given this variation so that one can observe the real effects of a liner on the propagation of the wave. A modified Muller's method was proposed to compute the radial wavenumbers. It was shown in the validation section that the Muller's method applied to the proposed formulation presents robust results, when compared to the literature, in a very low computational cost.

Different impedance models with different profiles throughout the frequency were analysed by evaluating the dispersion curves for the axial wavenumber obtained by the proposed semi-empirical scheme which uses an numerical root finding algorithm to calculate the complex roots of the transcendental equation arising from the analytical formulation. It is shown that they present significant qualitative and quantitative differences in terms of attenuation performance and main attenuation mechanism. In order to further understand the characteristics that arised from the dispersion curves for some of the models analysed the evaluation of the radial modal shape was

performed.

Also, the evaluation of each geometrical parameter of the liner construction was studied. The inserted effects by the variation of those parameters were interpreted and such, a modified impedance model based on the real liner was devised and its effects on the dispersion curves discussed as form of validation of the practical applicability of the methodology proposed in the present work.

The proposed approach has the potential of being used as a low cost computational design methodology for acoustic attenuation in lined ducts. Future work includes investigating different liner models on the attenuation performance and using the presented method as a benchmark for further non-linear analysis and parametric studies involving Machine Learning to assess the parameter sensitivity when very low-cost calculations are needed. Also the insertion of a more robust root finding algorithm can prove itself worth in order to decrease numerical error and sensitivity to the initial guesses.

REFERÊNCIAS BIBLIOGRÁFICAS

[1] SMITH, M. J. Aircraft noise. Cambridge University Press, 2004.

[2] SPILLERE, A. M. N. et al. Towards optimal design of acoustic liners in turbofan aero-engines. Universidade Federal de Santa Catarina, 2017.

[3] WECKMÜLLER, C.; GUÉRIN, S.; ASHCROFT, G. Cfd/caa coupling applied to dlr uhbr-fan: Comparison to experimantal data. In: *15th AIAA/CEAS Aeroacoustics Conference (30th AIAA Aeroacoustics Conference)*. [S.l.: s.n.], 2009. p. 3342.

[4] LI, Q.; PEAKE, N.; SAVILL, M. Large eddy simulation for fan-ogv broadband noise prediction. In: *14th AIAA/CEAS Aeroacoustics Conference (29th AIAA Aeroacoustics Conference)*. [S.l.: s.n.], 2008. p. 2843.

[5] PASCUAL, B. J. *A Study of the Viscous Effects over an Acoustic Liner using the Linearised Navier-Stokes equations in the Frequency Domain*. 2016.

[6] MOTSINGER, R.; KRAFT, R. Design and performance of duct acoustic treatment. 1991.

[7] MASON, W. H. Configuration aerodynamics. *Virginia Tech*, p. 3–41, 2006.

[8] PIMENTA, B. G. Simulação numérica de ondas não-lineares em dinâmica dos gases e ruído de interação rotor-estator em turbofans aeronáuticos. *Universidade de Brasília*, 2016.

[9] GLEGG, S.; DEVENPORT, W. Aeroacoustics of low mach number flows: fundamentals, analysis, and measurement. Academic Press, 2017.

[10] MALDONADO, A. L. P. *On the Prediction of the Effect of Interstage Liners in Turbofan Engines*. Tese (Doutorado) — University of Southampton, 2015.

[11] SUTLIFF, D. L. A 20 year retrospective of the advanced noise control fan–contributions to turbofan noise research. In: *AIAA Propulsion and Energy 2019 Forum*. [S.l.: s.n.], 2019. p. 3824.

[12] TAM, C. K.; AURIAULT, L. Time-domain impedance boundary conditions for computational aeroacoustics. *AIAA journal*, v. 34, n. 5, p. 917–923, 1996.

[13] BUSSE-GERSTENGARBE, S. et al. Impedance eduction based on microphone measurements of liners under grazing flow conditions. *AIAA journal*, v. 50, n. 4, p. 867–879, 2012.

[14] BURD, D. et al. Effects of two dof lining tolerances on modeled inlet acoustic attenuation. In: CITESEER. *15th AIAA/CEAS Aeroacoustics Conference, Miami*. [S.l.], 2009.

[15] SÁNCHEZ, J. R. *Étude théorique et numérique des modes propres acoustiques dans un conduit avec écoulement et parois absorbantes*. Tese (Doutorado) — Toulouse, ISAE, 2016.

[16] ORGANIZATION, W. H. et al. *Burden of disease from environmental noise: Quantification of healthy life years lost in Europe*. [S.l.]: World Health Organization. Regional Office for Europe, 2011.

[17] ENVIRONMENTAL Technical Manual Volume I: Procedures for the Noise Certification of Aircraft. 3rd. ed. [S.l.]: ICAO, 2018.

[18] MISERDA, R. F. B.; PIMENTA, B. G.; ROCHA, L. S. da. Numerical Simulation of Rotor-Stator Interaction Noise in Transonic Cascades. *Jounal of Propulsion and Power*, v. 36, n. 3, May-June 2020.

[19] TESTER, B. Some aspects of "sound" attenuation in lined ducts containing inviscid mean flows with boundary layers. *Journal of Sound and Vibration*, Elsevier, v. 28, n. 2, p. 217–245, 1973.

[20] TESTER, B. Acoustic energy flow in lined ducts containing uniform or "plug" flow. *Journal of Sound and Vibration*, Elsevier, v. 28, n. 2, p. 205–215, 1973.

[21] MAUNUS, J.; GRACE, S. M.; SONDAK, D. L. Effect of rotor wake structure on fan interaction tone noise. *AIAA journal*, v. 50, n. 4, p. 818–831, 2012.

[22] POLACSEK, C. et al. Numerical simulations of fan interaction noise using a hybrid approach. *AIAA journal*, v. 44, n. 6, p. 1188–1196, 2006.

[23] SHARMA, A. et al. Numerical prediction of exhaust fan-tone noise from high-bypass aircraft engines. *AIAA journal*, v. 47, n. 12, p. 2866–2879, 2009.

[24] GRACE, S. et al. Hybrid prediction of fan tonal noise. In: *14th AIAA/CEAS Aeroacoustics Conference (29th AIAA Aeroacoustics Conference)*. [S.l.: s.n.], 2008. p. 2992.

[25] HASE, T.; YAMASAKI, N.; OOISHI, T. Numerical simulation for fan broadband noise prediction. *Journal of Thermal Science*, Springer, v. 20, n. 1, p. 58–63, 2011.

[26] HU, B.-b. et al. Numerical prediction of the interaction noise radiated from an axial fan. *Applied acoustics*, Elsevier, v. 74, n. 4, p. 544–552, 2013.

[27] KAZAWA, J. et al. Numerical study on fan noise generated by rotor-stator interaction. In: *13th AIAA/CEAS Aeroacoustics Conference (28th AIAA Aeroacoustics Conference)*. [S.l.: s.n.], 2007. p. 3681.

[28] DUNN, M.; TWEED, J.; FARASSAT, F. The application of a boundary integral equation method to the prediction of ducted fan engine noise. *Journal of sound and vibration*, Elsevier, v. 227, n. 5, p. 1019–1048, 1999.

[29] ASTLEY, R.; HII, V.; GABARD, G. A computational mode matching approach for propagation in three-dimensional ducts with flow. In: *12th AIAA/CEAS Aeroacoustics Conference (27th AIAA Aeroacoustics Conference)*. [S.l.: s.n.], 2006. p. 2528.

[30] ASTLEY, R.; CUMMINGS, A. A finite element scheme for attenuation in ducts lined with porous material: comparison with experiment. *Journal of Sound and Vibration*, Elsevier, v. 116, n. 2, p. 239–263, 1987.

[31] EVERSMAN, W. Effect of local impedance variation and non-linearity on multiple tone attenuation. In: *16th AIAA/CEAS Aeroacoustics Conference*. [S.l.: s.n.], 2010. p. 3825.

[32] SACK, S.; ÅBOM, M. Modal filters for mitigation of in-duct sound. In: ACOUSTICAL SOCIETY OF AMERICA. *Proceedings of Meetings on Acoustics 172ASA*. [S.l.], 2016. v. 29, n. 1, p. 040004.

[33] MEDURI, S. S. S.; SUNDARAM, V. et al. *A Novel Approach to Optimize the Resonators for Air Induction System*. [S.l.], 2016.

[34] TAM, C. K.; KURBATSKII, K. A. Microfluid Dynamics and Acoustics of Resonant Liners. *AIAA journal*, v. 38, n. 8, p. 1331–1339, 2000.

[35] BIELAK, G. W.; HERSH, A. S. Advanced turbofan duct liner concepts. NASA Langley Technical Report Server, 1999.

[36] TAM, C. K. *Computational Aeroacoustics: A Wave Number Approach*. [S.l.]: Cambridge University Press, 2012.

[37] RIENSTRA, S. Impedance models in time domain, including the extended helmholtz resonator model. In: *12th AIAA/CEAS Aeroacoustics Conference (27th AIAA Aeroacoustics Conference)*. [S.l.: s.n.], 2006. p. 2686.

[38] ESCOUFLAIRE, M. *Theoretical and Numerical Investigation of Time-Domain Impedance Models for Computational AeroAcoustics*. Tese (Doutorado) — Le Mans, 2014.

[39] MALMARY, C. *Etude théorique et expérimentale de l'impédance acoustique de matériaux en présence d'un écoulement d'air tangentiel*. Tese (Doutorado) — Le Mans, 2000.

[40] GUESS, A. Calculation of perforated plate liner parameters from specified acoustic resistance and reactance. *Journal of Sound and Vibration*, Elsevier, v. 40, n. 1, p. 119–137, 1975.

[41] KINSLER, L. E. et al. *Fundamentals of acoustics*. [S.l.]: John wiley & sons, 2000.

[42] MORSE, P. M.; INGARD, K. U. *Theoretical acoustics*. [S.l.]: Princeton university press, 1986.

[43] INGARD, U. On the theory and design of acoustic resonators. *The Journal of the acoustical society of America*, Acoustical Society of America, v. 25, n. 6, p. 1037–1061, 1953.

[44] RICE, E. J. *A model for the acoustic impedance of a perforated plate liner with multiple frequency excitation*. [S.l.], 1971.

[45] INGARD, U.; ISING, H. Acoustic nonlinearity of an orifice. *The journal of the Acoustical Society of America*, Acoustical Society of America, v. 42, n. 1, p. 6–17, 1967.

[46] HIRSCHBERG, A.; RIENSTRA, S. W. An introduction to aeroacoustics. *Eindhoven university of technology*, 2004.

[47] BUTKOV, E. Física matemática, ed. *Guanabara, Rio de Janeiro*, 1988.

[48] MYERS, M. On the acoustic boundary condition in the presence of flow. *Journal of Sound and Vibration*, Elsevier, v. 71, n. 3, p. 429–434, 1980.

[49] WAKI, Y. *On the application of finite element analysis to wave motion in one-dimensional waveguides*. Tese (Doutorado) — University of Southampton, 2007.

[50] KOUSEN, K. A. Eigenmodes of ducted flows with radially-dependent axial and swirl velocity components. 1999.

[51] VO, P.; EVERSMAN, W. A method of weighted residuals with trigonometric basis functions for sound transmission in circular ducts. *Journal of Sound and Vibration*, Elsevier, v. 56, n. 2, p. 243–250, 1978.

[52] MACE, B. R.; MANCONI, E. Wave motion and dispersion phenomena: Veering, locking and strong coupling effects. *The Journal of the Acoustical Society of America*, v. 131, p. 1015–1028, 2 2012. ISSN 0001-4966. Disponível em: <https://asa.scitation.org/doi/10.1121/1.3672647>.

[53] ARFKEN, G. B.; WEBER, H. J. *Mathematical methods for physicists*. [S.l.]: AAPT, 1999.

[54] BATCHELOR, C. K.; BATCHELOR, G. *An introduction to fluid dynamics*. [S.l.]: Cambridge university press, 2000.

Appendix A

Curvilinear Coordinate Theory

Often the physical problems are described in Cartesian coordinates, the Cartesian coordinate system has a great advantage that all three unit vectors ($\hat{x}$, $\hat{y}$, $\hat{z}$) are constant in both direction and magnitude. However, not all physical problems are well expressed in the Cartesian coordinate system [53].

In this way, the coordinate system must be chosen in a way that fits the problem in such a manner that any restrictions or symmetries that the problem presents can be explored. Thus, a solution can be obtained following a simpler path.

Naturally , there is a price to pay for using non-Cartesian coordinates. Expressions for vector calculus should be developed in a general way that is consistent with the proposed [53] system

In a Cartesian coordinate system, we deal with three families of mutually perpendicular planes where $x = cte$, $y = cte$, $z = cte$. Thus, to define a curvilinear system, three other families of surfaces are superimposed on this system.

$$q_i(x, y, z) \text{ onde } i = 1, 2 \text{ ou } 3 \tag{A.1}$$

where none of the surfaces of the family q_i need to be parallel to each other or plane. Such surfaces also do not need to be mutually perpendicular, but for reasons of simplification, such a condition is imposed since, in physical application problems, orthogonal systems are more common and adequate. The orthogonality of the system implies that infinitesimal areas and infinitesimal volumes are products of coordinate differencials.

Given these assumptions, one can develop the formalism for orthogonal curvilinear coordinates by deriving the differential coordinates from geometry and using them as line, area, and volume elements for vector operations.

Any point in space can be described as the intersection of Cartesian planes or the intersection of the surfaces of the curvilinear system. Describing the curvilinear coordinates as $q_1 = cte$, $q_2 = cte$, $q_3 = cte$, one can identify the point by (q_1, q_2, q_3) as well as by (x, y, z)

$$
\begin{aligned}
& q_1, q_2, q_3 \\
x &= x(q_1, q_2, q_3) \\
y &= y(q_1, q_2, q_3) \\
z &= z(q_1, q_2, q_3)
\end{aligned} \tag{A.2}
$$

$$
\begin{aligned}
q_1 &= q_1(x, y, z) \\
q_2 &= q_2(x, y, z) \\
q_3 &= q_3(x, y, z)
\end{aligned} \tag{A.3}
$$

With each surface family $q_i = cte$, one can associate a unit vector $\hat{q_i}$ normal to its respective surface and in the direction of growth. In general these unit vectors will depend on their position in space. So a vector $\boldsymbol{V}$ can be written as

$$
\boldsymbol{V} = \hat{q_1} V_1 + \hat{q_2} V_2 + \hat{q_3} V_3 \tag{A.4}
$$

Differentiating the equation A.2 in x, we have that

$$
dx = \frac{\partial x}{\partial q_1} dq_1 + \frac{\partial x}{\partial q_2} dq_2 + \frac{\partial x}{\partial q_3} dq_3 \tag{A.5}
$$

similarly, the same process can be carried out for the variables y and z, in vector notation we have

$$
d\boldsymbol{r} = \sum \frac{\partial \boldsymbol{r}}{\partial q_i} dq_i \tag{A.6}
$$

from the Pythagorean theorem in Cartesian coordinates the square of the distance between two points is given by

$$
ds^2 = dx^2 + dy^2 + dz^2 \tag{A.7}
$$

Substituting the equation A.6 in the equation A.7, we have

$$
\begin{aligned}
ds^2 = d\boldsymbol{r} \cdot d\boldsymbol{r} = d\boldsymbol{r}^2 = \sum \frac{\partial \boldsymbol{r}}{\partial q_i} \cdot \frac{\partial \boldsymbol{r}}{\partial q_j} dq_i dq_j = \\
g_{11} dq_1 dq_1 + g_{12} dq_1 dq_2 + g_{13} dq_1 dq_3 \\
g_{21} dq_2 dq_1 + g_{22} dq_2 dq_2 + g_{23} dq_2 dq_3 \\
g_{31} dq_1 dq_1 + g_{32} dq_1 dq_2 + g_{33} dq_3 dq_3 = \sum g_{ij} dq_i dq_j
\end{aligned} \tag{A.8}
$$

where

$$g_{ij}(q_1, q_2, q_3) = \frac{\partial x}{\partial q_i}\frac{\partial x}{\partial q_j} + \frac{\partial y}{\partial q_i}\frac{\partial y}{\partial q_j} + \frac{\partial z}{\partial q_i}\frac{\partial z}{\partial q_j} = \frac{\partial \boldsymbol{r}}{\partial q_i} \cdot \frac{\partial \boldsymbol{r}}{\partial q_j} \tag{A.9}$$

it is observed that the expression for g_{ij} is the dot product between the vectors tangent to the curves $\boldsymbol{r}$ for $q_j = cte$ and $j \neq i$. Collectively, these coefficients are referred to as the coordinate system metric.

Limiting ourselves to orthogonal systems, we have that

$$g_{ij} = 0 \text{ para } i \neq j \text{ e } \hat{q_i} \cdot \hat{q_j} = \delta_{ij} \tag{A.10}$$

and simplifying the notation as

$$g_{ii} = h_i^2 \tag{A.11}$$

therefore

$$ds^2 = (h_1 dq_1)^2 + (h_2 dq_2)^2 + (h_3 dq_3)^2 = \sum (h_i dq_i)^2 \tag{A.12}$$

Orthogonal coordinate systems are described by specifying these positive scaling factors h_1, h_2, h_3. On the other hand, scale factors can be identified by the relationships

$$ds_i = h_i dq_i, \ \frac{\partial \boldsymbol{r}}{\partial q_i} = h_i \hat{q_i} \tag{A.13}$$

for any q_i, keeping the other q constant. In this way the differential $d\boldsymbol{r}$ can be written as

$$d\boldsymbol{r} = h_1 dq_1 \hat{q_1} + h_2 dq_2 \hat{q_2} + h_3 dq_3 \hat{q_3} \tag{A.14}$$

The orthogonality of the coordinate system leads to

$$\frac{\partial \boldsymbol{r}}{\partial q_1} \cdot \frac{\partial \boldsymbol{r}}{\partial q_2} = 0 \tag{A.15}$$

with the two other similar relations [54] and having that

$$\frac{\partial}{\partial q_3}\left(\frac{\partial \boldsymbol{r}}{\partial q_1}\frac{\partial \boldsymbol{r}}{\partial q_2}\right) = \frac{\partial}{\partial q_1}\left(\frac{\partial \boldsymbol{r}}{\partial q_3}\right) \cdot \frac{\partial \boldsymbol{r}}{\partial q_2} + \frac{\partial \boldsymbol{r}}{\partial q_1}\frac{\partial}{\partial q_2}\left(\frac{\partial \boldsymbol{r}}{\partial q_3}\right) = -2\frac{\partial \boldsymbol{r}}{\partial q_3} \cdot \frac{\partial^2 \boldsymbol{r}}{\partial q_1 \partial q_2} \tag{A.16}$$

it can be observed that

$$\frac{\partial^2 \boldsymbol{r}}{\partial q_1 \partial q_2} = \frac{\partial h_2 \hat{q_2}}{\partial q_1} \text{ ou } \frac{\partial h_1 \hat{q_1}}{\partial q_2} \tag{A.17}$$

thus,

$$\frac{\partial \hat{q_1}}{\partial q_2} = \frac{1}{h_1}\frac{\partial h_2}{\partial q_1}\hat{q_2} \ , \ \frac{\partial \hat{q_2}}{\partial q_1} = \frac{1}{h_2}\frac{\partial h_1}{\partial q_2}\hat{q_1} \tag{A.18}$$

similarly one can obtain four other relations. And it follows that

$$\frac{\partial \hat{q_1}}{\partial q_1} = -\frac{1}{h_2}\frac{\partial h_1}{\partial q_2}\hat{q_2} - \frac{1}{h_3}\frac{\partial h_1}{\partial q_3}\hat{q_3} \tag{A.19}$$

following the process for the other directions, the relation for $\hat{q_2}$ and for $\hat{q_3}$ is obtained.